NONEQUILIBRIUM PHASE BEHAVIOUR AND MASS TRANSFER OF ALKANE SOLVENT(S)–CO_2–HEAVY OIL SYSTEMS UNDER RESERVOIR CONDITIONS

A Thesis

Submitted to the Faculty of Graduate Studies and Research

In Partial Fulfillment of the Requirements

For the Degree of

Doctor of Philosophy

in

Petroleum Systems Engineering

University of Regina

By

Yu Shi

Regina, Saskatchewan

July, 2017

UNIVERSITY OF REGINA

FACULTY OF GRADUATE STUDIES AND RESEARCH

SUPERVISORY AND EXAMINING COMMITTEE

Yu Shi, candidate for the degree of Doctor of Philosophy in Petroleum Systems Engineering**,** has presented a thesis titled, ***Nonequilibrium phase behaviour and mass transfer of alkane solvent(s)-CO2-heavy oil systems undue reservoir conditions,*** in an oral examination held on June 16, 2017. The following committee members have found the thesis acceptable in form and content, and that the candidate demonstrated satisfactory knowledge of the subject material.

External Examiner:	*Dr. Brij Maini, University of Calgary
Supervisor:	Dr. Daoyong Yang, Petroleum Systems Engineering
Committee Member:	*Dr. Ezeddin Shirif, Petroleum Systems Engineering
Committee Member:	Dr. Amornvadee Veawab, Environmental Systems Engineering
Committee Member:	Dr. Hairuo Qing, Department of Geology
Chair of Defense:	Dr. David Gerhard, Department of Computer Science

*via SKYPE
**Not present at defense

ABSTRACT

During primary heavy oil recovery, a unique phenomenon has been found to be closely associated with an unexpected high recovery factor, a remarkably low gas-oil ratio, and a higher-than-expected well production rate due mainly to the foamy nature of viscous oil containing gas bubbles. Even for secondary and tertiary recovery techniques, it is possible to artificially induce foamy oil flow in heavy oil reservoirs by dissolution with injected gases (e.g., CO_2 and alkane solvents), which is characterized by time-dependent (i.e., nonequilibrium) phase behaviour. The entrained gas bubbles in the heavy oil are considered as the main mechanism accounting for such distinct phase behaviour. Therefore, it is of fundamental and practical importance to quantify the nonequilibrium phase behaviour and mass transfer of alkane solvent(s)–CO_2–heavy oil systems under reservoir conditions.

A novel and pragmatic technique has been firstly developed and validated to accurately quantify the preferential diffusion of each component in alkane solvent(s)-assisted recovery processes with consideration of natural convection induced by the heated and diluted heavy oil. The Peng-Robinson equation of state, heat transfer equation, and diffusion-convection equation are coupled to describe both mass and heat transfer for the aforementioned systems. The individual diffusion coefficient between each component of a gas mixture and liquid phase is respectively determined once either the deviation between the experimentally measured and theoretically calculated mole fraction of CO_2/solvents or the deviation between the experimentally measured dynamic swelling factors and the theoretically calculated ones has been minimized.

A robust and pragmatic technique has also been developed to quantify nonequilibrium phase behaviour of alkane solvent(s)–CO_2–heavy oil systems at a constant volume expansion rate and a constant pressure decline rate, respectively. Experimentally, constant-composition expansion (CCE) tests have been conducted for alkane solvent(s)–CO_2–heavy oil systems with a PVT setup, during which not only pressure and volume are simultaneously monitored and measured, but also gas samples were respectively collected at the beginning and the end of experiments to perform compositional analysis. Theoretically, mathematical formulations have been developed to quantify the amount of the evolved gas as a function of time, while mathematical models for compressibility and density of the oleic phase mixed with the entrained gas (i.e., foamy oil) are respectively formulated. In addition to a mechanistic model for quantifying a single gas bubble growth, a novel and pragmatic technique has been proposed and validated to quantify dynamic volume of foamy oil for the aforementioned systems under nonequilibrium conditions by taking preferential mass transfer of each component in a gas mixture into account.

The individual diffusion coefficient of each gas component with consideration of natural convection is found to be larger than that obtained with conventional methods. An increase in either volume expansion rate or pressure decline rate would increase the critical supersaturation pressure, whereas a high temperature leads to a low critical supersaturation pressure. When pressure is below the pseudo-bubblepoint pressure, density and compressibility of foamy oil are found to sharply decrease and increase at the pseudo-bubblepoint pressure, respectively. Also, pseudo-bubblepoint pressure and rate of gas exsolution is found to be two mechanisms dominating the volume-growth rate of the evolved gas, which is directly proportional to supersaturation pressure, pressure decline rate, and concentration of each gas component under nonequilibrium conditions.

ACKNOWLEDGEMENTS

Firstly of all, I would like to express my deepest appreciation and respect to my academic supervisor, Dr. Daoyong (Tony) Yang, for his invaluable guidance, endless patience, continuous encouragement, and generous financial support throughout my Ph.D. graduate studies at the University of Regina. Without Dr. Yang's genuine trust and persistent help, I would have not been able to have such a precious opportunity to pursue my Ph.D. degree at the University of Regina, not to mention carrying it on to completion.

I would like to thank my past and present research group members, Dr. Huazhou Li, Dr. Yin Zhang, Dr. Xiaoli Li, Dr. Sixu Zheng, Dr. Zhaoqi Fan, Mr. Chengyao Song, Mr. Deyue Zhou, Mr. Feng Zhang, Ms. Min Yang, Ms. Ping Yang, Ms. Xiaoyan Meng, Mr. Hyun Woong Jang, Mr. Abdou Maiga, Mr. Romauld Moiffo Tene, and Mr. Rui Li, for their inspired suggestions and selfless assistance.

I am truly thankful to the research fund awarded to Dr. Yang from the Petroleum Technology Research Centre (PTRC), a Discovery Development Grant, a Discovery Grant, and a Collaborative Research and Development (CRD) grant from the Natural Sciences and Engineering Research Council (NSERC) of Canada, and EHR Enhanced Hydrocarbon Recovery Inc. for the financial support.

I also thank the Faculty of Graduate Studies and Research (FGSR) for awarding the Graduate Scholarship and Teaching Assistantship during my Ph.D. graduate studies at the University of Regina.

Last but not least, I wish to express my sincere gratitude to my parents, Mr. Qingwei Shi and Mrs. Yan Fu, for their endless love, enormous support, and continuous encouragement throughout my Ph.D. graduate studies at the University of Regina.

DEDICATIOIN

This dissertation is gratefully dedicated to my beloved wife, Mrs. Wenyu Yang,

and my dear son, Hanzhang Shi.

TABLE OF CONTENTS

LIST OF TABLES

LIST OF FIGURES

NOMENCLATURE

Notations

a	a parameter representing the bubble growth rate
A	constant in Equation [3-7]
A_c	cross-sectional area of the PVT cell, m^2
A_{li}	constant unique to the i^{th} component of liquid mixture
B	constant in Equation [3-7]
B_g	constant in Equation [2-1]
B_{li}	constant unique to the i^{th} component of liquid mixture
$c(r,t)$	gas concentration at radius r and time t, mol/m^3
c_{bd}	dispersed gas concentration, $gmol/m^3$
c_{do}	compressibility of dead oil, kPa^{-1}
c_{en}	compressibility of entrained gas, kPa^{-1}
c_{fo}	compressibility of foamy oil, kPa^{-1}
c_{gd}	dissolved gas concentration, $gmol/m^3$
c'_{gd}	dissolved gas solubility, $gmol/m^3$
c_i	the i^{th} solvent or CO_2 concentration in the liquid phase, mol/m^3
c_{i0}	initial concentration of the i^{th} solvent or CO_2, mol/m^3
c_{pl}	heat capacity of the liquid phase, $J/(kg \cdot K)$

c_{sat}	solvent concentration at the gas-liquid interface, mol/m^3
c_{sg}	compressibility of solution gas, kPa^{-1}
c_t	compressibility of liquid under equilibrium conditions, kPa^{-1}
d	bubble growth rate coefficient
d_p	pressure decline rate, kPa/s
D_{go}	diffusion coefficients of gas solvent in heavy oil, m^2/s
D_i	the i^{th} solvent or CO_2 diffusion coefficient, m^2/s
D_{og}	diffusion coefficient of heavy oil in gas solvent, m^2/s
f	a function of site geometry and wettability
f_m	foam quality
f_{en}, f_o	volume fraction of entrained gas and heavy oil
f_v	volume fraction of the dispersed phase
$G_{1,2}$	the gas bubble growth parameters
J	the number of bubble per unit time and unit volume of a liquid
J_0	the number of molecules per unit of volume
K	Boltzmann's constant
K_h	kinetic constant
K_s	solubility constant
l_0	initial height of the liquid phase, m
$l(t)$	height of the liquid phase at time t, m

m	mass of a molecule, g
m_1	bubble growth coefficient at $t < t_{pb}$
m_2	bubble growth coefficient at $t \geq t_{pb}$
$m_{a,b,c}$	constant in Table 2-1
m_{fo}	mass of foamy oil, g
m_t	total mass of gas-heavy oil mixture, g
MW_{free}	molecular weight of free gas, g/mol
n	mole of gas, mol
n_{en}	mole of entrained gas, mol
n_{eq}	mole of evolved gas under thermodynamic conditions, mol
n_{ev}	mole of the evolved gas under nonequilibrium conditions, mol
n_{free}	mole of free gas, mol
Δn_s	supersaturation expressed in moles of gas, mole
$N_{1,2}$	nucleation parameters
N_b	total number of gas bubbles in oleic phase
N_g	number of gas solvent component
N_m	number of experimental data
p_g	pressure of gas bubble, kPa
p_l	pressure of liquid phase, kPa

P_b	bubblepoint pressure, kPa
P_c	critical pressure, kPa
P_e	pressure at the end of CCE experiment, kPa
P_i	initial pressure of the entire system, kPa
P_i^{cal}	calculated pressure corresponding to the i^{th} measured pressure point, kPa
P_i^m	the i^{th} measured pressure point, kPa
P_{pb}	pseudobubble point pressure, kPa
P_{pi}	parachor of the i^{th} component
P_{ref}	reference pressure, 101.325 kPa
P_s	apparent critical supersaturation pressure, kPa
$P(t)$	pressure at time t, kPa
ΔP	pressure deviation from atmospheric pressure, MPa
ΔP_{lg}	pressure difference between gas and liquid in critical bubble, kPa
ΔP_s	supersaturation pressure, kPa
q	volume increment of entire system per unit time, m^3/s
r	radial distance from the center of the liquid shell, μm
$r_a^{1,2}$	mass transfer rates per unit volume per unit time of dissolved gas into dispersed bubbles, $kg/m^3 \cdot s$
r_{b0}	radius of an initial gas bubble, μm
$\dot{r}_b$	change of r_b over time, μm/s

$r_b(t)$	radius of the gas bubble at time *t*, μm
r_c	radius of a capillary, μm
$r_d^{1,2}$	mass transfer rates of dispersed bubbles into connected bubbles, kg/m^3·s
r_e	outer boundary radius of the liquid shell, μm
R	universal gas constant, kPa·m^3/K·mol
R_s, R_{so}	solution gas-oil ratio and gas-oil ratio, respectively, m^3/m^3
s	swelling factor
s_i^{cal}	calculated dynamic swelling factor
s_i^m	measured dynamic swelling factor
t	time, s
t_c	interaction time between two bubbles, s
t_{dg}	age of the dispersed gas, s
t_{eq}	time required to reach thermodynamic conditions, s
t_i	time of the liquid film trapped between the bubbles to drain, s
t_{pb}	critical time corresponding to the pseudo-bubblepoint pressure, s
Δt	time step size, s
T	temperature, K
T_c	critical temperature, K
T_h	temperature of the PVT chamber, K
T_l	temperature of liquid phase, K

T_{li} initial temperature of liquid phase, K

T_r reduced temperature

u velocity of natural convection, m/s

u_r radial fluid velocity, μm/s

$V(t)$ total volume of mixture, m^3

$\bar{V}$ corrected molar volume, m^3/kmol

V_c critical volume of each component, m^3/kmol

V_{fo} volume of an alkane solvent(s)–CO_2–heavy oil system, m^3

V_{free} volume of free gas, m^3

$V_g(t)$ volume of gas phase, m^3

V_i^{cal} calculated volume corresponding to the i^{th} measured pressure point , m^3

V_i^m the i^{th} measured volume point, m^3

V_i^p the i^{th} component corrections

$V_l(t)$ volume of liquid phase, m^3

V_{li} initial volume of liquid phase, m^3

V_M molar volume, m^3/kmol

V_{Mx}^0, V_{Mx}^t molar volume of oleic phase at initial stage and time t, respectively, m^3/kmol

V_T^c, V_T^m calculated and measured volume of experimental fluids, respectively, m^3

ΔV total increased volume of the liquid phase, m^3

w_i	i^{th} component mass fraction in the liquid phase
W	a nucleation site of width, m
x	distance in x axis, m
x_{gi}	composition of the i^{th} gas solvent in the liquid phase
x_i	composition of the i^{th} component in the liquid phase
x_i^{cal}	calculated mole fraction of the i^{th} component in liquid phase
x_i^m	measured mole fraction of the i^{th} component in liquid phase
y_{cal}	calculated mole fraction in gas phase
$y_{\exp}$	measured mole fraction in gas phase
y_i	mole composition of the i^{th} component in gas phase
z	compressibility factor of gas phase
z_{RA}	Rackett parameter

Greek Letters

$\alpha(T_r, \omega)$	alpha function
α_g	fraction of the flashed gas that is entrained in oleic phase
α_i	viscosibility parameter of the i^{th} component in the liquid phase
α_l	viscosibility parameter of liquid mixture
β	coefficient in Equation [3-4]

β_l	constant in Equation [2-8]
δ_{ij}	binary interaction parameter between the i^{th} and j^{th} components
ε	tolerance for convergence, unit depending on the variable
θ_l	constant in Equation [2-14]
λ_{dg}	decay coefficient of dispersed gas, s^{-1}
λ_l	thermal conductivities of the liquid phase, W/(m·K)
λ_s	rate coefficient for the decay of supersaturation
μ	viscosity, cP
$\mu^0(T)$	dynamic viscosity of mixture at temperature T and atmospheric pressure, cP
ρ_{fo}	density of foamy oil, kg/m^3
ρ_g, ρ_l	density of the gas and liquid phase, kg/m^3
ρ_{sat}	saturation density, kg/m^3
ρ^L	molar densities of liquid, mol/cm^3
ρ^V	molar densities of gas, mol/cm^3
σ	interfacial tension, mN/m
ϕ_g	ratio of the volume of gas flashed to the volume of the total solution gas
ω	acentric factor

CHAPTER 1 INTRODUCTION

1.1 Heavy Oil Primary Recovery

With the continuously increasing oil consumption, oil production from unconventional resources (e.g., heavy oil, tight oil, and shale gas) will gradually occupy more and more market shares around the world. Such an increasing trend can be peeped from the fact that the United States has been ranked as the number one oil producer of the world in 2014 with the contribution of tight oil production (Smith, 2014). Similar to tight oil, heavy oil inarguably, is one of the most important unconventional oil resources, though its recovery cost is still high. The estimated volume about 434 billion barrels of technically recoverable heavy oil (100 cP < viscosity < 10000 cP and API < 22°) in the known accumulations accounts for 45.8% of the remaining conventional oil reserves (viscosity < 100 cP and API > 22°) in the world (Meyer and Attanasi, 2003).

In addition to minimizing greenhouse gas emissions (mainly CO_2) and thus reducing the carbon footprint, heavy oil recovery has to face more challenges than that of conventional oils due mainly to its remarkably high viscosity under reservoir conditions. Numerous efforts have been made to facilitate mobilizing the residual heavy oil by using heat, CO_2, water, solvent(s), and polymer during the so-called secondary and tertiary recovery stages (Butler, 1991; Bulter and Mokrys, 1992; Farouq Ali, 2003; Santos *et al*., 2014). Although those techniques can effectively boost the heavy oil production, the relatively high recovery cost is still an inevitable disadvantage. For example, the ratio of the energy used to the energy produced can even reach 30% for extracting the extra heavy oil compared

to 6% of conventional oil and gas because of the required significant amount of heat (Seljom, 2010). Also, thermal recovery methods normally require huge amount of water while emitting a large amount of greenhouse gases (e.g., CO_2). Therefore, it is of fundamental and practical importance to enhance the primary recovery factor for heavy oil reservoirs while mitigating the negative environmental impact in a cost-effective and sustainable manner.

In fact, primary recovery or solution-gas drive plays an important role for heavy oil production with a recovery factor of 5–15% of the original-oil-in-place (OOIP) (Maini, 1996; 2001; Firoozabadi, 2001; Arora and Kovscek, 2003). The oil production driven by solution gas drive usually shows much better performance than that of a conventional oil reservoir. Such a unique phenomenon is always accompanied with an unexpected high recovery factor, remarkably low gas-oil ratio (GOR), and a larger-than-expected well production rate (Sarma and Maini, 1992; Sheng, 1997; Kamp *et al*., 2001). Numerous efforts have been made to identify the underlying mechanisms of primary recovery of heavy oil, among which the so-called foamy oil has been, eventually, accepted to be the main mechanism (Maini *et al*., 1993; Sheng *et al*., 1996; Mastmann *et al*., 2001; Bennion *et al*., 2003). Even for the secondary and tertiary recovery techniques, it is possible to artificially induce foamy oil flow in heavy oil reservoirs with non-hydrocarbon gases, such as CO_2 (Or *et al*., 2014). As CO_2 solubility in heavy oil is limited, addition of alkane solvent(s) to the CO_2 stream is able to accelerate the mass transfer between gas phase and heavy oil (Li, 2013; Li *et al*., 2013a; b; Zheng *et al*., 2016b). Nonequilibrium phase behaviour is essentially associated with *in-situ* generation of foamy oil, delivering a

greater recovery potential with less reservoir pressure decline as well as lower GOR than those predicted by using the existing reservoir simulators that are based on thermodynamic equilibrium. Therefore, both pragmatic and fundamental works need to be conducted in terms of nonequilibrium phase behaviour and mass transfer in order to effectively utilize the energy originated from the solution gas and maximize the corresponding recovery factor.

1.2 Objectives of the Study

Nonequilibrium phase behaviour of foamy oil is physically stemmed from the fact that the gas evolved from the saturated heavy oil with a decrease of pressure is partially or entirely entrained in the liquid phase rather than directly released to be free gas. The distinct phase behaviour of foamy oil, evidently, is strongly associated with the amount of the entrained gas in the liquid (Kraus *et al*., 1993; Sheng *et al*., 1995; Wang *et al*., 2009). Consequently, an experimental and theoretical work to examine effects of gas bubbles on the foamy oil shall serve as the necessary foundation for addressing the issue of nonequilibrium phase behaviour of foamy oil.

The major objective of this research is aiming to develop experimental and theoretical techniques to quantify the nonequilibrium behaviour and the corresponding physical properties of foamy oil used for numerical simulation and mass transfer processes occurring between gas phase (including free gas and gas bubble) and liquid phase for alkane solvent(s)–CO_2–heavy oil systems under reservoir conditions. The detailed objectives are listed as follows:

1). To perform PVT experiments for quantifying equilibrium and nonequilibrium phase behaviour for the alkane solvent(s)–CO_2–heavy oil systems under reservoir conditions while examining the effects of addition of alkane solvent(s) to the CO_2 stream on heavy oil properties;

2). To formulate theoretical models to determine the individual diffusion coefficient of each component in a alkane solvent(s)–CO_2–heavy oil mixture with consideration of natural convection induced by swelling effect and heat;

3). To theoretically quantify the nonequilibrium phase behaviour and mass transfer of the aforementioned systems under reservoir conditions and thus predict the physical properties of foamy oil;

4). To develop a mechanistic model for formulating gas bubble growth processes by taking into account the contribution of each individual component of a gas mixture under reservoir conditions; and

5). To apply the newly developed mechanistic model to quantify the actual nonequilibrium phase behaviour with consideration of preferential diffusion.

1.3 Outline of the Study

In total, eight chapters are included in this dissertation. Chapter 1 briefly introduces background of the research topic together with the detailed research objectives. Chapter 2 summarizes the updated literature review associated with nonequilibrium phase behaviour and related mechanisms of gas bubble formation. Chapter 3 proposes a novel mathematical model to determine the individual diffusion coefficient of each component in alkane solvent(s)–CO_2–heavy oil systems with consideration of natural convection

induced by the diluted and heated heavy oil. Chapters 4 and 5 respectively present a pragmatic and robust technique to experimentally and theoretically quantify the nonequilibrium phase behaviour together with foamy oil properties of alkane solvent(s)–CO_2–heavy oil systems under a constant volume expansion rate and a constant pressure decline rate. A mechanistic model has been developed and validated to describe a single gas bubble growth process by taking into account the contribution of each individual component of a gas mixture under reservoir conditions in Chapter 6. Furthermore, Chapter 7 extends the newly proposed single gas bubble model to formulate the dynamic volume growth of foamy oil with consideration of preferential diffusion of the aforementioned systems. Finally, Chapter 8 summarizes the major contributions together with the main scientific findings on this research, while recommendations for future work are accordingly introduced.

CHAPTER 2 LITERATURE REVIEW

2.1 Introduction

A number of heavy oil reservoirs under solution gas drive show anomalously good primary performance featured by high oil production rates, low producing gas-oil ratio (GOR) and high oil recovery compared with that of conventional oil reservoirs (Sarma and Maini, 1992; Sheng, 1997; Kamp *et al*., 2001). Nonequilibrium phase behaviour has been considered as an important aspect (e.g., in-situ generation of foamy oil during production) for increasing primary heavy oil recovery, while it can be found in solvent(s)-assisted heavy oil recovery processes. Physically, nonequilibrium phase behaviour is closely associated with the *in-situ* generation of foamy oil in heavy oil reservoirs where dispersed gas remains in the viscous liquid phase at pressures below the thermodynamic bubblepoint pressure (Thomas *et al*., 2014). As for the mechanisms of gas bubble formation in heavy oil, time evidently plays a key role on the understanding of foamy oil generation and quantification of the amount of the entrained gas (Sheng *et al*., 1999b). In addition, as a nonequilibrium thermodynamic system, the phase behaviour of foamy oil is characterized by some specific properties, such as supersaturation (Maini, 2001) and the so-called "pseudo-bubblepoint pressure" (Kraus, 1993). Such characteristics make foamy oil obviously be distinguished from equilibrium thermodynamic systems under the same conditions. Essentially, the nonequilibrium phase behaviour is resulted from the capture of the evolved gas in the liquid phase and eventually induces the aforementioned oil production performance during primary recovery of heavy oil.

2.2 Mechanisms of Gas Bubble Formation

The solution gas drive of heavy oil includes a large number of mechanisms as similar as those found in conventional oil reservoirs (Sheng *et al*., 1999c). In general, gas bubble formation in heavy oil involves three stages, i.e., bubble nucleation, bubble growth, and bubble coalescence, which are same as those in conventional oils (Firoozabadi *et al*., 1992; Kashchiev and Firoozabadi, 1993; Sheng *et al*., 1999c). The notable difference is that all of the three stages are supposed to instantly occur in conventional light oils; however, as for heavy oil, the entire gas bubble formation processes would only take place during a certain period.

2.2.1 Gas bubble nucleation

The physical implication of gas bubble nucleation can be understood as a volatile fluid in contact only with other condensed phases (Blander, 1979). The occurrence of gas nucleation is mainly resulted from either a pressure decline below the bubblepoint pressure or a temperature increase above the boiling point, i.e., the so-called cavitation and boiling, respectively (Kumar, 1999). Accordingly, for heavy oil recovery, the cavitation shall be the main mechanism of gas bubble nucleation taking place in reservoirs.

As for the experimental quantification of gas bubble nucleation in the oil industry, Chatenever *et al*. (1959) initiated research early in this regard with 116 laboratory experiments performed in glass-bead packing and thin sections of natural sandstone and limestone. It has been found that supersaturation is necessary for the nucleation of gas

bubbles, though the supersaturation behaviour is not stable and thus difficult to be reproduced even for the same systems. Li and Yortsos (1991) observed that nucleation of gas bubbles is originated from different locations in the glass micromodels utilized in their experiments. To identify the mechanisms accounting for the anomalous heavy oil production, Sarma and Maini (1992) experimentally examined effects of gas nucleation on heavy oil recovery and found that nucleation cannot improve the mobility of the liquid phase. After examining the effect of interfacial tension (IFT) on the gas nucleation, Mackay *et al*. (1998) concluded that high values of gas/oil IFT lead to increasing levels of supersaturation with relatively fewer bubbles nucleating on the water-solid surface under waterflooding conditions. It is interesting to note that two types of contrary experimental results are obtained for gas nucleation processes. By utilizing transparent micromodels to understand the mechanisms of gas bubble nucleation with pressure decline in a CO_2–water system, Yousfi *et al*. (1997) observed that gas bubble nucleation is basically instantaneous except for those captured by capillary force in porous media. Also, the total number of gas bubbles can be expressed as a function of supersaturation. A similar phenomenon of gas nucleation has also been found in a Berea sandstone sample held with a visualized coreholder by Firoozabadi and Aronson (1999). On the contrary, Bora *et al*. (1997) experimentally found that the bubble nucleation is not an instantaneous process, i.e., the nucleation of new bubbles continues to appear late in the pressure depletion processes from a series of flow visualization experiments.

For the theoretical study of nucleation, development of classical nucleation theory (CNT) can be traced back to almost a century ago (Volmer and Weber, 1925; Reguera and

Miguel, 2015). Since then, numerous efforts have been made to quantify the nucleation due to its frequent occurrence and extensive applications in different industries (Farkas, 1927; Zeldovich, 1943; Deryagin, 1994; Frank *et al*., 2007). Traditional nucleation theory generally classifies gas nucleation as two types of nucleation processes, namely, homogeneous nucleation and heterogeneous nucleation, based on characteristics of the interface between gas phase and the enclosing phase (Blander, 1979; Avedisian, 1985; Li and Yortsos, 1995; Delale *et al*., 2003). More specifically, theoretical rate for homogeneous nucleation is able to be expressed as follows (Wilt, 1986; Oxtoby, 1998),

$$J = J_0 \left(\frac{2\sigma B_g}{\pi m} \right) \exp\left(\frac{-16\pi\sigma^3}{3KT\Delta P_{\mathrm{lg}}^2} \right) \qquad [2\text{-}1]$$

where J is the number of bubble per unit time and unit volume of a liquid; J_0 is the number of molecules per unit of volume; K is Boltzmann's constant; T is absolute temperature; σ is IFT between gas and liquid; ΔP_{lg} is the pressure difference between gas phase and liquid phase in critical bubble; m is mass of a molecule; and $B_g = 1$ or $B_g \approx \frac{2}{3}$ for chemical equilibrium and mechanical equilibrium, respectively.

Yortsos and Parlar (1989) postulated that heterogeneous nucleation is the most plausible mechanism pertaining to the nucleation of porous media owing mainly to a relatively low supersaturation (i.e., possible several thousand psi less than that of the homogeneous nucleation) and rough interface between liquid and solid. Then, a heterogeneous nucleation rate model is proposed as follows (Moulu, 1989; Yortsos and Parlar, 1989),

$$J = K_h \exp\left(\frac{-16\pi\sigma^3}{3KT\Delta P_{\mathrm{lg}}^2} f \right) \qquad [2\text{-}2]$$

where K_h is a kinetic constant; f is a function of site geometry and wettability, ranging from 0 to 1 to represent from the homogeneous nucleation to completely heterogeneous nucleation. Kashchiev and Firoozabadi (1993) further indicated that, if the radius of grains in porous media is much larger than 10 nm, f can be formulated as follows,

$$f(\theta) = \frac{2 + 3\cos\theta - \cos^3\theta}{4} \qquad [2\text{-}3]$$

where θ is the wetting angle between liquid and grain.

An alternative model, which is expressed as follows, presented that nucleation activation is only dependent on the local variables (Li and Yortsos, 1995),

$$K_s c - P_l \geq \frac{\sigma}{W} \qquad [2\text{-}4]$$

where K_s is solubility constant; c is concentration of solute (i.e., dissolved gas); P_l is liquid pressure, and W is crevice mouth size. Although such nucleation condition does not involve any intrinsic kinetic mechanisms of classical nucleation theory (i.e., whether homogeneous or heterogeneous), it is still of the nature of heterogeneous nucleation (Sheng *et al*., 1999c).

Although the nucleation rate has been effectively quantified with the aforementioned models rooted in classical nucleation theory, an argument associated with the nucleation processes still exists between the two contradictory theories, i.e., instantaneous nucleation (IN) model and progressive nucleation (PN) model (Kashchiev and Firoozabadi, 1993; Li and Yortsos, 1995; Firoozabadi and Kashchiev, 1996). In terms of the former, all nucleus bubbles are assumed to form at once and then gradually grow (Kashchiev and

Firoozabadi, 1993; Firoozabadi and Kashchiev, 1996). In contrast, as for the latter, new bubbles are assumed to continuously nucleate among the growing ones with consideration of the density of bubbles as a function of time (Kashchiev and Firoozabadi, 1993; Li and Yortsos, 1995).

Firoozabadi and Kashchiev (1996) employed the gas volume expression, which is derived from the incorporation of a nucleation rate model and a bubble growth model, to examine the reliability of the IN and PN models, respectively. It is found that the calculated results with PN model are not supported by the experimental data because the pronounced effect of IFT on supersaturation is not observed in the laboratory experiments. However, Yortsos (1997) concluded that the nucleation process is essentially progressive due to the heterogeneous nucleation occurring in porous media. In detail, the activation of nucleation in porous media is dependent on the condition of Equation [2-4]. Nucleation, therefore, would take place at the different time by taking different characteristics of nucleation sites into account (Li and Yortsos, 1995). Sheng *et al*. (1999c) also asserted that the IN process actually is a special case of the PN process when supersaturation is instantly achieved by a rapid one-step pressure drop. This is because the initial supersaturation, evidently, is the maximum one when a rapid one-step pressure drop is utilized to induce the supersaturation. Consequently, no more sites can be activated after the pressure drop since all sites that can be activated have been triggered to nucleate by the supersaturation based on Equation [2-4]. In spite of the inconsistent understanding about the nucleation process, the mechanistic model developed by Arora and Kovscek

(2003) theoretically found that both the IN model and the PN model can be successfully used to match the experimental measurements for light oil and viscous oil, respectively.

2.2.2 Gas bubble growth

When gas bubble has nucleated in the enclosing liquid phase, the gas bubble volume will continuously increase if the radius of gas bubble is larger than a critical value. Scriven (1959) proposed a generalized model to mathematically describe the growth process of a single gas bubble based on the equation of continuity, equation of motion, equation of energy flow, and equation of mass flow. Such a complicated equation matrix makes the solving of the proposed mathematical model extremely difficult. Accordingly, numerous efforts have been made to analytically or numerically solve the aforementioned model for accurately quantifying the growth of a single gas bubble involved in chemical engineering, petroleum engineering, geology science, and food engineering. In particular, as for the heavy oil recovery, the bubble growth can be postulated as a process induced by pressure depletion (rather than heat) in a Newtonian liquid. Therefore, numerous attempts have been focused on examining effects of liquid inertia, surface tension, viscous forces, and natural convection on the bubble growth (Szekely and Martins, 1971; Patel, 1980; Kumar, 1999; Sheng *et al*., 1999c; Wong and Maini, 2007).

Szekely and Martins (1971; 1973) numerically solved the model to address the growth of a stationary spherical gas bubble in a quiescent liquid with the assumption of a constant liquid pressure and infinite liquid volume. With the comparison between experimental measurements and theoretical calculation of C_5–C_{14} systems, they concluded that the

liquid inertia plays an important role in determining the growth rate at the very initial stage; however, hydrodynamic and surface kinetic effects tend to dramatically diminish in their importance with an increase of gas bubble volume. Such results are consistent with those reported in previous work (Birkhoff *et al*., 1958). After the very beginning stage of bubble growth, mass transfer becomes an important factor controlling the gas bubble growth (Kashchiev and Firoozabadi, 1993; Sheng *et al*., 1999c).

Obviously, the simplification of infinite liquid volume in Szekely and Martins (1971)' works cannot be used to effectively represent the actual physical processes of the gas bubble growth in the liquid phase due to the indeed limited amount of the dissolved gas. Rosner and Epstein (1972) theoretically quantified the bubble growth process with taking into account of interface motion and self-induced radial fluid motion. Arefmanesh *et al*. (1992), eventually, provided accurately numerical solutions of a single gas bubble growth with a limited dissolved gas concentration in a Newtonian fluid. The gas bubble radius is found to be a function of time before time reaches its threshold value. After that, the radius of gas bubble stops increasing owing to the limited amount of the dissolved gas. Combining with the heterogeneous bubble nucleation model, Moulu (1989) extended the aforementioned single bubble growth model to a theoretical equation matrix accounting for the relationship between gas saturation and pressure. Similar theoretical efforts have also been made with the boundary conditions of gradual volume expansion and pressure depletion (Kumar and Pooladi-Darvish, 2001). Wong and Maini (2007) further applied the single bubble growth model to interpret the nonequilibrium phase behaviour of pore pressure and volume changes by taking the liquid compressibility into account.

Physically, a gas bubble evolved from the heavy oil usually is a multicomponent vapour system comprising the dissolved gas and/or the injected solvent(s)/CO_2. So far, few attempts have been made to determine the mass transfer rate of different components as a function of gas concentration, diffusion coefficient, temperature, and pressure, not to mention the bubble growth rate and the nonequilibrium behaviour of foamy oil under such complicated conditions. Cable and Frade (1987) presented both analytical and numerical solutions for a single gas bubble growth in an infinite volume liquid phase with several independently diffusing gases, while Gor and Kuchma (2009) developed and analytically solved the model describing the growth process of a two-component gas bubble based on the assumption of a steady-state composition in the gas bubble.

Although the aforementioned theoretical descriptions can be employed to effectively quantify the characteristics of gas bubble growth and be generally accepted, it is a time-consuming process to numerically solve the equation matrix due to the complicated procedure where many parameters are involved. After summarizing a number of experimental and theoretical works on bubble growth, Jones *et al.* (1999) concluded that a power function associated with time, which can be used to simply describe the relationship between the bubble radius and time, i.e.,

$$r \sim t^a \qquad [2\text{-}5]$$

where r is the radius of a gas bubble, t is time, and a is a parameter representing the bubble growth rate. The range of such parameter, a, has been found to be large due to the possible effects of different factors (Scriven, 1959; Moulu, 1989; Jones *et al*., 1999). Kashchiev and Firoozabadi (1993) also indicated that three regimes of gas bubble growth

respectively dominated by inertia of the liquid, evaporation and condensation, and diffusion result in three different $r_b(t)$ dependencies. Since the radius of a gas bubble is evidently proportional to its volume, Sheng *et al*. (1995; 1997; 1999c) further quantified the amount of the evolved gas, n_{ev}, as a power function of time, i.e.,

$$n_{ev}(t) = n_{eq}\left(\frac{t}{t_{eq}}\right)^{d} \qquad [2\text{-}6]$$

where n_{ev} is the amount of gas evolved at thermodynamic equilibrium; t_{eq} is the time required to reach the thermodynamic equilibrium; and d is the gas-bubble growth rate coefficient.

2.2.3 Gas bubble coalescence

Bubble coalescence is a process occurring when two bubbles come close to each other in a gas-liquid dispersion (Kumar, 1999). It is one of important processes that not only govern the distribution of gas bubble size, but also affect the interfacial mass transfer rate owing to the renewal of bubble surfaces (Chen *et al*., 1998; Laari and Turunen, 2005). It is desired to accurately quantify bubble coalescence because the physical laws that dominate the bubble coalescence have not yet been completely understood, especially in porous media (Kumar, 1999; Sheng *et al*., 1999c; Laari and Turunen, 2005; Slettebø, 2009). Basically, three regimes are recognized to be involved during the entire bubble coalescence process (see Figure 2-1): (1) bubble collision, trapping a small amount of liquid; (2) liquid film drainage, draining liquid film between two bubbles; and (3) rupture of the film, forming a larger bubble (Slettebø, 2009).

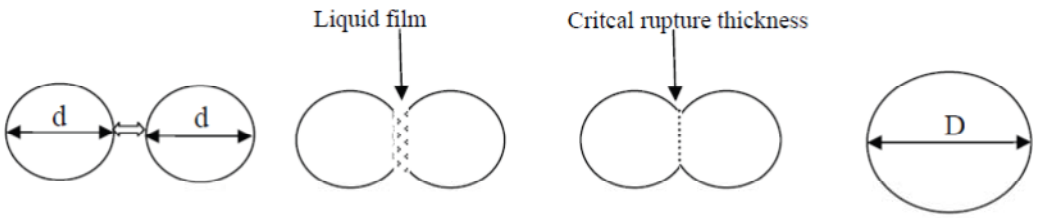

Figure 2-1 The three regimes occurring in bubble coalescence: Collision, liquid film drainage, and rupture (Slettebø, 2009)

Marrucci (1969) proposed a theory in which the thinning of a liquid film between two contacting bubbles was divided into two stages: (1) an extremely rapid thinning of film down to a quasi-equilibrium thickness and (2) further thinning of quasi-equilibrium film down to the rupture. It is suggested that the diffusion on the border of the film determine the thinning rate, and then predictive equations for the coalescence time can be quantified. Chesters (1991) presented that the drainage time (i.e., the time of the liquid film trapped between the bubbles to drain) and the interaction time between two bubbles can be expressed as,

$$t_i \cong \left(\frac{\rho_l r^3}{2\sigma} \right)^{1/2} \qquad [2\text{-}7a]$$

$$t_c \cong \frac{1}{2} \frac{\rho_l r^2 V_r}{\sigma} \qquad [2\text{-}7b]$$

where V_r is the relative velocity of the colliding bubbles; ρ_l is the density of liquid. Slettebø (2009) pointed out that drainage time must be shorter than interaction time so that the collisions of two bubbles can lead to coalescence.

In particular, as for the study of bubble coalescence in foamy oil, Geilikman *et al*. (1995) categorized gas bubbles of heavy oil into rigid (small) bubbles and soft (large) bubbles based on the interrelation between fluid pressure and capillary pressure. The rigid bubble is not only more stable than the soft one, but also more difficult to coalesce because of the compression of capillary pressure. Bora *et al*. (2003) experimentally found that the coalescence of gas bubbles in foamy oil is mostly caused by two distinct mechanisms in porous media: (1) approaching coalescence of two adjoining gas bubbles during their

growth processes and (2) colliding coalescence of two gas bubbles during their flow processes. Based on mechanism (1), therefore, the coalescence rate of gas bubbles in heavy oil would be decreased to some degree because of high viscosity. Such findings, in fact, have also been observed in other laboratory experiments (Dusseault, 1993; Pooladi-Darvish and Firoozabadi, 1999). Although numerous attempts have been made to develop theoretical models for quantifying the bubble coalescence processes since 1950s (Luo, 1993), most of which are still only applicable for a limited range of the conditions and materials because of the extremely complicated physical processes and a great number of factors involved in the coalescence, such as IFT, liquid viscosity, and buoyancy (Homayouni *et al*., 2008).

2.2.4 Mass transfer during gas bubble formation

Mass transfer between gas and liquid phase plays a critical role on gas bubble formation (Li, 1996; Jones *et al*., 1999; Lillico *et al*., 2001). Especially, for gas bubble growth in a hydrocarbon liquid, mass transfer process is indispensable to be investigated because most of the amount of dissolved gas comes out of the liquid in this stage considering the tiny volume of the critical embryo during the nucleation process (Yortsos and Parlar, 1989; Kashchiev and Firoozabadi, 1993). In other words, the phenomenon of either the gas bubble growth at micro-scale or exsolution of dissolved gas at macro-scale is dominated by the process of gas component transferring from liquid phase to gas phase. Molecular diffusion has been apparently believed to be the main mechanism accounting for such mass transfer process, though the factors that govern this process are not well understood yet (Jones *et al*., 1999). Accordingly, considering that the concentration of

gas solvent in oleic phase is relatively easily obtained, diffusion coefficient becomes a key parameter required for accurately quantifying the mass transfer process and thus describing the gas bubble growth.

Until now, numerous efforts have been made to experimentally and theoretically determine diffusion coefficients for solvent(s)–heavy oil systems under various conditions (Yang and Gu, 2006a; Luo and Kantzas, 2008; Guerrero-Aconcha *et al*., 2008; Song *et al*., 2010; Li and Yang, 2016; Zheng and Yang, 2016). In general, diffusion coefficient can be obtained indirectly by minimizing the deviation between the experimental measurements and theoretical calculations from various mathematical models. As for such an indirect determination, PVT tests, X-ray method, and NMR approach are found to be effectively experimental approaches for quantifying mass transfer of a solvent in heavy oil (Wen *et al*., 2005; Li, 2006; Song *et al*., 2010). Both analytical and numerical solutions of mathematical models have been used to determine diffusion coefficients with Fick's law, depending on the complexity of history matching experimental processes (Renner, 1988; Sachs, 1998; Civan and Rasmussen, 2006).

During diffusion experiments, fluids flow or convection cannot be avoided due to experimental procedures or swelling effect induced by the heated or diluted crude oil. Since numerical solutions related to mass transfer models for accurately describing the fluid flow are complex, it is difficult to isolate the contribution of convection to the mass transfer, which has been vaguely combined with diffusion mechanisms as stated in most of the literatures (Wen *et al*., 2005; Civan and Rasmussen, 2006; Yang and Gu, 2006b;

Moghaddam *et al*., 2011). Such a vague combination can cause the to-be-measured diffusion coefficient deviated from its true value up to two orders of magnitude (Yang and Gu, 2006b). To examine effects of heat or natural convection, Farajzadeh *et al*. (2007) initiated a study on diffusion coefficients of the CO_2–water systems by considering the density-driven natural convection. As for CO_2–*n*-$C_{16}H_{34}$ systems, Li and Dong (2009) calculated the velocity resulted from the swelling effect in a porous medium and thus indirectly determined the corresponding diffusion coefficients, accounting for both effect of convection and diffusion mechanism. By treating heavy oil as one pseudocomponent (Sun *et al*., 2014; Li *et al*., 2016) and multiple pseudocomponents (Zheng and Yang, 2016; Zheng *et al*., 2016a; Zheng and Yang, 2017), generalized methods have been developed to determine individual diffusion coefficients for alkane solvent(s)–heavy oil systems at high pressures and elevated temperatures without considering convection. So far, no attempts have been made to determine individual diffusion coefficient with consideration of natural convection (Li and Yang, 2016; Zheng *et al*., 2016a), though natural convection may impose a great impact on the mass transfer rate as documented elsewhere (Li and Dong, 2009).

2.3 Nonequilibrium Phase Behaviour

2.3.1 Supersaturation

For saturated oil, supersaturation is defined as the pressure difference between bubblepoint pressure (P_b) and actual pressure of the liquid phase (Kamath and Boyer, 1995). It is mainly utilized to indicate the supersaturated degree of a liquid system, i.e., the degree that the amount of the dissolved gas at actual given pressure and temperature exceeds that of gas dissolved under equilibrium conditions (Kennedy and Olson, 1952).

Physically, gas bubble nucleation and gas bubble growth are found to have a close relationship with supersaturation. When pressure is lower than the bubblepoint pressure during a pressure depletion process, the live oil turns into a supersaturated system. Then, the gas bubbles begin to form once a supersaturation threshold is reached (Kamath and Boyer, 1995).

As early as 1950s, laboratory experiments revealed that the bubble formation frequency is a function of supersaturation in a CH_4–kerosene mixture within both silica and calcite systems (Kennedy and Olson, 1952; Firoozabadi *et al*., 1992). Wieland and Kennedy (1957) further indicated that the rate of gas bubble formation increases with an increase in supersaturation. Meanwhile, both homogeneous and heterogeneous nucleation models presented that there is a firmly positive correlation between supersaturation and bubble nucleation rate (Wilt, 1986; Yortsos and Parlar, 1989; Oxtoby, 1998). In other words, once a gas bubble is formed, the mass transfer of gas from the enclosing liquid to the gas bubble can reduce the degree of supersaturation and prevent new bubbles from forming in the vicinity of the existing bubble (Kortekaas and van Poelgeest, 1991).

Based on supersaturation, as for bubble growth, Yortsos and Parlar (1989) asserted that the bubble growth process can be divided into three regimes, i.e., (1) low supersaturation ($\Delta P_s \ll p_l$), (2) moderate supersaturation ($\Delta P_s \sim p_l$) and (3) large supersaturation ($\Delta P_s \gg p_l$), where ΔP_s is supersaturation and p_l is pressure of a liquid mixture, which is lower than the bubblepoint pressure. For the first two regimes (i.e., low supersaturation and moderate supersaturation), gas bubble growth processes are mainly controlled by

mass transfer since the inertial and viscous forces can be neglected. On the contrary, the inertial and viscous forces play an important role at the early stage of the bubble growth under the condition of large supersaturation. Kashchiev and Firoozabadi (1993) proposed a bubble growth model that quantified bubble growth rate as a power function of supersaturation, stating that the bubble growth rate increases with an increase in supersaturation of the liquid system. Namely, the higher the supersaturation is, the larger the bubble formation rate will be (Stewart *et al*., 1954).

The magnitude of supersaturation is remarkably affected by the characteristics of the involved system, operating conditions, and the pressure depletion level (Sheng *et al*., 1999c). Kortekaas and van Poelgeest (1991) pointed out that the degree of supersaturation developed under low pressure decline rate will most likely differ from those developed under high pressure decline rates. In particular, a low pressure decline rate would result in a low supersaturation (Bauget and Lenormand, 2002). Such findings have been previously reported and verified by a number of researchers (Stewart *et al*., 1954; Handy, 1958; Moulu, 1989; Firoozabadi *et al*., 1994; Sheikha and Pooladi-Darvish, 2009).

The properties of porous medium also show their influences on the supersaturation. A porous medium composed of random packing and sharp-edged grains leads to a low supersaturation under the same conditions (Chatenever *et al*., 1959). Firoozabadi *et al*. (1992) experimentally found that a porous medium with small pore space may result in a relatively low supersaturation compared with those having a large pore space. Meanwhile,

a larger capillary force existing in porous media can result in a higher degree of supersaturation (Kamath and Boyer, 1995).

2.3.2 Pseudo-bubblepoint pressure

Pseudo-bubblepoint pressure (P_{pb}) represents the pressure at which the entrained gas in heavy oil begins to form either free gas phase (Chen *et al*., 2015) or continuous gas phase (de Mirabal *et al*., 1996; Wang *et al*., 2008). It is worthwhile noting that pseudo-bubblepoint pressure is a parameter likely associated with rheological properties of the oil and the producing reservoirs or sandpack models. The pseudo-bubblepoint pressure is not a thermodynamic property and could vary with time (Joseph and Kamp, 2002).

Pseudo-bubblepoint pressure is assumed to be an adjustable parameter in the so-called pseudo-bubblepoint pressure model in order to match field or laboratory measurements of foamy oil (Kraus *et al*., 1993), whereas, under certain conditions, it can be accurately determined with experimental methods (Wang *et al*., 2008). Two main techniques are generally utilized to identify the occurrence of pseudo-bubblepoint pressure during the pressure depletion processes, i.e., (1) the turning point of volume-pressure curve and (2) the change of gas-oil ratio (GOR). As for the former, the pseudo-bubblepoint pressure is physically equal to the nucleation pressure documented elsewhere (Sheng *et al*., 1999c). During constant-composition expansion (CCE) experiments, nucleation pressure can be determined by the turning point of compressibility of the mixture (Firoozabadi *et al*., 1992). Therefore, the pseudo-bubblepoint pressure under nonequilibrium conditions can be located with similar methods used for finding the bubblepoint pressure in the pressure-

volume diagram under equilibrium conditions. As for the latter, Wang *et al*. (2008) pointed out that, when pressure of the mixture system drops to the pseudo-bubblepoint pressure, the gas entrained in liquid phase begins to evolve out of the oil and form free gas. This implies that GOR of the effluent fluid should decline for a short period of time since the portion of the depleted oil is driven out from the porous medium. Then, an increase in GOR can be soon observed as the free mobile gas is expelled. Such features related to GOR changes, therefore, are able to be utilized for the identification of pseudo-bubblepoint pressure.

Based on the aforementioned two methods, several attempts have been made to determine the pseudo-bubblepoint pressures experimentally. Wang *et al*. (2008) determined the pseudo-bubblepoint pressure of the Orinoco-belt heavy oil to be 4.7 MPa within artificial core samples. Sun *et al*. (2013) found that the pseudo-bubblepoint pressures of a heavy oil sample decrease from 3.44 MPa to 1.89 MPa with an increase in pressure depletion rate. Both the above results revealed that the pseudo-bubblepoint pressure under nonequilibrium conditions is lower than the corresponding bubblepoint pressure under equilibrium conditions. Mastmann *et al*. (2001) attributed the difference between bubblepoint pressure and pseudo-bubblepoint pressure to the fact that the high viscosity of heavy oil hinders the gas bubbles immediately coalesce together to form bubbles large enough to be evolved from the liquid phase. So far, limited efforts have been made to theoretically and experimentally determine pseudo-bubblepoint pressure of heavy oil, though its concept has been proposed for more than 20 years (Kraus *et al*., 1993).

2.4 Properties of Foamy Oil

Properties of foamy oil are strongly related to the foamy oil flow behaviour. Similar to the conventional oils, numerically evaluating performance of heavy oil reservoirs requires accurate foamy oil properties for history matching and future prediction (Sheng, 1997; Mastmann *et al*., 2001; Chen *et al*., 2015). Physically, the properties of foamy oil are greatly affected by the growth and decay of dispersed gas bubbles in the oleic phase (Sheng *et al*., 1995), implying that properties of foamy oil are time-dependent. Particularly, for the same mixture, the properties of foamy oil generated under different pressure depletion rates are different, even though those properties are measured at the same designated pressure and temperature.

2.4.1 Compressibility

It has been an interesting topic to determine compressibility of foamy oil for more than 20 years in the oil and gas industry because such a parameter is closely associated with the primary recovery factor of heavy oil reservoirs (Smith, 1988; Kraus *et al*., 1993; Sheng *et al*., 1999b; Bora *et al*., 2003). Two methods are mainly applied for determining compressibility of foamy oil, i.e., (1) semi-empirical method and (2) linear mixing method. By assuming the components of Lloydminster heavy oil to be methane and heavy oil, Smith (1988) proposed the expression of compressibility of foamy oil as follows based on Henry's law,

$$c_{fo} = \frac{\beta_l}{P} \qquad [2\text{-}8]$$

where c_{fo} is compressibility of foamy oil; P is pressure; β_l is a constant (for a Lloydminster oil, β_l is 0.25, which implies that the compressibility of foamy oil is about

one fourth of that for ideal gas under the same conditions). Similar to the pseudo-bubblepoint pressure, the compressibility of foamy oil is also a non-thermodynamic parameter depending on the time. The Smith's model cannot be used to effectively capture such an essential characteristic of foamy oil compressibility.

The methodology utilized in the linear mixing method is, actually, similar to that used in the determination of total compressibility of reservoirs; namely, the compressibility of foamy oil is regarded as a summation of compressibilities of the components constituting foamy oil. More specifically, three components, i.e., dead heavy oil, solution gas, and the entrained gas, are assumed to be included in foamy oil (Kraus *et al*., 1993). Correspondingly, Sheng *et al*. (1997; 1999b) developed a mathematical model for compressibility of foamy oil, which treated the compressibility as a linear combination of the aforementioned three components, i.e.,

$$c_{fo} = -\frac{1}{V_{fo}}\left(V_{Mdo}x_{do}c_{do} + V_{Msg}x_{sg}c_{sg} + V_{Men}x_{en}c_{en}\right) \qquad [2\text{-}9a]$$

where

$$V_{fo} = V_{Mdo}c_{do} + V_{Msg}c_{sg} + V_{Men}c_{en} \qquad [2\text{-}9b]$$

where V_{Mdo}, V_{Msg}, and V_{Men} are the molar specific volumes of dead oil, solution gas, and the entrained gas, respectively; c_{do}, c_{sg}, and c_{en} are the compressibilities of dead oil, solution gas, and the entrained gas, respectively; and x_{do}, x_{sg}, and x_{en} are the mole fraction of dead oil, solution gas, and the entrained gas in the oleic phase, respectively. Since mole fraction of the dispersed gas varies with time, the compressibility calculated by Equation [2-9a] is a function of time as well.

An important difference between foamy oil compressibility and that of conventional oils is that the former is much larger than the latter under a certain range of pressure below the pseudo-bubblepoint pressure (Sheng, 1997; Xiao and Zhao, 2013). This can be explained by the fact that the evolved gas bubbles entrained in the oleic phase dominate the magnitude of compressibility due to the inherently high compressibility of gas phase (Xiao and Zhao, 2013). As such, the compressibility of foamy oil is more gas-like than liquid-like in nature to some extent (Mastmann *et al*., 2001). The pressure, therefore, is able to impose a great impact on the compressibility of foamy oil, which can be briefly evaluated with Equation [2-8]. Meanwhile, based on Equation [2-9a], Sheng *et al*. (1995; 1997) pointed out that the trend of compressibility of foamy oil varying with time keeps its pace with that of the entrained gas mole fraction. More specifically, as for a saturated heavy oil sample, when the pressure suddenly drops lower than its bubblepoint pressure and then keeps stable, the compressibility gradually increases to its maximum and then declines to a certain value approaching to that of a live oil. Apart from the pressure, thus, the factors that can exert effects on the amount of the entrained gas, such as temperature and composition, are able to indirectly affect the compressibility of foamy oil owing to a strong relationship between compressibility and the amount of the entrained gas (Kraus *et al*., 1993; Sheng *et al*., 1995). It is noteworthy that the compressibility of heavy oil is basically same as that of live oil when the gas bubble is not nucleated (Firoozabadi *et al*., 1992).

2.4.2 Viscosity

Effect of the entrained gas on the viscosity of foamy oil is still controversial, while the viscosity of foamy oil is one of the factors affecting the solution-gas drive performance of

heavy oil reservoirs (Chen *et al*., 2015). The key disagreement is whether viscosity of foamy oil (i.e., oil with the dispersed gas bubbles) is reduced or not in comparison with that of a live oil under the same conditions. Viscosity of foamy oil can then be determined with the following proposed correlations as a function of gas phase volume fraction (Smith, 1988),

$$\mu_{fo} = f_o \mu_o + f_{en} \mu_{en} \qquad [2\text{-}10a]$$

or (Smith, 1988; Islam and Chakma, 1990),

$$\mu_{fo} = \mu_o^{f_o} \mu_{en}^{f_{en}} \qquad [2\text{-}10b]$$

where μ_o and μ_{en} are the viscosities of heavy oil and the entrained gas, respectively; f_o and f_{en} are the volume fraction of heavy oil and the entrained gas, respectively. Based on the aforementioned models, the viscosity of foamy oil is expected to be reduced due to a minor effect of the entrained gas in the oleic phase. Subsequently, several viscosity models were also postulated based on the suggestion that attributes the decline of foamy oil viscosity to one of the mechanisms accounting for the anomalous production of heavy oil reservoirs (Poon and Kisman, 1992; Claridge and Prats, 1995). It should be noted that Islam and Chakma (1990) experimentally measured the viscosity of foamy oil and presented that it is decreased with an increase in the gas volume fraction. Albartamani *et al*. (1999), however, argued that such results not only contradict the theoretical prediction of viscosity for a suspension, but also are not reliable since the details pertaining to the calculation of foamy oil viscosity and comparison between the calculated and predicted viscosity values are not presented.

The classical viscosity theory of a suspension mixture described that, when tiny solid particles or immiscible fluid droplets exist in a continuous liquid phase, the viscosity of the suspension mixture is supposed to be increased owing to the additional energy dissipation (Shen and Batycky, 1999). A viscosity model was proposed for an extremely dilute mixture involving small solid particles ($f_v < 0.05$) by Einstein in 1906 (Bora, 1998; Shen and Batycky, 1999),

$$\mu_s = \mu_l \left(1 + 2.5 f_v\right) \qquad [2\text{-}11]$$

where μ_l is viscosity of the continuous liquid phase; μ_s is the viscosity of the suspension mixture; f_v is the volume fraction of the dispersed phase. Following Einstein's work, Taylor (1932) developed a viscosity model for the liquids containing small droplets of another liquid in the suspensions.

$$\mu_s = 1 + 2.5\left(\frac{\mu_d + 0.4\mu_l}{\mu_d + \mu_o}\right) f_v \qquad [2\text{-}12]$$

where μ_d is the viscosity of the dispersed liquid droplet. Since then, numerous efforts have been made for accurately predicting viscosity of the suspension mixture with different liquids or high concentration suspensions as compared to the low concentration constraint (< 0.05) in Einstein's work (Pal *et al*., 1992). More specifically, for oil industry, Mitchell (1971) quantified the viscosity of foam as a piece-wise equation depending on the range of foam quality on the basis of traditional viscosity theory of suspension.

$$u_s = \begin{cases} \mu_l \left(1.0 + 3.6 f_m\right) & 0 < f_m \le 0.54 \\ \dfrac{\mu_l}{\left(1.0 + 3.6 f_m\right)} & 0.54 < f_m < 0.96 \end{cases} \qquad [2\text{-}13]$$

where f_m is the foam quality. Shen and Batycky (1999) proposed a specific viscosity model of foamy oil, which is derived from the modification of an early proposed viscosity of suspension by Roscoe (1952). Then, Kumar and Mahadevan (2012) developed a similar model based on the Einstein relationship. In addition to the aforementioned methods, several other types of viscosity models were also established (Romero *et al*., 2001; Chen *et al*., 2015). A summary for foamy oil viscosity models is tabulated in Table 2-1.

Meanwhile, a number of laboratory experiments have been conducted for the measurement of foamy oil viscosity, and found that there is no viscosity decline of the liquid phase when gas bubbles are dispersed in heavy oil. Bora (1998) experimentally examined the effects of temperature, pressure, bubble size, and shear rate on the viscosity of foamy oil. In general, it is found that the viscosity of foamy oil is close to or slightly higher than that of the live oil under the same conditions. Especially, viscosity of foamy oil increases when the conditions are beneficial to the increase of dispersed phase volume fraction. Goodarzi *et al*. (2007) claimed that the viscosities of liquid oil measured by CT and NMR techniques under the equilibrium and nonequilibrium conditions are similar. Also, Alshmakhy and Maini (2012) systematically measured and discussed the viscosities of foamy oil under different conditions, including flow rate, gas volume fraction, and even the type of viscometers used. Although the measured viscosities of foamy oil are greatly affected by the measurement methods, they are still close to that of the live oil in a certain range of gas volume fractions (<40%). Overall, based on the existing experimental and theoretical work, foamy oil viscosity seems to be similar or slightly

Table 2-1 Summary of foamy oil viscosity models

Model	Source
$\mu_{fo} = f_o \mu_o + f_{en} \mu_{en}$	Smith (1988)
$\mu_{fo} = \mu_o^{f_o} \mu_{en}^{f_{en}}$	Smith (1988) Islam and Chakma (1990)
$\mu_{fo} = \begin{cases} \mu_l \left(1.0 + 3.6 f_m\right) & 0 < f_m \le 0.54 \\ \dfrac{\mu_l}{\left(1.0 + 3.6 f_m\right)} & 0.54 < f_m < 0.96 \end{cases}$	Mitchell (1971)
$\mu_{fo} = \left(1 - \alpha f_{en}\right)^{-\beta_f}$	Shen and Batycky (1999)
$\mu_{fo} = \mu_0 \left(1 + m_a f_{en}\right)$	Kumar and Mahadevan (2012)
$\mu_{fo} = \begin{cases} 0.5\left(\mu_l^{x_{gm}} + \mu_g^{x_{om}}\right) + 0.25\left[\left(x_{om}\mu_l + x_{gm}\mu_g\right) + \mu_l^{x_{gm}} \mu_g^{x_{om}}\right] & p \le p_b \\ 0.55 x_{om}\left(p - p_b\right) + \mu_{ob} & p > p_b \end{cases}$	Romero *et al*. (2001)
$\mu_{fo} = \begin{cases} \mu_{oc} \exp\left[m_b \left(R_s - R_{so}\right)\right] & p \le P_{pb} \\ \mu_{oc} \exp\left[m_c \left(p - p_0\right)\right] & p > P_{pb} \end{cases}$	Chen *et al*. (2015)
$\mu_{fo} = \dfrac{\mu_o}{1 - \left(r_b / r_c\right)^4}$	Sheng (1997)

Note: α is the reciprocal of maximum volume fraction of the suspended phase; μ_0 is the viscosity of oil at zero flashed-gas fraction; μ_{ob} is the viscosity at bubblepoint pressure; μ_{oc} is the conventional oil viscosity; m_a, m_b, and m_c are constants; x_{gm} is mole fraction of gas phase in the equilibrium state; x_{om} is mole fraction of oil phase in the equilibrium state; P_{pb} is pseudo-bubblepoint pressure; R_s and R_{so} are the solution gas-oil ratio and gas-oil ratio, respectively; p_0 is initial reservoir pressure; r_b is the radius of a bubble; and r_c is radius of a capillary.

higher than that of live oil under the same conditions.

2.4.3 Density

Density of foamy oil is closely related to the reciprocal of formation volume factor that is one of the factors accounting for the anomalous primary recovery of heavy oil (Chen *et al*., 2015). Mastmann *et al*. (2001) experimentally measured the foamy oil density and found that, when pressure is higher than bubblepoint pressure, the density of foamy oil is exactly same as that of non-foamy oil since there, actually, is no gas bubble nucleating from the liquid phase, i.e., no foamy oil. Especially, it has been well-recognized that, when pressure declines to be lower than the bubblepoint pressure, density of conventional oils begins to increase owing to the gas released from liquid phase. In contrast, density of foamy oil decreases due to the entrapment of gas bubbles in the oleic phase as pressure decreases below the pseudo-bubblepoint pressure (Bennion *et al*., 2003).

Smith (1988) developed an empirical correlation of foamy oil density, ρ_{fo} as follows,

$$\rho_{fo} = \rho_{sat}\left(\frac{p}{p_{sat}}\right)^{\theta_l} \qquad [2\text{-}14]$$

where p_{sat} and ρ_{sat} are the saturation pressure and saturation density, respectively; θ_l is in the range of 0.25 to 0.40 for a Lloydminster heavy oil. The determination of parameter θ_l requires a great number of the measured data points of foamy oil density, which constrains the extensive application of such a correlation of foamy oil.

Kumar and Mahadevan (2012) proposed a general formulation that the density of foamy oil, ρ_{fo}, can be calculated by use of a simple mixing rule,

$$\rho_{fo} = \rho_o \left(1 - f_{en}\right) + \rho_g f_{en} \quad [2\text{-}15a]$$

$$f_{en} = \frac{\alpha_g \phi_g}{1 - \phi_g \left(1 - \alpha_g\right)} \quad [2\text{-}15b]$$

where ρ_g is gas density; ρ_o is density of live oil and given by Standing correlation; α_g is fraction of the flashed gas that is entrained in oleic phase; ϕ_g is the ratio of the volume of gas flashed to the volume of the total solution gas. Chen *et al*. (2015) also followed the aforementioned model to match the Mastmann's experimental results but with a different expression of dispersed gas density. Although the density is an important parameter for foamy oil, there are still no many efforts made on the determination of foamy oil density available for pragmatic usage.

2.5 Phase Behaviour Models of Foamy Oil

Phase behaviour of foamy oil is essentially featured by nonequilibrium processes where time is a critical parameter to affect the heavy oil properties. A complex interplay of gas bubble formation comprising nucleation, growth, and coalescence is usually involved.

2.5.1 Pseudo-bubblepoint model

Kraus *et al*. (1993) introduced a new concept, i.e., pseudo-bubblepoint pressure, to quantify the physical behaviour of foamy oil. All the evolved gas is assumed to be entrained in the liquid phase in this model when the pressure is higher than the pseudo-bubblepoint pressure but lower than the thermodynamic bubblepoint pressure. Once the

pressure is lower than the pseudo-bubblepoint pressure, a fraction of the evolved gas is released from the oleic phase to be free gas. Such a fraction is linearly proportional to the ratio of difference between system pressure and a reference pressure (lower than P_{pb}, usually 101.325 kPa) to the one between pseudo-bubblepoint pressure and the reference pressure.

Importantly, the pseudo-bubblepoint pressure is treated as an adjustable parameter for quantifying the fluid properties in the pseudo-bubblepoint model (Kraus *et al*., 1993). Dead oil, dissolved gas, and entrained gas are regarded as the three components constituting the foamy oil in their pseudo-bubblepoint model. Accordingly, a methodology of calculating the properties of foamy oil mainly including molar volume and isothermal compressibility has been developed.

The pseudo-bubblepoint model, on one hand, can be used to effectively adjust conventional black oil fluid properties typically measured in PVT tests to account for the enhanced compressibility effect found during the field production of foamy oil (Kraus *et al*., 1993). On the other hand, it is convenient to be coupled into the existing simulators and, actually, has been successfully used in several simulation tasks pertaining to foamy oil production (Mastmann *et al*., 2001; Chen *et al*., 2015). However, time is not included in the model, resulting in that the model fails to capture the essentially time-dependent features of foamy oil.

2.5.2 Dynamic model

Sheng (1997) proposed a dynamic model aiming to accurately predict the time-dependent behaviour of foamy oil. Three types of mathematical equations are employed to describe the varying amount of evolved gas from the liquid phase and entrained gas in heavy oil, respectively.

Model 1:

$$\alpha_{ev} = \left(\frac{t_{ev}^{i,j}}{t_{eq}} \right)^{b_1} \qquad [2\text{-}16a]$$

$$\alpha_{dg} = \exp\left(\lambda_{dg} t_{dg} \right) \qquad [2\text{-}16b]$$

where α_{ev} is the ratio of cumulative amount of gas evolved to gas flashed at thermodynamic equilibrium; $t_{ev}^{i,j}$ is the bubble age or the effective time which is from the time of this step change in pressure to the time of interest; t_{dg} is the age of the dispersed gas; α_{dg} is the ratio of amount of gas dispersed at t_{dg} to the amount of gas dispersed at $t_{dg} = 0$; and λ_{dg} is the decay coefficient of dispersed gas.

Model 2:

$$\Delta n_{sg \to ev}^{n+1} = \Delta n_s \left(\frac{\Delta t/2}{t_{eq}} \right)^{b_2} \qquad [2\text{-}17a]$$

$$n_{en}^{n+1} = n_{en}^{n} \exp\left(-\lambda_{dg} \Delta t \right) + \Delta n_{sg \to ev}^{n+1} \exp\left(-\lambda_{dg} \Delta t/2 \right) \qquad [2\text{-}17b]$$

where $\Delta n_{sg \to ev}^{n+1}$ is the mass of gas evolved from solution from time t^n to t^{n+1}; Δn_s is the supersaturation expressed in moles of supersaturated solution gas in the oil phase at time

t^n referred to the equilibrium state at t^{n+1}; Δt is time step size; and n_{en}^{n+1} is the entrained gas at t^{n+1}.

Model 3:

$$\Delta n_{sg\to ev}^{n+1} = \Delta n_s \left[1 - \exp\left(-\lambda_s \Delta t/2\right)\right] \qquad [2\text{-}18]$$

where λ_s is the rate coefficient for the decay of supersaturation. The other parameters are same as those of Model 2.

It can be found that dynamic models attempt to formulate the foamy oil phase behaviour by quantifying the entire history of gas bubble formation, i.e., nucleation, growth, and coalescence. Also, once the amount of the evolved gas and entrained gas are determined, the dynamic model postulates that foamy oil comprises three components, which is same as those of pseudo-bubblepoint model, in order to calculate the properties of foamy oil. This model has been successfully applied for matching the laboratory gas-solution experiments (Sheng *et al*., 1999a), though the complicated adjustable parameters cannot be determined independently.

2.5.3 Population balance model

Arora and Kovscek (2003) developed a mechanistic modeling framework stemmed from the bubble population balance framework to not only address the issue of gas bubble microstructure, but also elucidate the mechanisms of solution-gas drive performance in heavy oil. Such a mechanistic model integrates the conservation equation, which is relevant to the volume of stationary and flowing gas bubbles, and the bubble rate

equations, which take pore-level dynamic bubble nucleation and growth mechanisms into account. It is noted that either the IN model or the PN model can be incorporated into this framework. Then, the gas bubble growth model developed by Firoozabadi and Kashchiev (1996) is applied to characterize the gas bubble growth rate in the framework, while the properties of foamy oil are calculated with the procedure resembling that of the pseudo-bubblepoint model. The proposed mechanistic model has been effectively used for history matching the experimental measurements during pressure depletion processes. It is found that the mechanistic model has the capability of capturing the unique characteristics of foamy oil behaviour such as pseudo-bubblepoint pressure and the rebound in pressure occurring after the pseudo-bubblepoint pressure. However, the effects of gas mobility and bubble coalescence have not been examined.

2.5.4 Nonequilibrium reaction model

Coombe and Maini (1994) firstly proposed the so-called nonequilibrium reaction model based on the primary principle that includes two dynamic processes of gas bubble formation, i.e., (1) the dissolved gas changing into the gas dispersed in the form of microbubbles and (2) the dispersed gas changing into free gas. These two dynamic processes are modeled as chemical reactions with specified stoichiometry and reaction-rate constants (Maini, 2001). Arrhenius equation, in particular, is utilized to quantify the related dynamic gas bubble formation (Luigi *et al*., 1998).

On the basis of such a mathematical framework, a similar kinetic model was developed by Uddin (2005) as well. The entire dynamic gas formation is divided into four separated reactions as follows (Uddin, 2005; Istchenko and Gates, 2014),

Reaction 1: $g_d \rightarrow b_d$

Reaction 2: $g_d + b_d \rightarrow 2b_d$

Reaction 3: $b_d \rightarrow b_c$

Reaction 4: $g_d + b_d \rightarrow g_d + b_c$

where g_d and b_d are the dissolved gas and entrained gas in oleic phase; and b_c is the connected bubble component in gas phase. Correspondingly, four novel relationships instead of Arrhenius equation are suggested to formulate the aforementioned four reactions.

$$r_a^1 = N_1\left(c_{gd} - c'_{gd}\right) \quad [2\text{-}19a]$$

$$r_a^2 = N_2\left(c_{gd} - c'_{gd}\right)^2 c_{bd} \quad [2\text{-}19b]$$

$$r_d^1 = G_1 c_{bd} \quad [2\text{-}19c]$$

$$r_d^2 = G_1\left(c_{gd} - c'_{gd}\right)c_{bd} \quad [2\text{-}19d]$$

where c_{gd} and c_{bd} are defined as concentrations of the dissolved and dispersed gas, respectively; c'_{gd} is the dissolved gas concentration under equilibrium conditions; N_1 and N_2 are the nucleation parameters, respectively; r_a^1 and r_a^2 are the mass transfer rates per unit volume per unit time of dissolved gas into dispersed bubbles; r_d^1 and r_d^2 are the mass transfer rates of dispersed bubbles into connected bubbles; and G_1 and G_2 are the gas bubble growth parameters, respectively.

Nonequilibrium reaction models have been successfully employed for numerically simulating the foamy oil production performance by incorporating them into the existing commercial simulators (Luigi *et al*., 1998; Uddin, 2005). Although the distinct time-dependent characteristics in dispersion properties can be formulated by nonequilibrium reaction models, it is still impossible to evaluate the impact of time and position-dependent capillary number (Maini, 2001).

2.6 Summary

Foamy oil is a complicated nonequilibrium liquid system, characterized by the time-dependent phase behaviour and properties. Overall, it has to admit that the theoretical and experimental efforts on foamy oil are still not successful enough to satisfy the requirements of heavy oil recovery due mainly to the extremely complicated physical behaviour involved during the formation and flow of foamy oil. Physically, the unique behaviour of foamy oil is strongly related to the existence of the dispersed gas in oleic phase. It can be concluded that many aspects of physical phenomena associated with gas bubble formation (nucleation, growth, and coalescence) are still poorly understood based on the aforementioned discussions in this chapter, though molecular diffusion has been apparently considered as the main mechanism of gas bubble growth. On the other hand, the inherent characteristics of heavy oil, such as high viscosity and asphaltene content, also impose some distinct impacts on dynamic processes of the dispersed gas formation, such as the slow coalescence process and multi-component gas diffusion. Even for the corresponding mass transfer processes, diffusion isolated from natural convection has not been made available, not to mention to take preferential diffusion into account. In a word,

intensive and extensive efforts are still needed for exploration of the phase behaviour and mass transfer of foamy oil under equilibrium and nonequilibrium conditions in order to achieve more accurate and reliable prediction for recovering heavy oil from hydrocarbon reservoirs.

CHAPTER 3 DETERMINATION OF INDIVIDUAL DIFFUSION COEFFICIENTS OF ALKANE SOLVENT(S)–CO_2–HEAVY OIL SYSTEMS WITH CONSIDERATION OF NATURAL CONVECTION INDUCED BY SWELLING EFFECT

3.1 Introduction

It is well-known that diffusion of the dissolved gas from liquid phase to gas phase plays a key role in the gas bubble growth process except for its very beginning stage (Sheng *et al*., 1999c). Also, diffusion has been found to be an important mechanism accounting for mass transfer rate in solvent(s)-assisted recovery techniques (Luo and Kantzas, 2008). Compared with either the heat-alone or solvent-alone approach, hybrid thermal-solvent processes can take advantages of both solvent and heat, during which energy efficiency has been found to be significantly increased with the injection of solvent(s), while the cost of heat is greatly reduced (Gupta and Gittins, 2006; Frauenfeld *et al*., 2009). Not only can the heat carried by a hot CO_2/solvent remarkably decrease the viscosity of oleic phase (Zheng *et al*., 2016b), but also its mass transfer in heavy oil can be effectively accelerated due to the quick heat transfer with a larger swelling factor (Ivory et al., 2010; Li *et al*., 2011). As such, it is of practical and fundamental importance to accurately quantify the mass transfer rate for each individual component of a gas mixture during a CO_2/solvent(s)-assisted thermal recovery process.

In this chapter, by coupling heat and mass transfer as well as characterizing heavy oil as multiple pseudocomponents, a new and pragmatic technique has been developed to determine the individual diffusion coefficient of each component in alkane solvent(s)–CO_2–heavy oil systems with consideration of natural convection induced by oil swelling

effect (Shi *et al*., 2017). Peng-Robinson equation of state (PR EOS), one dimensional (1D) heat transfer equation, and 1D convection-diffusion equation are integrated to quantify both mass and heat transfer. The diffusion coefficient considering the effect of convection between each component of a gas mixture and liquid phase can be respectively obtained as a function of viscosity once either the deviation between the experimentally measured mole fractions of CO_2 and/or solvents and the calculated ones or the deviation between the experimentally measured dynamic swelling factors and theoretically calculated ones from the newly developed mathematical model is minimized. Furthermore, the effects of heat and natural convection induced by swelling effect on mass transfer rate are evaluated and discussed.

3.2 Mathematical Formulations

The PR EOS, heat transfer equation, and convection-diffusion equation constitute the mathematical matrix to quantify mass and heat transfer processes during the diffusion tests with natural convection based on the following assumptions:

(1) The PVT cell is a closed system;

(2) Dirichlet quasi-equilibrium is achieved at the gas-liquid interface (Tharanivasan *et al*., 2004; Li, 2013; Zheng and Yang, 2016; 2017);

(3) Heat transfer only starts from the interface of gas and liquid and the bottom of PVT cell (Sun *et al*., 2014);

(4) Convective heat transfer is neglected (Irani and Ghannadi, 2013);

(5) Mass transfer only occurs from the gas phase to liquid phase (Sun *et al*., 2014; Li and Yang, 2016; Zheng *et al*., 2016a);

(6) Cross-term diffusion coefficient between different gas components is not taken into account, considering that it is much smaller than main term diffusion coefficient (Li and Yang, 2016);

(7) Gas-phase temperature is constant and equal to the temperature of the PVT cell; and

(8) Thermophoresis is neglected (Sun *et al*., 2014; Zheng *et al*., 2016b; Zheng and Yang, 2016; 2017).

3.2.1 PR EOS

Since PR EOS has been extensively applied for quantifying phase behaviour in petroleum and chemical industries due to its robustness and accuracy, it is chosen in this study to determine solvent concentration at the solvent(s)–heavy oil interface. The PR EOS can be expressed as follows (Peng and Robinson, 1976),

$$P=\frac{RT}{V_M-b}-\frac{a}{V_M\left(V_M+b\right)+b\left(V_M-b\right)} \quad [3\text{-}1]$$

$$a = a_c\alpha\left(T_r,\omega\right) \quad [3\text{-}2a]$$

$$a_c=\frac{0.457235R^2T_c^2}{P_c} \quad [3\text{-}2b]$$

$$b=\frac{0.0777969RT_c}{P_c} \quad [3\text{-}2c]$$

where $\alpha\left(T,\omega\right)$ is alpha function; P is pressure; T is temperature; R is universal gas constant; P_c is critical pressure; T_c is critical temperature; T_r is reduced temperature; V_M is molar volume, and ω is acentric factor.

A recently proposed alpha function instead of the traditional one is used in this study to more accurately predict the phase behaviour of both pure substances (Li and Yang, 2011) and alkane solvent(s)–CO_2–heavy oil systems by treating heavy oil as one pseudocomponent (Li and Yang, 2013; Li *et al*. 2013a; Sun *et al*., 2014) and multiple pseudocomponents (Li *et al*., 2013b; 2014; Zheng and Yang, 2016; Zheng *et al*., 2016a). Such alpha function can be written as follows (Li and Yang, 2011),

$$\alpha = \exp\left\{\left(0.13280 - 0.05052\omega + 0.25948\omega^2\right)\left(1 - T_r\right) + 0.81769\ln\left[1 + \left(0.31355 + 1.86745\omega - 0.52601\omega^2\right)\left(1 - \sqrt{T_r}\right)\right]^2\right\} \quad [3\text{-}3]$$

The heavy oil is split into four pseudocomponents in order to not only accurately calculate the properties of heavy oil (AARD of saturation pressure < 4.8%) (Li *et al.*, 2013b), but also balance the computational time. Meanwhile, it is found that the binary interaction parameter (BIP) correlation proposed by Chueh (1967) for treating heavy oil as multi-pseudocomponents performs superior than others (Li *et al*., 2013b; Zheng and Yang, 2016; Zheng *et al*., 2016a), which is expressed as follows,

$$\delta_{ij} = 1 - \left[\frac{2\sqrt{V_{ci}^{1/3} V_{cj}^{1/3}}}{V_{ci}^{1/3} + V_{cj}^{1/3}}\right]^{\beta} \quad [3\text{-}4]$$

where V_c is the critical volume of each component; δ_{ij} is the BIP between the i^{th} and j^{th} component. The recommended value of exponent β is 1.5 according to the previous work (Li *et al*., 2013b). The detailed physical and critical properties of each pseudocomponent can be found in the work of Li *et al*. (2013b).

The EOS-calculated volume is corrected with a volume-translation approach proposed by Péneloux (1982) because the cubic equations of state cannot be used to accurately predict the molar volume for liquids (Milind *et al*., 1993). Also, the Péneloux's volume translation is found to provide the highest accuracy in terms of the swelling factor prediction for the alkane solvent(s)–CO_2–Lloydminster heavy oil systems (Li *et al.*, 2013b; Zheng and Yang, 2016; Zheng *et al*., 2016a).

$$\bar{V} = V - \sum_{i=1}^{n} x_i V_i^p \qquad [3\text{-}5a]$$

where $\bar{V}$ is the corrected molar volume; x_i is composition of the i^{th} component in liquid phase; V_i^p is the corrected volume for the i^{th} component (Péneloux *et al*., 1982),

$$V^p = 0.40768\left(\frac{RT_c}{P_c}\right)\left(0.29441 - z_{RA}\right) \qquad [3\text{-}5b]$$

z_{RA} is Rackett parameter.

3.2.2 Convection-diffusion equation

The 1D convection-diffusion equation is expressed as,

$$\frac{\partial c_i}{\partial t} = \frac{\partial}{\partial x}\left(D_i \frac{\partial c_i}{\partial x}\right) - u\frac{\partial c_i}{\partial x} \qquad [3\text{-}6]$$

where c_i is the concentration of the i^{th} solvent or CO_2 component in liquid phase; D_i is diffusion coefficient of the i^{th} solvent or CO_2 component; and u is velocity of natural convection in liquid phase.

In general, the following three conditions shall be satisfied so as to treat diffusion coefficient as a constant parameter (Guerrero-Aconcha *et al*., 2008): (1) diameter and shape of the involved molecules are similar; (2) the inter-molecular forces can be negligible; and (3) there exists a non-reacting environment. Since alkane solvent(s)–CO_2–heavy oil systems in this study only satisfy the third condition, diffusion coefficient is assumed to be viscosity-dependent as given by Hayduk and Cheng (1976),

$$D = A\mu^B \tag{3-7}$$

where A and B are constants, depending on each diffusing substance, and μ is liquid phase viscosity.

Yarranton *et al*. (2013) developed a Walther-type correlation with double logarithm for viscosity based on western Canadian oils to predict the viscosities of dead and live crude oil ranging from 0.5 to 500000 mPa·s with an accuracy of within 30%. Compared with the corresponding-states (CS) model and Lohrenz-Bray-Clark (LBC) model (Yarranton *et al*., 2013; Pedersen *et al*., 2014), such Walther-type correlation has been found to provide more accurate prediction for viscosity of the solvent(s)/CO_2–diluted heavy oil in this study,

$$\mu = \mu^0(T)\left[1+\alpha_l\left(1-0.0033T\right)\Delta P\right] \tag{3-8}$$

$$\log\left[\log\left(\mu^0(T)+1\right)\right] = \sum w_i\left(A_{li}+B_{li}\log T\right) \tag{3-9a}$$

$$\ln\left[\ln\left(\alpha_l+1\right)\right] = \sum w_i \ln\left[\ln\left(\alpha_i+1\right)\right] \tag{3-9b}$$

where $\mu^0(T)$ is the dynamic viscosity of liquid mixture at temperature T and atmospheric pressure; α_l and α_i are the viscosibility parameters of liquid mixture and

the i^{th} component in the mixture, respectively; ΔP is the pressure deviation from atmospheric pressure; w_i is the mass fraction of the i^{th} component; and A_{li} and B_{li} are constants unique to the i^{th} component of liquid mixture.

Swelling effect of the diluted heavy oil can result in the expansion of liquid volume for the alkane solvent(s)–CO_2–heavy oil systems in diffusion tests. Consequently, the increased volume of heavy oil induces the fluids flow from the bottom of liquid phase to the gas-liquid interface. The direction of fluids flow is evidently opposite to the direction of solvent(s)/CO_2 transfer resulted from concentration difference. Given a finite volume element in liquid phase from x to $x+\Delta x$ (see Figure 3-1), the increased volume during time interval Δt can be express as,

$$\Delta V_x^{t+\Delta t} = A_c \Delta x \left(\frac{s_x^{t+\Delta t} + s_{x+\Delta x}^{t+\Delta t}}{2} - \frac{s_x^t + s_{x+\Delta x}^t}{2} \right) \quad [3\text{-}10a]$$

Therefore, the total incremental volume of liquid phase can be calculated by the following equation,

$$\Delta V = \int_0^{l_{t+\Delta t}} A_c \left[s^{t+\Delta t}(x) - s^t(x) \right] dx \quad [3\text{-}10b]$$

where ΔV is total increased volume; A_c is cross-sectional area of the PVT cell; s is the dynamic swelling factor; and $l_{t+\Delta t}$ is the height of liquid phase at time $t+\Delta t$. Therefore, the velocity at location x can be written as,

$$u_x^{t+\Delta t} = \frac{\Delta V}{\Delta t A_c} = \frac{1}{\Delta t} \int_0^x \left[s^{t+\Delta t}(x) - s^t(x) \right] dx \quad [3\text{-}11]$$

As for the dynamic swelling factor of an alkane solvent(s)–CO_2–heavy oil mixture, it can be determined by the following equation (Teja and Sandler, 1980),

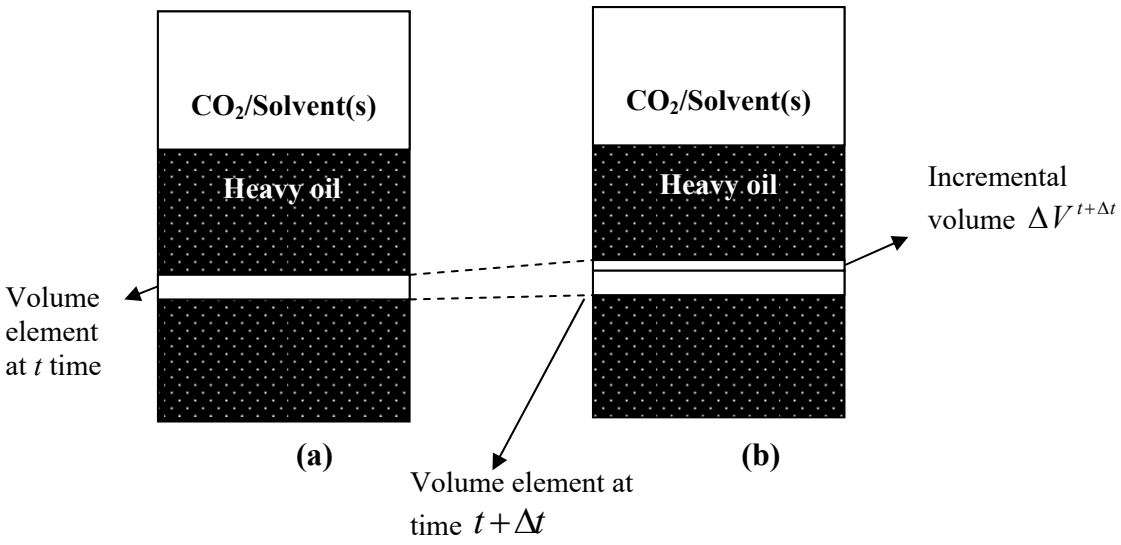

Figure 3-1 Schematic diagram of a finite volume element at **(a)** time t and **(b)** time $t+\Delta t$

$$s_x^t = \frac{V_{Mx}^t}{V_{Mx}^0} \frac{1}{1 - \sum_{j=1}^{n_g} x_{gi}^t} \quad [3\text{-}12]$$

where V_{Mx}^0 and V_{Mx}^t are molar volume of heavy oil at initial stage and solvent-diluted heavy oil and time *t*, respectively, x_{gi} is mole fraction of the i^{th} gas component in liquid phase, i.e., solvents/CO_2 mole fraction in the liquid phase in this study, and n_g is the number of gas components.

Compared to the CO_2-light/medium oil systems where density-driven natural convection may occur (Emera and Sarma, 2008), such a phenomenon may not take place for alkane solvent(s)–CO_2–heavy oil systems. This is ascribed to the fact that the density of alkane solvent(s)–CO_2–heavy oil systems is less than that of dead heavy oil at the same conditions based on the PR EOS calculations.

3.2.3 Heat transfer

Since heat transfer is assumed to only conduct from the gas-liquid interface and the bottom of the PVT cell to liquid phase and the convective heat transfer is neglected, the 1D heat equation in bulk liquid is employed to describe the heat transfer (Sun *et al*., 2014).

$$\rho_l c_{pl} \frac{\partial T_l}{\partial t} = \frac{\partial}{\partial x}\left(\lambda_l \frac{\partial T_l}{\partial x} \right) \quad [3\text{-}13]$$

where T_l , c_{pl} , ρ_l and λ_l are temperature, heat capacity, density, and thermal conductivity of the liquid phase, respectively.

3.2.4 Initial and boundary conditions

The initial conditions are expressed by,

$$\begin{aligned} &T_l = T_{li}, && 0 < x < l_0, && t = 0 \\ &c = 0, && 0 < x < l_0, && t = 0 \end{aligned} \qquad \text{[3-14a]}$$

where T_{li} is initial temperature of heavy oil and l_0 is initial height of liquid phase.

Based on the aforementioned assumptions and the PVT experiments, the Dirichlet quasi-equilibrium boundary condition at the gas-liquid interface is used, i.e.,

$$\begin{aligned} &T_l = T_h, && x = 0,\ l(t) && t > 0 \\ &c = c_{sat}\left[T_l(t), P(t)\right], && x = l(t), && t > 0 \\ &\frac{\partial c}{\partial x} = 0, && x = 0, && t > 0 \end{aligned} \qquad \text{[3-14b]}$$

where T_h is temperature of the PVT chamber, indicating a high temperature of solvent-assisted heat process; c_{sat} is solvent concentration at the gas-liquid interface at time *t*; and $l(t)$ is the height of the heated and diluted heavy oil at time *t*.

3.2.5 Numerical solution

Due to variable properties of alkane solvent(s)–CO_2–heavy oil mixture and velocity resulted from natural convection during the diffusion tests, this coupled equation matrix is non-linear. In this way, numerical methods are employed to solve the matrix of equations. To ensure the numerical convergence, an implicit finite difference technique, i.e., the Crank-Nicolson method, is used to discretize the proposed model. Diffusion coefficient is determined once the deviation between the experimentally measured and

theoretically calculated mole fractions or the deviation between the measured dynamic swelling factors and the calculated ones is minimized by using the particle swarm optimization (PSO) algorithm. Two objective functions are respectively defined as follows,

$$O(m)=\sqrt{\frac{1}{N_g}\sum_{i=1}^{N_g}\left(x_i^{cal}-x_i^{m}\right)^2} \qquad [3\text{-}15a]$$

or

$$O(s)=\sqrt{\frac{1}{N_m}\sum_{i=1}^{N_m}\left(\frac{s_i^{cal}-s_i^{m}}{s_i^{m}}\right)^2} \qquad [3\text{-}15b]$$

where x_i^{cal} and x_i^{m} is the calculated and measured mole fraction of the i^{th} component in liquid phase at the end of the diffusion test; N_g is the number of gas-phase component; s_i^{cal} and s_i^{m} is the calculated and measured dynamic swelling factor of i^{th} data point; N_m is the number measured from the experiment. Equations [3-15a] and [3-15b] are aimed to minimize the deviation between the calculated and measured mole fraction of CO_2 and solvents as well as the calculated and measured dynamic swelling factors, respectively. Once the prespecified accuracy has been satisfied, the calculated mole fractions or swelling factors can be considered as an accurate match of the measured value, and thus the corresponding diffusion coefficient can be treated as the actual one. Otherwise, the iterations with the new *A* and *B* in Equation [3-7] will be conducted until the objective function meets the termination requirements. The corresponding flowchart is depicted in Figure 3-2. It shall be noted that Equation [3-15b] is used for a non-intrusive system, i.e., there is no need to collect gas samples at the beginning and the end of the diffusion tests

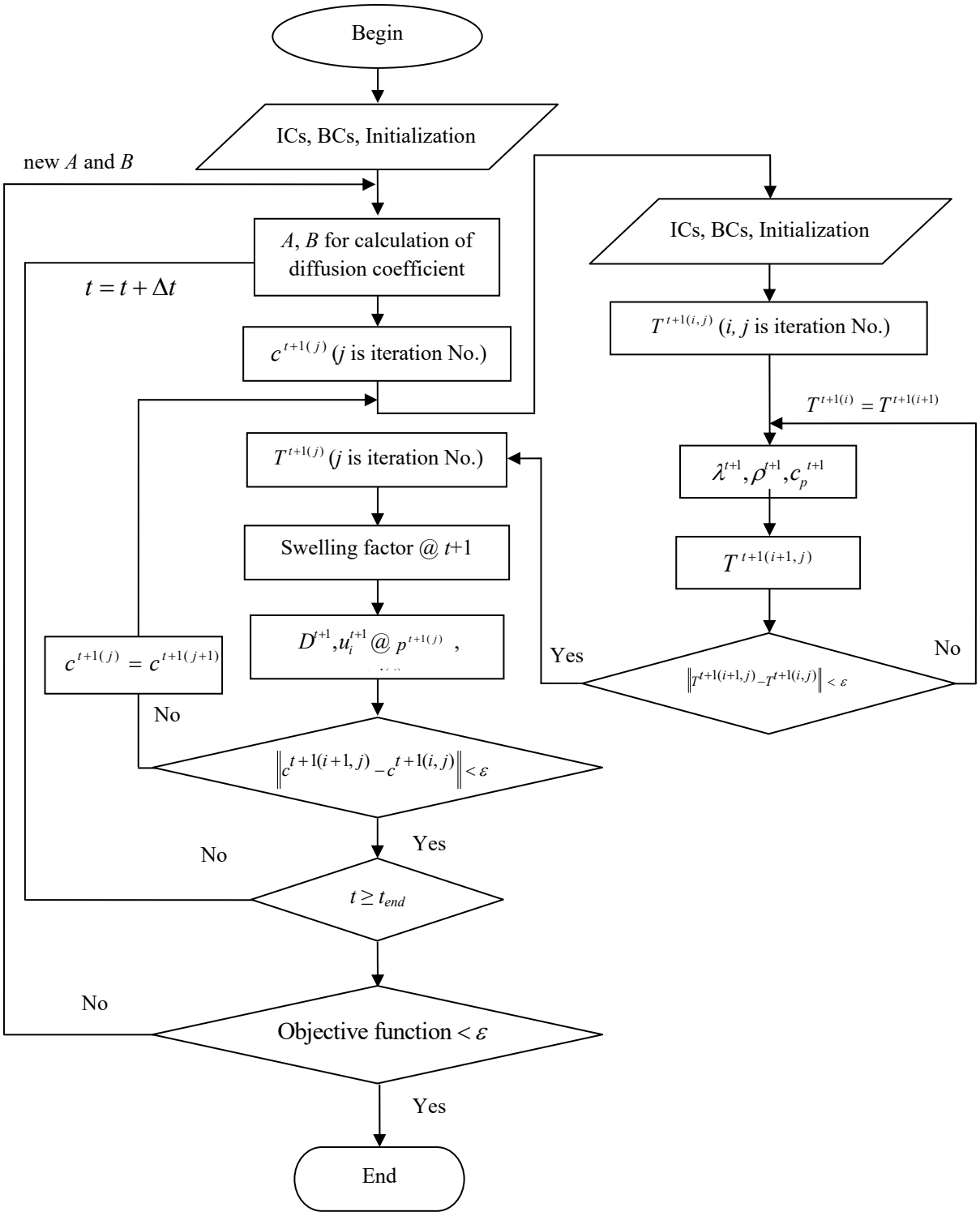

Figure 3-2 Flowchart of numerically solving the equation matrix

for Gas chromatography (GC) analysis, but accurate diffusion coefficients can still be obtained.

3.2.6 Model validation

Analytical solutions of both convection-diffusion and heat transfer equation are used to validate the numerical solutions of the equation matrix, respectively. Based on the literature, the analytical solution of 1D convection-diffusion equation can be expressed by Kumar *et al*. (2009),

$$
\begin{aligned}
&c = c_o A(x,t) \\
&A(x,t) = \frac{1}{2} erfc\left(\frac{x-ut}{2\sqrt{D_i t}}\right) + \frac{1}{2}\exp\left(\frac{ux}{D_i}\right) erfc\left(\frac{x+ut}{2\sqrt{D_i t}}\right) \\
&\quad + \frac{1}{2}\left[2 + \frac{u\left(2l(t)-x\right)}{D_i} + \frac{u^2 t}{D_i}\right] \times \exp\left(\frac{ul(t)}{D_i}\right) erfc\left[\frac{\left(2l(t)-x\right)+ut}{2\sqrt{D_i t}}\right] \\
&\quad - \left(\frac{u^2 t}{\pi D_i}\right)^{1/2} \exp\left[\frac{ul(t)}{D_i} - \frac{\left(2l(t)-x+ut\right)^2}{4D_i t}\right]
\end{aligned}
\qquad [3\text{-}16]
$$

The 1D heat transfer equation without convection term can be solved as follows,

$$
T_l(x,t) = T_0 + \left(T_{li} - T_0\right)x + \sum_{h=0}^{\infty} B_h \sin\frac{h\pi x}{l} e^{-h^2\pi^2\varphi^2 t/l^2} \qquad [3\text{-}17]
$$

Where

$$
B_h = 2\int_0^l \left[f(x) - T_0 - \left(T_{li} - T_0\right)x\right] \sin\frac{h\pi x}{l} dx \qquad [3\text{-}18]
$$

As shown in Figure 3-3, there exists an excellent match between the analytical and numerical solution of the convection-diffusion equation and heat transfer equation, respectively.

As shown in Table 3-1, there is an excellent agreement between the experimentally measured CH_4 mole fraction in liquid phase (Riazi, 1996) and the theoretical one with Equation [3-15a]. As such, the diffusion coefficient of CH_4 without convection is calculated to be 1.50×10^{-8} m^2/s, which is basically same as the reported value (1.51×10^{-8} m^2/s: Riazi, 1996). Also, when the natural convection is considered, the calculated diffusion coefficient is increased to be 2.71×10^{-8} m^2/s.

In the pressure decay experiment of CH_4 and *n*-C_5H_{12} mixture, the convection induced by density does not occur in the liquid phase due to the negative density gradient in vertical direction. However, volumetric increase of the liquid phase due to the increased dissolution of CH_4 generates a natural convection from the bottom of liquid phase to the gas-liquid interface. Physically, the direction of natural convection resulted from the swelling effect is opposite to that of mass transfer during the pressure decay tests. This phenomenon, therefore, slows down the rate of mass transfer caused by diffusion between CH_4 and *n*-C_5H_{12} system. As such, the diffusion coefficient calculated by using the conventional methods where molecular diffusion is offset by natural convection to some extent due to the vague combination, shall be lower than the one calculated by using the newly proposed technique in which the effect of natural convection on mass transfer is isolated from the molecular diffusion.

Table 3-1 The measured and calculated mole fractions of CO_2/solvent(s) at the end of experiments

Mixture system	Concentration mol%			Measured concentration source
	Gas	Measured	Calculated	
CH_4–*n*-C_5H_{12} system	CH_4	33.00	32.99	Riazi (1996)
CO_2–heavy oil system	CO_2	28.92	28.93	Li and Yang (2016)
C_3H_8–CO_2–heavy oil system	CO_2	22.92	22.92	
	C_3H_8	13.01	13.01	
n-C_4H_{10}–CO_2–heavy oil system	CO_2	4.72	4.72	
	C_4H_{10}	4.55	4.55	
n-C_4H_{10}–CO_2–heavy oil system	CO_2	91.76	94.88*	Zheng and Yang (2016)
	C_4H_{10}	8.24	5.12*	
C_3H_8–*n*-C_4H_{10}–CO_2–heavy oil system	CO_2	91.22	89.17*	
	C_3H_8	7.22	8.75*	
	C_4H_{10}	1.56	2.08*	

Note: * The mole fractions are obtained with the matching dynamic swelling factors

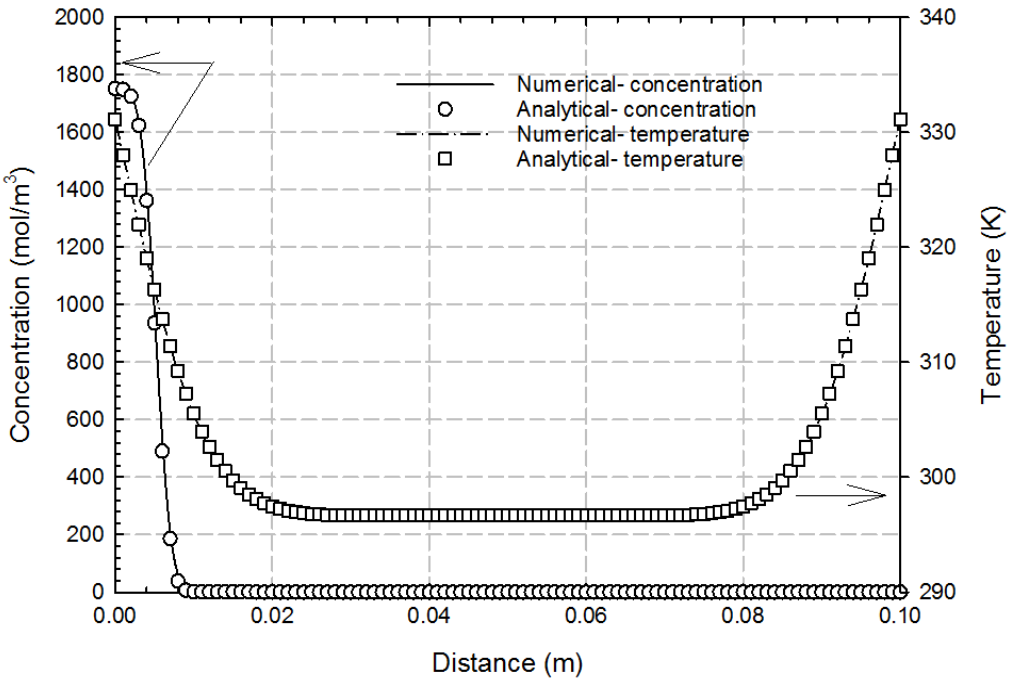

Figure 3-3 Comparison of concentration profiles of numerical and analytical solutions for the convection-diffusion equation at u=0.0001 m/s and t=49 s

3.3 Results and Discussion

The individual diffusion coefficients of CO_2 and solvents are firstly determined and discussed with the newly proposed technique on the basis of two types of diffusion tests, which were conducted under the conditions of (1) a decaying pressure and constant temperature and (2) an elevated temperature and constant pressure, respectively, in this study. Furthermore, three diffusion tests of CO_2–heavy oil system conducted with different system temperatures are utilized to examine the effect of heat and natural convection on mass transfer processes.

3.3.1 Individual diffusion coefficient

1) Decaying pressure and constant temperature

Individual diffusion coefficients have been determined for three sets of pressure-decay experiments under a constant temperature (Li, 2013; Li and Yang, 2016). The measured viscosities of heavy oil at atmospheric pressure are first regressed with Equation [3-8] (see Figure 3-4) so as to obtain the values of A_l, B_l of the heavy oil to be 9.4669 and 3.5861, respectively. The recommended values of A_l, B_l for pure CO_2, C_3H_8 and C_4H_{10} in Yarranton's correlations (2013) are utilized in this study. Table 3-1 shows that there exists a good agreement between the measured and calculated mole fractions for the CO_2–heavy oil, CO_2–C_3H_8–heavy oil, and CO_2–*n*-C_4H_{10}–heavy oil systems, respectively. Meanwhile, Figure 3-5a shows the matching results of dynamic swelling factors for three CO_2/solvent(s)–heavy oil systems with objective function [3-15a]. The dynamic swelling factors at the end of the experiments are respectively calculated to be 1.039, 1.066, and 1.015 for CO_2–heavy oil, CO_2–C_3H_8–heavy oil, and CO_2–*n*-C_4H_{10}–heavy oil systems,

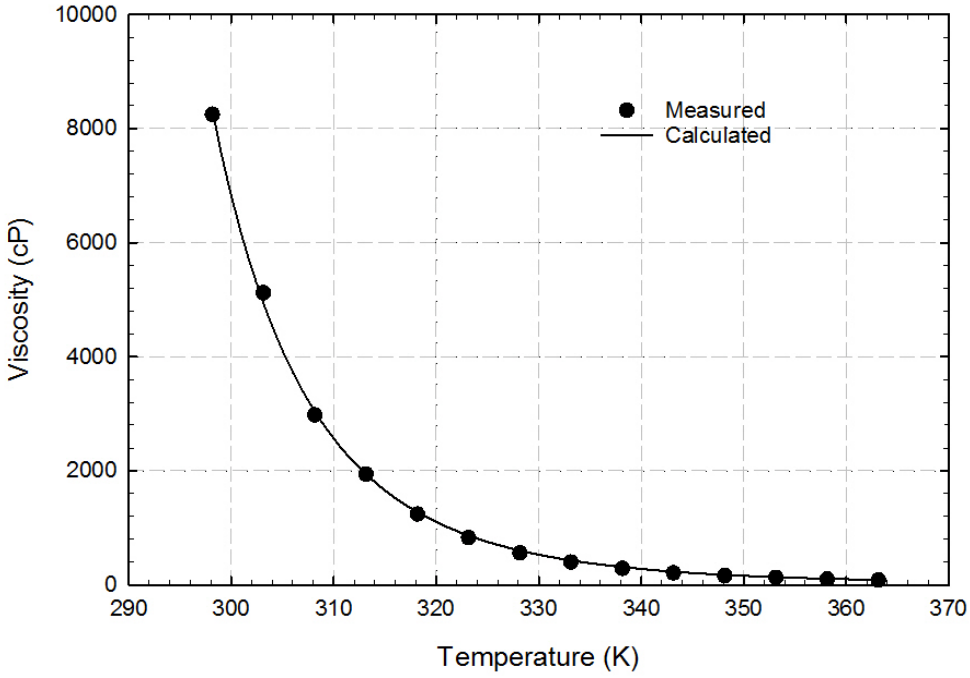

Figure 3-4 Measured and calculated viscosity of heavy oil

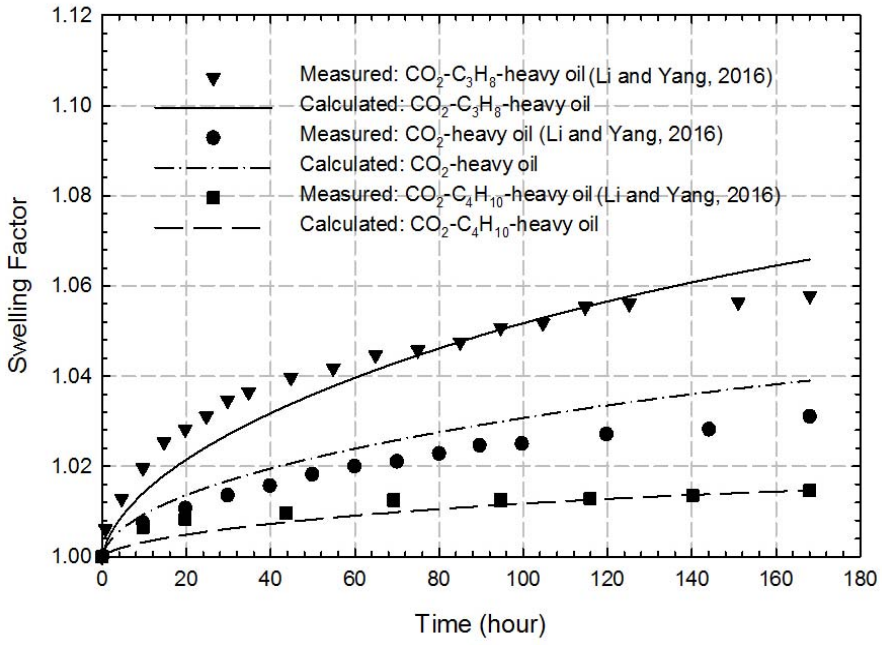

(a)

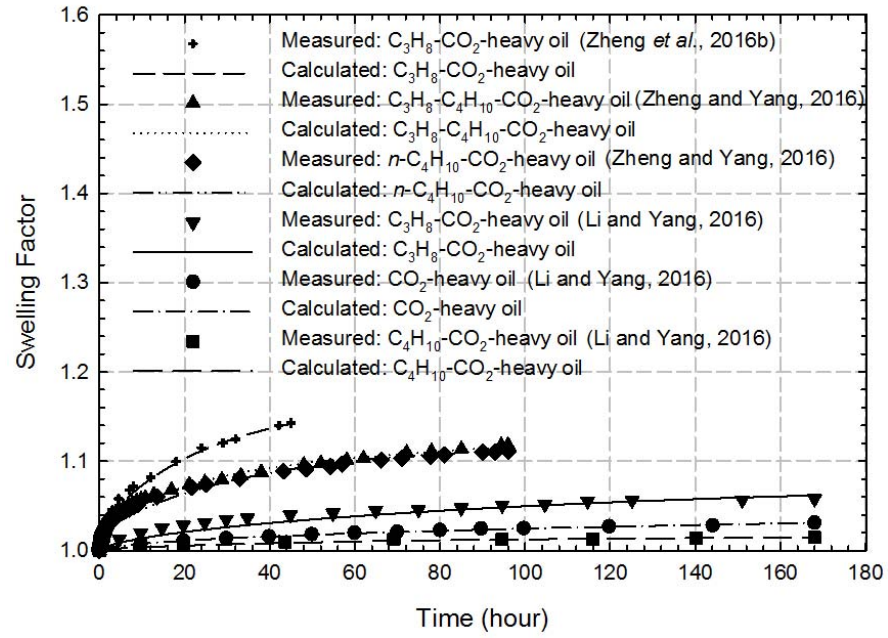

(b)

Figure 3-5 Measured and calculated dynamic swelling factor profiles for the CO_2–heavy oil systems, C_3H_8–CO_2–heavy oil systems, *n*-C_4H_{10}–CO_2–heavy oil systems and CO_2–C_3H_8–*n*-C_4H_{10}–heavy oil systems with **(a)** Objective function [3-15a] and **(b)** Objective function [3-15b]

while their related values are measured to be 1.031, 1.058 and 1.015, respectively (Li and Yang, 2016). Such minor differences between the measured and calculated dynamic swelling factors confirm that there exists a natural convection from the bottom of liquid phase to the gas-liquid interface, and thus reducing the dynamic swelling factors. Figure 3-5b presents the matching results of dynamic swelling factor with objective function [3-15b] which provides more reliable diffusion coefficients under dynamic and equilibrium conditions because all the measured swelling factors are employed during the matching processes with comparison of the objective function [3-15a] that uses only two data points of mole fraction at the beginning and end of the experiments. In this way, dynamic and equilibrium diffusion coefficients calculated with objective functions [3-15a] and [3-15b] for all three alkane solvent(s)–CO_2–heavy oil systems are presented in Table 3-2. Overall, the diffusion coefficients obtained with the two objective functions, i.e., Equations [3-15a] and [3-15b], are similar for all three alkane solvent(s)–CO_2–heavy oil systems, respectively. Also, it is worthwhile mentioning that, for the aforementioned three alkane solvent(s)–CO_2–heavy oil systems, the corresponding diffusion coefficient correlations for CO_2 are slightly different. This is mainly ascribed to the fact that each solvent has its preferential diffusion in the alkane solvent(s)–CO_2–heavy oil systems (Zheng *et al*., 2016a; b; Li and Yang, 2016; Zheng and Yang, 2016; 2017). Such preferential diffusion is physically caused by the difference of mass transfer rate among gas components resulted from different diffusivities. More specifically, a gas component with a relatively fast mass transfer rate would firstly result in the changes of oleic phase properties (such as viscosity), and further affect the diffusivity of other gas components in the oleic phase.

Table 3-2 Coefficients in Equation [3-7] and diffusion coefficients of alkane solvent(s)–CO_2–heavy oil systems with two types of objective functions

Mixture system	Gas	Equation [3-15a]			Equation [3-15b]					
		Coefficients in Equation [3-7]		Diffusion coefficient at equilibrium state ($\times10^{-10}$ m^2/s)	Coefficients in Equation [3-7]				Diffusion coefficient at equilibrium state ($\times10^{-10}$ m^2/s)	
		A ($\times10^{-8}$)	B		A ($\times10^{-8}$)		B			
CO_2–heavy oil (Li and Yang, 2016)	CO_2	1.9107	0.3942	9.82	3.2987		0.5131		6.64	
C_3H_8–CO_2–heavy oil (Zheng *et al*., 2016b)	CO_2	7.0402	0.3780	4.79	2.3000	0.3436*	0.2775	0.1704*	3.19	18.05*
	C_3H_8	4.0944	0.4588	16.03	1.1890	1.5189*	0.2795	0.1163*	16.30	97.89*
n-C_4H_{10}–CO_2–heavy oil (Zheng and Yang, 2016)	CO_2	4.3981	0.6014	3.19	5.4810	0.3315*	0.6652	0.0001*	2.27	33.13*
	C_4H_{10}	5.2433	0.3915	16.30	5.7237	0.8563*	0.3533	0.1907*	17.03	35.13*
C_3H_8–n-C_4H_{10}–CO_2–heavy oil (Zheng and Yang, 2016)	CO_2	–	–	–	0.0991*		0.0662*		7.52*	
	C_3H_8	–	–	–	0.6762*		0.0294*		59.85*	
	C_4H_{10}	–	–	–	0.7534*		0.0300*		66.51*	

*Based on the experiment data at the elevated temperatures of 329 K.

Li and Yang (2016) presented the diffusion coefficients of CO_2/solvents in the same heavy oil with the conventional method, i.e., solving the diffusion equation instead of the diffusion-convection equation (see Table 3-3). Since the objective function [3-15a] is exactly same as that of Li and Yang (2016)'s work, the diffusion coefficients calculated with objective function [3-15a] is employed for the comparison purpose. It is evidently found that all of the previously reported diffusion coefficients of CO_2/solvents are slightly lower than the calculated ones under the equilibrium conditions in this study. Natural convection originated from the swelling effect is supposed to be responsible for such a difference. The effect of the diluted heavy oil expanding from the bottom to the top of liquid phase hinders the molecular diffusion of CO_2/solvent(s) from the top to the bottom of liquid phase. This is similar to the process of the aforementioned CH_4–*n*-C_5H_{12} systems. Physically, a molecular diffusion process weakened by natural convection resulted from swelling effect is regarded as the actual molecular diffusion process and then utilized for solving the diffusion equation in conventional methods. Therefore, once the effect of natural convection is isolated from the molecular diffusion process, the calculated diffusion coefficients with the newly proposed model would be larger than the reported ones but closer to their actual values.

It can be concluded that the mass transfer rate of CO_2 is significantly lower than that of C_3H_8 and *n*-C_4H_{10} under the same conditions. More specifically, the diffusion coefficients of CO_2 are found to be respectively determined with three different equations on account of the variations of viscosities resulted from the different components and pressures in the three experiments. In addition, the diffusion coefficients of C_3H_8 and *n*-C_4H_{10} in this

Table 3-3 Comparison of the diffusion coefficients for CO_2 and/or solvent(s) in different heavy oils

Gas system	Sources	Heavy oil	Viscosity (cP)	Pressure (kPa)	Temperature (K)	Diffusion coefficient at equilibrium conditions (10^{-10} m^2/s)
CO_2	This study	Lloydminster heavy oil	12854 @ 294.55 K	3741-3371	294.55	6.64
	Li and Yang (2016)	Lloydminster heavy oil	12854 @ 294.55 K	3741-3371	294.55	8.24
	Upreti and Mehrotra (2000)	Athabasca Bitumen	N/A	4000	298.15-363.15	1.6-4.7l
	Zheng *et al*. (2016a)	Lloydminster heavy oil	12854 @ 294.55 K	3741-3371	294.55	4.3
	Zheng and Yang, (2016)	Lloydminster heavy oil	12854 @ 294.55 K	5400	317.65	14.97
	Upreti and Mehrotra (2002)	Athabasca Bitumen	821000 @ 298.15 K	4000 8000	298.15-363.15 323.15-363.15	1.3-4.3 4.0-9.3
	Sun *et al*. (2014)	Lloydminster heavy oil	12854 @ 294.55 K	5500	331.15	21
	Zhang *et al*. (2000)	Hamaca Oil	5000 @ 293.15 K	3471	294.15	48
	Yang and Gu (2006a)	Ontario heavy oil	N/A	2900	298.15	11.4
	Yang and Gu (2006c)	Lloydminster heavy oil	23000 @ 297.05 K	2000-6000	297.05	2.0-5.5
	Li *et al*. (2016)	Lloydminster heavy oil	13924 @ 293.85 K	3950	293.85	10.59
CO_2: 84.38 mol% C_3H_8: 15.62 mol%	This study	Lloydminster heavy oil	12854 @ 294.55 K	3741-3371	294.55	3.19 (CO_2) 16.30 (C_3H_8)
	Li and Yang (2016)	Lloydminster heavy oil	12854 @ 294.55 K	3741-3371	294.55	4.06 (CO_2) 13.34 (C_3H_8)
	Zheng *et al*. (2016a)	Lloydminster heavy oil	12854 @ 294.55 K	3741-3371	294.55	1.05 (CO_2) 13.70 (C_3H_8)
CO_2: 87.3 mol% C_3H_8: 12.7 mol%	Li *et al*. (2016)	Lloydminster heavy oil	13924 @ 293.85 K	3945	293.85	8.68 (CO_2) 18.19 (C_3H_8)
CO_2: 70 mol% C_3H_8: 30 mol%	Yang and Gu (2006c)	Lloydminster heavy oil	23000 @ 297.05 K	3005-1003	297.05	0.82-8.20*
CO_2: 86.64 mol% C_3H_8: 13.36 mol%	Sun *et al*. (2014)	Lloydminster heavy oil	12854 @ 294.55 K	3741-3371	331.15	17*
CO_2: 64.9 mol% C_3H_8: 35.1 mol%	This study	Lloydminster heavy oil	12854 @ 294.55 K	5500	329.15	18.05 (CO_2) 97.89 (C_3H_8)
	Zheng *et al*.(2016b)	Lloydminster heavy oil	12854 @ 294.55 K	5500	329.15	9.36 (CO_2) 22.37 (C_3H_8)
CO_2: 88.33 mol% C_4H_{10}: 11.67 mol%	This study	Lloydminster heavy oil	12854 @ 294.55 K	3741-3371	294.55	2.27 (CO_2) 17.03 (n-C_4H_{10})
	Li and Yang (2016)	Lloydminster heavy oil	12854 @ 294.55 K	3741-3371	294.55	1.92 (CO_2) 13.41 (n-C_4H_{10})
	Zheng *et al*. (2016a)	Lloydminster heavy oil	12854 @ 294.55 K	3741-3371	294.55	1.01 (CO_2) 15.30 (n-C_4H_{10})
CO_2: 90.29 mol% C_4H_{10}: 9.71 mol%	This study	Lloydminster heavy oil	12854 @ 294.55 K	5520	329.15	33.13 (CO_2) 35.13 (n-C_4H_{10})
	Zheng and Yang (2016)	Lloydminster heavy oil	12854 @ 294.55 K	5520	329.15	19.5 (CO_2) 27.5 (n-C_4H_{10})
CO_2: 80.55 mol% C_3H_8: 13.88 mol% C_4H_{10}: 5.57 mol%	This study	Lloydminster heavy oil	12854 @ 294.55 K	5540	329.25	7.52 (CO_2) 59.8 (C_3H_8) 66.51 (n-C_4H_{10})
	Zheng and Yang (2016)	Lloydminster heavy oil	12854 @ 294.55 K	5540	329.25	7.02 (CO_2) 25.63 (C_3H_8) 29.04 (n-C_4H_{10})

*Note: Apparent diffusion coefficient of a gas mixture.

study are evidently larger than those of C_3H_8–heavy oil systems ($0.9–6.8\times10^{-10}$ m^2/s at a pressure range of 400-900 kPa and 297.05 K: Yang and Gu, 2006c) and *n*-C_4H_{10}–heavy oil systems (1.84×10^{-10} m^2/s at 150 kPa and 298 K: Ganapathi, 2009). Such large diffusion coefficients can be likely attributed to the high pressure of gas solvents during the experiments in this study. Numerous experimental results indicate that diffusion coefficients of alkane solvents are increased with an increase in pressure when the pressure is lower than its dewpoint pressure at a constant temperature (Yang and Gu, 2006c; Marufuzzaman and Henni, 2014). Since the effect of CO_2 on the properties of gas mixture, the dewpoint pressures of CO_2–C_3H_8 systems and CO_2–*n*-C_4H_{10} systems are much higher than those of pure C_3H_8 and C_4H_{10} under the same conditions, implying there shall lead to large diffusion coefficients of C_3H_8 and C_4H_{10} at relatively high pressures in this chapter.

Under comparable conditions, it is found that both pressure and gas concentration dominate the mass transfer for the alkane solvent(s)–CO_2–heavy oil systems. As for the same oil samples at almost same temperature (see Table 3-3), both diffusion coefficient for pure CO_2 and individual diffusion coefficients for CO_2-C_3H_8 mixture obtained under the condition of decaying pressure (Initial pressure: 3741 kPa) in this study are respectively smaller than those attained under a constant pressure (CO_2–heavy oil systems: 3950 kPa and CO_2–C_3H_8–heavy oil systems: 3945 kPa) in the literature (Li *et al*., 2016). Also, a large gas concentration has been experimentally found to increase its mass transfer (i.e., diffusion coefficient) in a liquid (Yang *et al*., 2006; Yang and Gu, 2008).

2) Constant pressure and elevated temperatures

The experimental results of C_3H_8–CO_2–heavy oil system, *n*-C_4H_{10}–CO_2–heavy oil system and C_3H_8–*n*-C_4H_{10}–CO_2–heavy oil system documented in the literature (Zheng and Yang, 2016; Zheng *et al*., 2016b) were then utilized for determining individual diffusion coefficients at elevated temperatures by using objective function [3-15b]. Figure 3-5b shows that good agreements have been achieved between the measured dynamic swelling factors and the calculated ones. Also, there exists good agreements between the measured and calculated mole fractions of *n*-C_4H_{10}–CO_2–heavy oil system and C_3H_8–*n*-C_4H_{10}–CO_2–heavy oil system (see Table 3-1). The minor deviations are due mainly to the complicated and intrusive gas sampling processes. The good agreements of both dynamic swelling factors and mole fractions confirmed the validity of the newly proposed technique under the condition of elevated temperatures.

The coefficients in Equation [3-7] for calculating the dynamic diffusion coefficients of CO_2, C_3H_8, and *n*-C_4H_{10} in three alkane solvent(s)–CO_2–heavy oil systems and their diffusion coefficients under equilibrium conditions are presented in Tables 3-2 and 3-3, respectively. Since the same oil sample is used in the diffusion tests of this study and those in Li and Yang's work (2016), some comparisons between the results based on these two sets of experiments can be carried out. One can find that, similar to the aforementioned results with the decaying pressure and constant temperature in previous section, the individual diffusion coefficients of CO_2 and solvents under the elevated temperatures are also larger than those calculated with conventional method in the literature because of the natural convection. Furthermore, the increments of diffusion

coefficients at elevated temperatures are higher than those at a constant and relatively low temperature (see Table 3-3). More specifically, the individual diffusion coefficients of CO_2 and *n*-C_4H_{10} at 294.55 K in *n*-C_4H_{10}–CO_2–heavy oil system are increased by 1.26×10^{-10} m^2/s and 1.73×10^{-10} m^2/s, respectively, in comparison with the results of Zheng *et al*. (2016a) at the same temperature. At 329.15 K, the increments of individual diffusion coefficients of CO_2 and *n*-C_4H_{10} can respectively reach 13.63×10^{-10} m^2/s and 7.63×10^{-10} m^2/s for *n*-C_4H_{10}–CO_2–heavy oil systems, which is much higher than those at 294.55 K. The similar trend is also able to be observed in C_3H_8–CO_2–heavy oil systems (see Table 3-3). Such an enhanced swelling effect mainly resulted from the high temperature shall be the underlying mechanism accounting for the large individual diffusion coefficients. The swelling factors at the end of the diffusion experiments for the C_3H_8–CO_2–heavy oil system (45 hours) and the *n*-C_4H_{10}–CO_2–heavy oil system (96 hours) at 329.15 K have been measured to be 1.14 and 1.11, respectively, which are much larger than the corresponding values (i.e., 1.04 and 1.01) at 294.55 K at the same time. Accordingly, a faster velocity of natural convection caused by the enhanced swelling effect is generated at 329.15 K, leading to a greater hindrance for mass transfer of CO_2, C_3H_8, and *n*-C_4H_{10} in heavy oil.

3.3.2 Effect of temperature and natural convection on mass transfer

Diffusion tests of three CO_2–heavy oil systems under different system temperatures (Test #1: 298.6 K; Test #2: 316.7 K; Test #3: 336.7 K: Zheng and Yang, 2017) are employed to examine the effects of heat and natural convection on the mass transfer processes. Figure 3-6 shows that the calculated dynamic swelling factors with the proposed model are

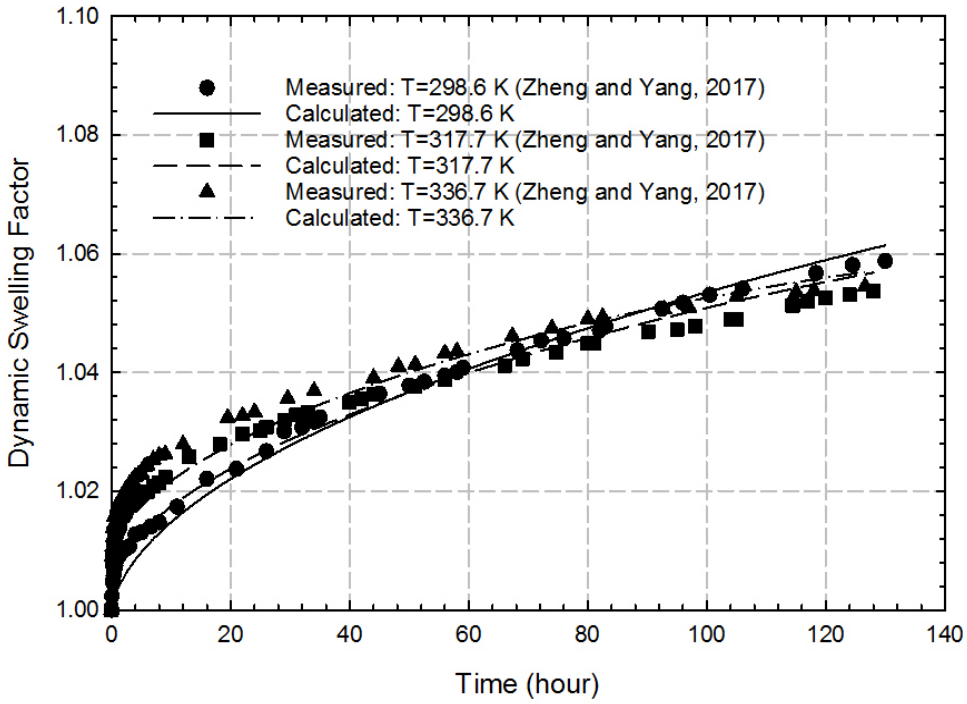

Figure 3-6 Measured and calculated dynamic swelling factor profiles for the CO_2–heavy oil systems at different temperatures

consistent with the experimental measurements for all three tests. Then, the physical properties associated with the mass transfer processes, such as dynamic CO_2 mole fraction, viscosity of the diluted heavy oil and natural convection velocity, are computed based on the matching results. As for evaluating the natural convection effect on mass transfer process, three designed cases (Cases #1–3) featured by neglecting natural convection are simulated with completely same input parameters of Tests #1–3, respectively.

1) Thermal effect

Figure 3-7a depicts CO_2 mole fractions as a function of time for Tests #1–3, respectively. It can be found that the dynamic CO_2 mole fractions gradually decline with an increase in system temperature. It is well recognized that CO_2 solubility in heavy oil is increased with a decrease in temperature. A higher solvent concentration gradient on the phase contact is generated under the condition of a lower temperature and thus improves the mass transfer rate. On the other hand, the entire system gradually approaches its equilibrium state as time proceeds, and then a larger mole fraction of CO_2 in the diffusion test with a lower system temperature is inevitably achieved compared with those with higher temperatures.

Meanwhile, the dynamic average viscosities of the diluted heavy oil in Tests #1–3 are calculated and depicted in Figure 3-7b. One can find that the viscosities not only decline with time proceeding in every individual diffusion test, but also decrease with an

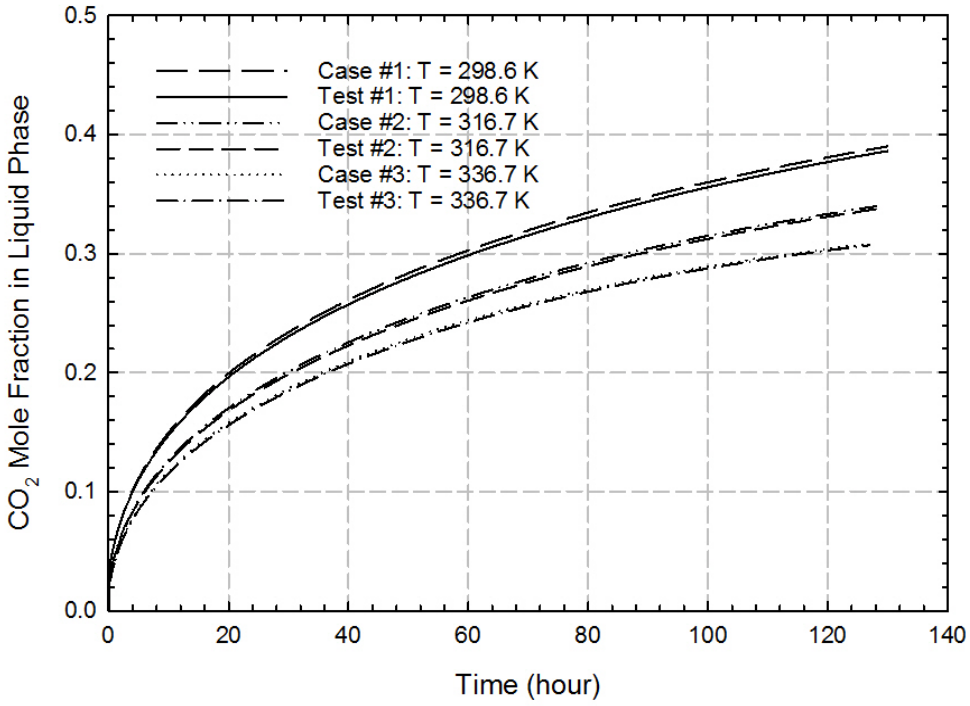

(a)

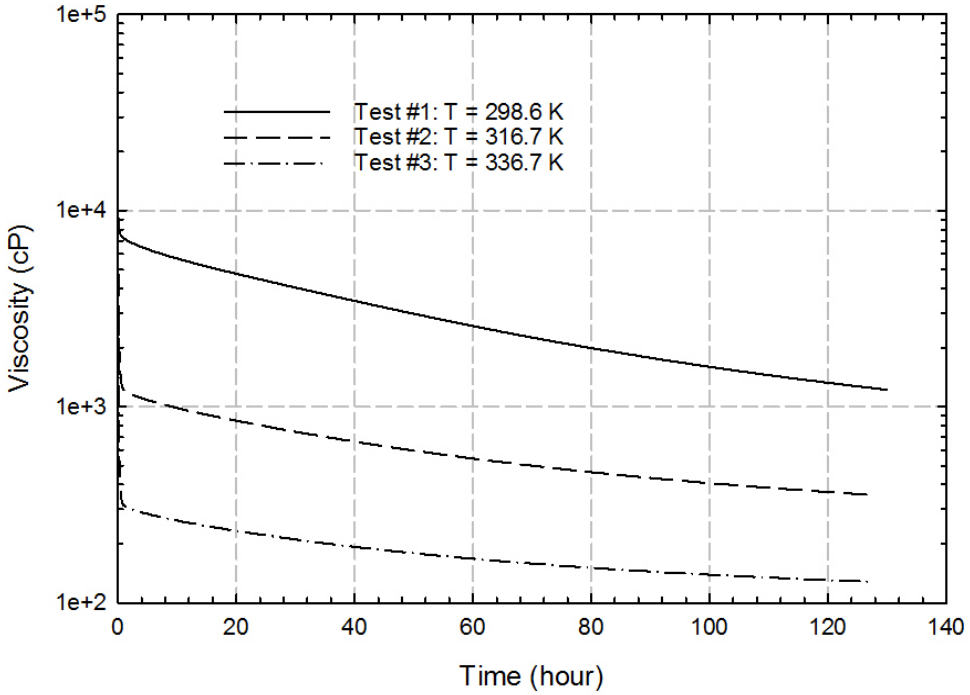

(b)

Figure 3-7 (a) Calculated CO_2 mole fraction profiles of Tests #1–3 and Cases #1–3 and **(b)** calculated average liquid viscosity profiles of Tests #1–3

increase of temperature among three tests at the same time. Such a reduced viscosity results in a large diffusion coefficient on the basis of Equations [3-7]–[3-9].

As indicated in Figures 3-7a and b, the mole fraction profiles reveal that a high solvent concentration at the interface originated from the relatively low temperature and a large diffusion coefficient resulted from the reduced viscosity of the heated heavy oil do not impose a similar impact on the mass transfer rate at the same time. Accordingly, the CO_2 concentration at the bottom of the PVT cell is utilized to examine the effects of the aforementioned high solvent concentration and large diffusion coefficient because such CO_2 concentration is a direct reflection of mass transfer rate in the entire liquid phase (see Figure 3-8). As can be seen, CO_2 mole fraction increases with an increase of system temperature before 110 hours, showing that a negative effect of the reduced solvent concentration from the high temperature on the mass transfer rate can be counteracted by the positive effect of the high diffusion coefficient. As such, the hybrid thermal-solvent processes can effectively enhance mass transfer rate of a solvent in heavy oil within a certain range of temperature and time. When the experimental time is longer than 110 hours in this study, the order of CO_2 mole fractions of Tests #1–3 is the converse of previous one since CO_2 solubility, physically, is declined with an increase of temperature.

Figure 3-9 depicts the distribution profiles of the normalized concentration (c/c_{sat}) at 126 hours from the bottom of PVT cell to the gas-liquid interface, implying that a high temperature can accelerate the mass transfer processes so as to reduce the time required to achieve the concentration equilibrium. In addition, as for Tests #1–3, the required

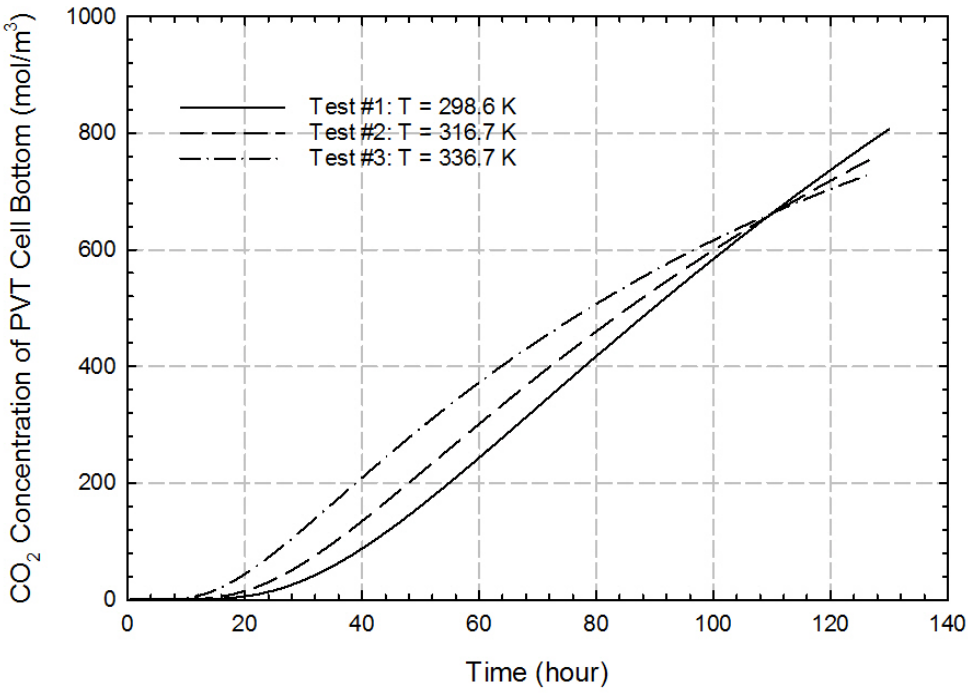

Figure 3-8 Dynamic CO_2 concentrations at bottom of PVT cell in Tests #1–3

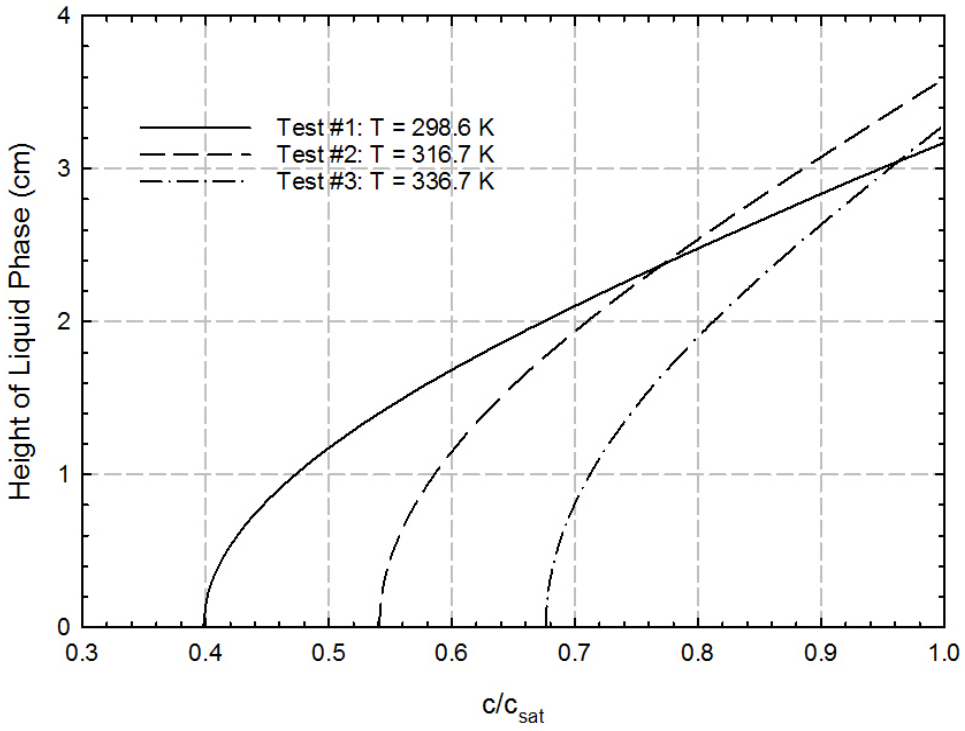

Figure 3-9 Calculated normalized concentrations profiles of Tests #1–3 at 126 hours

times for reaching temperature equilibrium state are found to be 60, 111, and 105 minutes (see Figure 3-10), respectively. It is noted that the required time of temperature equilibrium state in Test #3 is slightly shorter than that of Test #2, though system temperature of the former is higher than that of the latter. This may be ascribed to the fact that a larger CO_2 mole fraction in Test #2 retards the heat transfer rate in comparison to that of Test #3. Also, the durations of Tests #1–3 to achieve temperature equilibrium are much shorter than that of CO_2 mass transfer since the concentration distribution of CO_2 has not even reached the equilibrium state at the end of simulation. This evidently shows that the heat transfer rate is much larger than that of CO_2 mass transfer in heavy oil.

2) Natural convection

Physically, natural convection induced by swelling effect stems from an increase of the diluted liquid volume. Such fluids flow from the bottom to the top of the liquid phase slows the CO_2 mass transfer since the direction of fluids flow is opposite to that of mass transfer. Figure 3-11 shows the velocity distributions of Tests #1–3. It can be found that the velocity of natural convection gradually decreases with time because the swelling effects induced by the gradients of both temperature and CO_2 concentration decline over time. Also, the average natural convection velocities of the gas-liquid interface during the experimental processes of Tests #1–3 are 1.70×10^{-9} m/s, 1.78×10^{-9} m/s, and 1.57×10^{-9} m/s, respectively. The difference among average velocities in Tests #1–3 are caused by the differences of thermal energy and compositions of mixture. More specifically, the reduced viscosity resulted from the heated heavy oil and diluted heavy oil firstly enhances the mass transfer rate of CO_2. Then, a larger CO_2 mole fraction leads to a higher

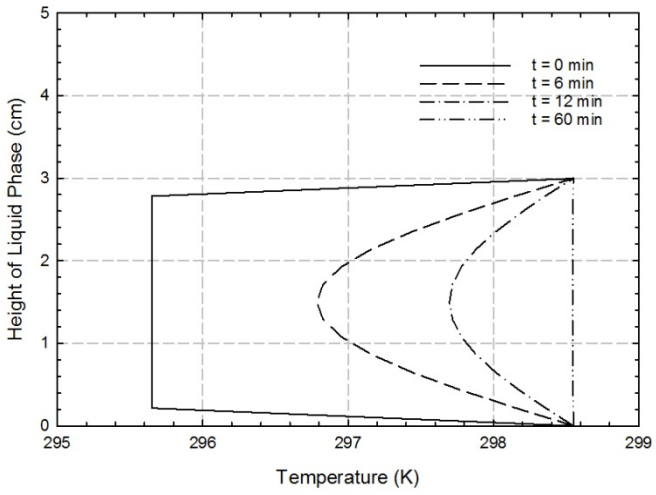

(a)

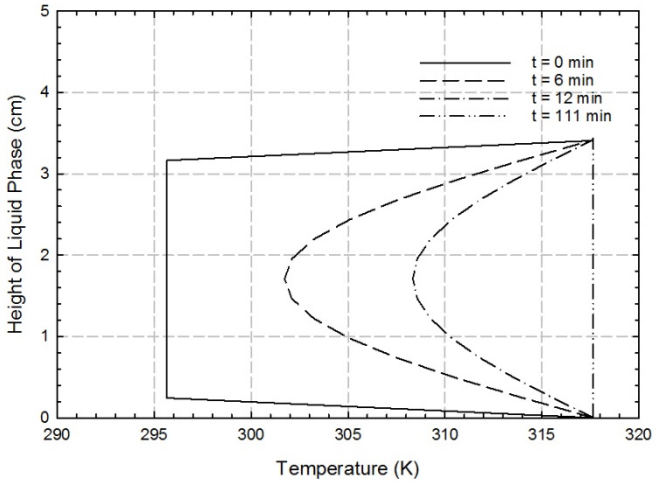

(b)

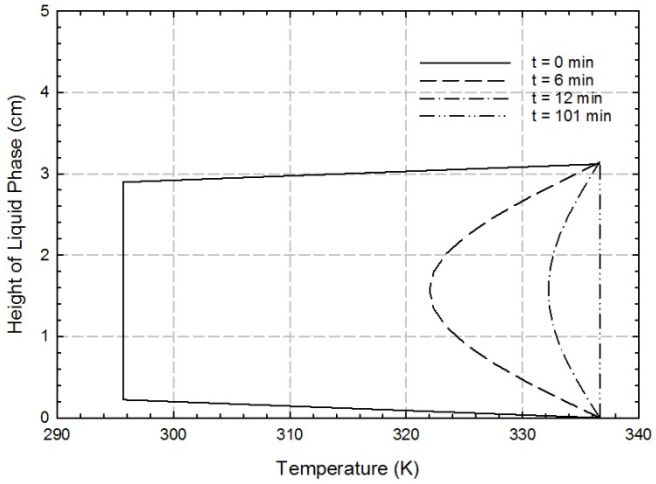

(c)

Figure 3-10 Temperature distributions at different time for **(a)** Test #1, **(b)** Test #2 and **(c)** Test #3

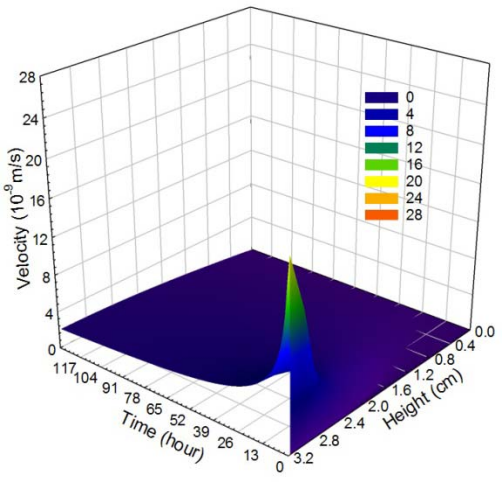

(a)

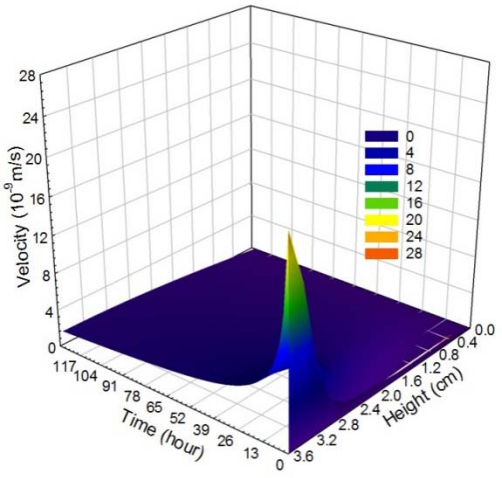

(b)

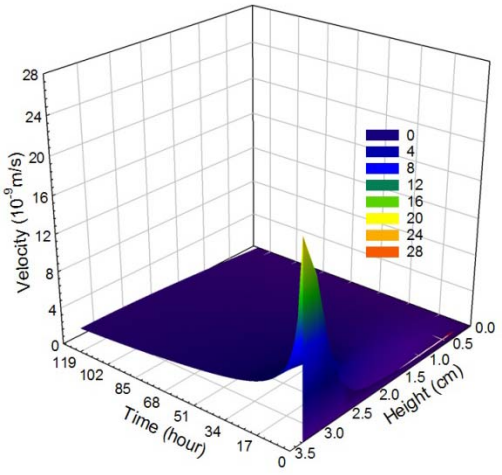

(c)

Figure 3-11 Velocity distributions as a function of time and liquid height for **(a)** Test #1, **(b)** Test #2, and **(c)** Test #3

swelling factor based on Equation [3-12], and further results in a higher velocity of natural convection.

As for the designed Cases #1–3, since the natural convections are neglected, the mole fractions of CO_2 are slightly higher than those of Tests #1–3 (see Figure 3-7a). This implies that the natural convection actually weakens the mass transfer rate from the gas-oil interface to the liquid phase in Tests #1–3. Figure 3-12 shows the incremental mole fraction percentages of Cases #1–3 in comparison to those of Tests #1–3, respectively. It can be found that the increment of CO_2 mole fraction first reaches its maximum at the early stage due mainly to the effect of the heat transfer and a large CO_2 concentration gradient. In addition, the maximum increment of mole fraction gradually declines with an increase in system temperature mainly owing to an enlarged temperature gradient between liquid phase and gas phase that usually leads to an increase of natural convection velocity. Then, increments of CO_2 mole fraction in pairs of Test #1–Case #1, Test #2–Case #2, and Test #3–Case #3 begin to decline as time proceeds after their corresponding maximum values. This can be explained by the fact that the entire system gradually approaches its equilibrium state, and the impact from the natural convection on the mass transfer must inevitably be tapered off. Also, the decline rate of mole fraction is increased with an increase in system temperature because a high system temperature is beneficial to approach the equilibrium state, and then results in a low natural convection velocity (see Figure 3-9).

The average velocities of Tests #1–3 are only in the range of $1.50–1.80\times10^{-9}$ m/s. It is the

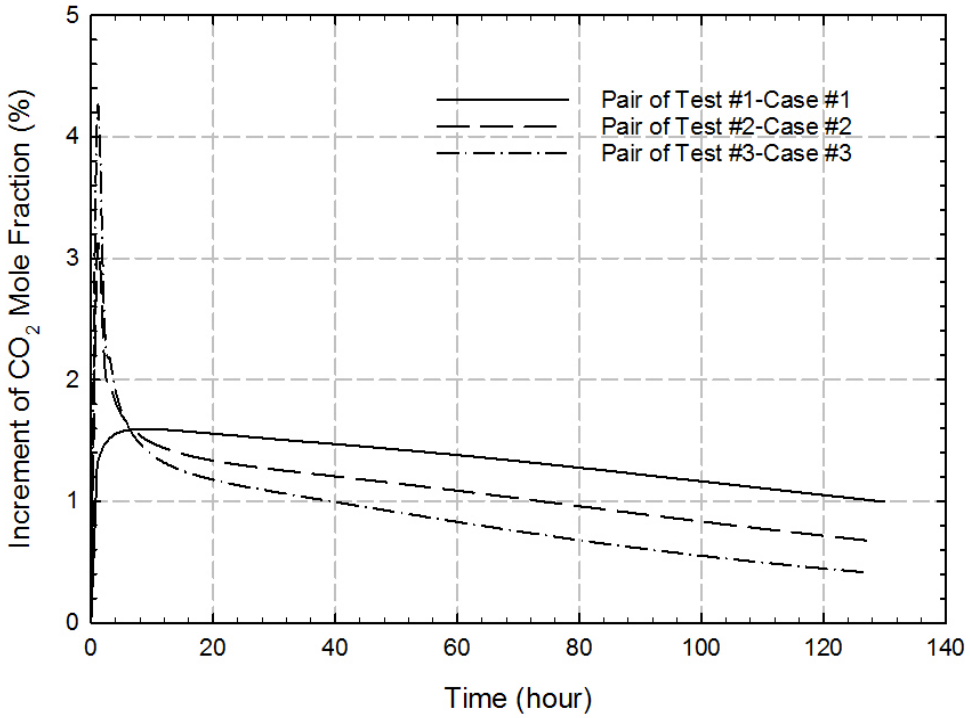

Figure 3-12 Increment of CO_2 mole fraction between pair of Test #1–Case #1, Test #2–Case #2, and Test #3–Case #3

reason why the average increments of CO_2 mole fraction in pairs of Test #1–Case #1, Test #2–Case #2, and Test #3–Case #3 are only 1.32%, 1.08% and 0.88%, respectively, though the corresponding related maximum increments of CO_2 mole fraction are 1.59%, 3.06% and 4.22%, respectively. Such a minor difference implies that the natural convection effect can be neglected in the CO_2–heavy oil system. However, as for the C_3H_8–CO_2–heavy oil system, *n*-C_4H_{10}–CO_2–heavy oil system and C_3H_8–*n*-C_4H_{10}–CO_2–heavy oil system in this study, the average velocities can reach 13.50×10^{-9} m/s, 4.45×10^{-9} m/s, and 4.26×10^{-9} m/s, respectively. Such relatively large differences are mainly caused by the relatively large swelling factors induced by the dissolution of alkane solvents. More specifically, the increasing rates of the oil swelling, defined as the average increment of swelling height of the liquid phase per second, of the three alkane solvent(s)–CO_2–heavy oil systems (Tests #4–6) are larger than 9.31×10^{-9} m/s, which is much higher than average one (3.83×10^{-9} m/s) of the CO_2–heavy oil systems (Tests #1–3). Consequently, for the sake of simplifying the procedure of determining diffusion coefficients for the alkane solvent(s)–CO_2–heavy oil systems, it seems that the effect of natural convection can be neglected when the increasing rate of oil swelling is smaller than 3.83×10^{-9} m/s.

3.4 Summary

By coupling heat and mass transfer and treating heavy oil as multiple pseudocomponents, a novel and pragmatic technique has been developed and validated to determine individual diffusion coefficient of each component for the alkane solvent(s)–CO_2–heavy oil systems with consideration of natural convection induced by the swelling effect. The

PR EOS, heat transfer equation, and convection-diffusion equation are integrated to quantify the heat and mass transfer. The individual diffusion coefficient considering the effect of natural convection on the mass transfer can be quantified as a function of viscosity of the solvent-saturated heavy oil. The individual diffusion coefficients are found to be larger than those calculated ones with the conventional methods under equilibrium conditions. This can be attributed to the fact that the conventional methods allow molecular diffusion to be offset by natural convection to some extent due to the vague combination, while the newly proposed technique isolate natural convection from the molecular diffusion.

Based on the measured and calculated results of three diffusion tests conducted with CO_2–heavy oil systems, mass transfer rate of CO_2 in heavy oil with heat is found to be increased owing to the large diffusion coefficient resulted from the reduced viscosity of the heated heavy oil within a certain range of temperature and time. The natural convection induced by swelling effect for the CO_2–heavy oil systems can be neglected, whereas it needs to take into account for the alkane solvent(s)–CO_2–heavy oil systems due to the preferential dissolution of alkane solvents.

CHAPTER 4 NONEQUILIBRIUM PHASE BEHAVIOUR OF ALKANE SOLVENT(S)–CO_2–HEAVY OIL SYSTEMS UNDER CONSTANT VOLUME EXPANSION RATES

4.1 Introduction

This chapter developed a robust and pragmatic technique to experimentally and theoretically quantify the nonequilibrium phase behaviour of alkane solvent(s)–CO_2–heavy oil systems under reservoir conditions (Shi *et al*., 2015; 2016; Shi and Yang, 2017c). Experimentally, a mercury-free PVT setup has been utilized to perform constant-composition expansion (CCE) experiments with a constant volume expansion rate for quantifying the equilibrium and nonequilibrium phase behaviour of alkane solvent(s)–CO_2–heavy oil systems. Theoretically, real gas equation of state and a time-dependent power-law relation are incorporated into a newly proposed mathematical model to bridge the dynamic relationship between pressure and the expanded volume of the CCE experiments, while the PR EOS is used to calculate the equilibrium-properties by treating heavy oil as multiple pseudocomponents. Then, the properties of foamy oil (i.e., compressibility and density) are determined and analyzed accordingly.

4.2 Experimental

4.2.1 Materials

Heavy oil sample used in the experiment is collected from Lloydminster area in Saskatchewan, Canada. Molecular weight is measured to be 482 g/mol, while the compositional analysis (see Table 4-1) of the heavy oil sample is conducted by using the simulated distillation method. The CO_2, CH_4, and C_3H_8 (Praxair, Canada) have purities of

Table 4-1 Compositional analysis of the Lloydminster heavy oil

Carbon No.	wt%	mol%	Carbon No.	wt%	mol%
C_1	0.000	0.000	C_{32}	1.329	1.310
C_2	0.000	0.000	C_{33}	0.981	0.940
C_3	0.000	0.000	C_{34}	1.083	1.010
C_4	0.000	0.000	C_{35}	1.307	1.180
C_5	0.000	0.000	C_{36}	1.343	1.180
C_6	0.000	0.000	C_{37}	0.917	0.780
C_7	0.000	0.000	C_{38}	0.900	0.750
C_8	0.000	0.000	C_{39}	1.583	1.290
C_9	0.786	2.730	C_{40}	1.600	1.270
C_{10}	0.844	2.640	C_{41}	0.750	0.580
C_{11}	1.037	2.960	C_{42}	0.830	0.630
C_{12}	1.267	3.320	C_{43}	1.380	1.020
C_{13}	1.817	4.390	C_{44}	0.929	0.670
C_{14}	1.950	4.380	C_{45}	0.929	0.650
C_{15}	2.300	4.830	C_{46}	0.700	0.480
C_{16}	2.143	4.220	C_{47}	0.833	0.560
C_{17}	2.286	4.240	C_{48}	0.792	0.530
C_{18}	2.238	3.920	C_{49}	0.792	0.510
C_{19}	2.048	3.400	C_{50}	0.733	0.460
C_{20}	1.857	2.930	C_{51}	0.750	0.470
C_{21}	2.071	3.110	C_{52}	0.717	0.440
C_{22}	1.329	1.910	C_{53}	0.717	0.430
C_{23}	1.743	2.390	C_{54}	0.683	0.400
C_{24}	1.571	2.070	C_{55}	0.650	0.370
C_{25}	1.714	2.170	C_{56}	0.650	0.370
C_{26}	1.600	1.950	C_{57}	0.667	0.370
C_{27}	1.583	1.850	C_{58}	0.667	0.360
C_{28}	1.650	1.860	C_{59}	0.667	0.360
C_{29}	1.452	1.580	C_{60}	0.767	0.410
C_{30}	1.281	1.350	C_{61+}	35.397	14.600
C_{31}	1.390	1.420	Total	100.000	100.000

Note: The compositional analysis was conducted by the Saskatchewan Research Council (SRC)

99.998 mol%, 99.97 wt%, and 99.5 wt%, respectively. The compositions of alkane solvent(s)–CO_2–heavy oil systems in this experiment are tabulated in Table 4-2.

4.2.2 Experimental setup

In this study, constant-composition expansion experiments are performed with a mercury-free DBR PVT system (PVT-0150-100-200-316-155, DBR, Canada) for the alkane solvent(s)–CO_2–heavy oil systems. Figure 4-1 depicts the schematic diagram of the PVT experimental setup. The entire experimental system mainly includes four parts, i.e., a visual and high pressure PVT cell, a recording subsystem, an injection subsystem, and an air bath. As for the visual and high pressure PVT cell, the fluids are contained in the glass tube with an inner diameter of 3.177 cm and a length of 20.320 cm. Maximum operating pressure and temperature are 69000 kPa and 473.15 K, respectively. A floating piston, which is driven by a high-pressure automatic positive-displacement pump (PMP-0500–1–10-MB-316-M4-C0, DBR, Canada), is positioned in the PVT cell to separate the hydraulic oil from experimental fluids. The volume and pressure of fluids can be controlled by vertically moving the floating piston upwards and downwards. The recording subsystem includes a high-precision pressure sensor (PM Series, 5000 psia, Heise, USA) with a full-scale accuracy of 0.025% and a video-based digital cathetometer with a resolution of 0.002 cm. The injection subsystem mainly consists of two high-precision syringe pumps (500HP, ISCO Inc., USA) that are applied for injecting alkane solvent(s), CO_2, and heavy oil into PVT cell. As for the air bath, the temperature of entire experimental system is maintained at a pre-specified temperature with an accuracy of ±0.1 K.

Table 4-2 Compositions of alkane solvent(s)–CO_2–heavy oil systems

Feed No.	Composition (mol%)			
	CH_4	CO_2	C_3H_8	Heavy oil
1	0.0	27.7	0.0	72.3
2	0.0	19.7	28.7	51.6
3	14.4	0.0	0.0	85.6

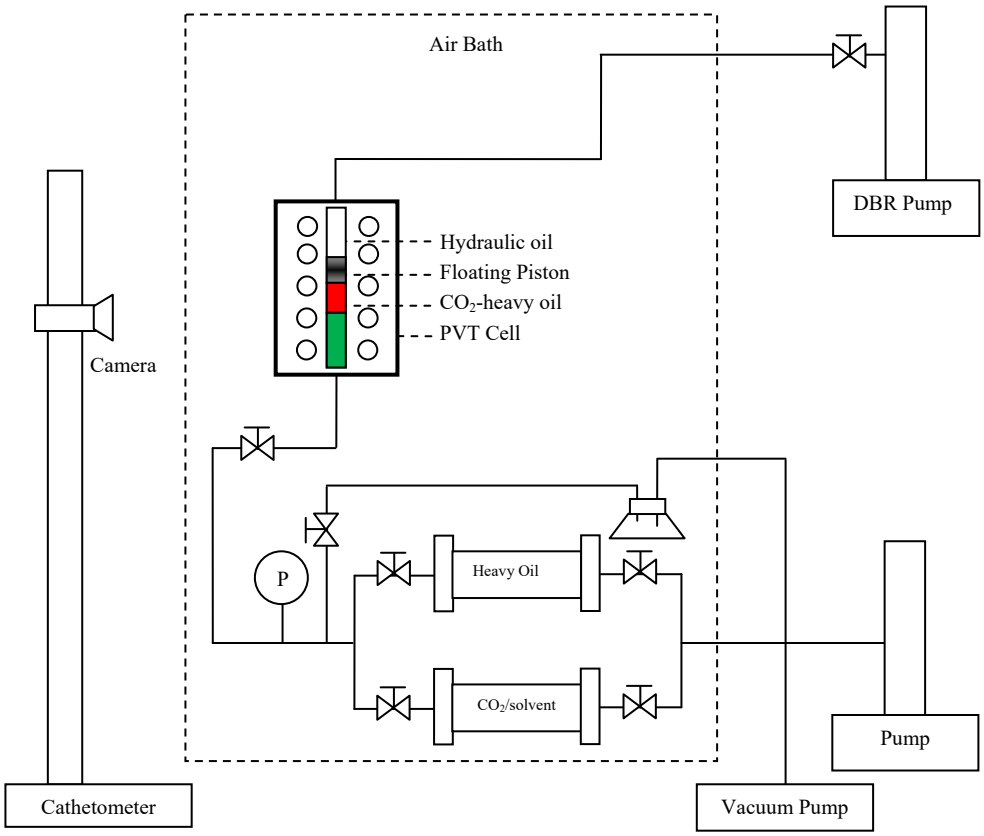

Figure 4-1 Schematic diagram of the PVT experimental setup

4.2.3 Experimental procedures

The experimental procedures of nonequilibrium conditions for CO_2–heavy oil system can be briefly described as follows:

1) Prior to constant-composition expansion experiments, leakage test for the PVT cell is firstly conducted with nitrogen. Then, the PVT cell is completely cleaned with kerosene and flushed with air;
2) The vacuum pump is employed to evacuate the air in the PVT cell and flowlines. Subsequently, CO_2 is introduced into the PVT cell from a gas cylinder;
3) The heavy oil sample is slowly injected into PVT cell. After closing the inlet valve, the entire CO_2–heavy oil system is isolated and to be vigorously agitated more than 16 hours with the equipped mixer at the bottom of the PVT cell to ensure that the entire system reaches the equilibrium state at the given temperature and pressure; and
4) When the equilibrium state is established, the mixer is turned off to stop agitating. Floating piston in the PVT cell is started to move up for enlarging the volume by withdrawing hydraulic oil at a constant rate. Meanwhile, pressure of the PVT cell is continuously recorded, while the height of the liquid phase is simultaneously measured by using the cathetometer. Thus, relationship between the volume of CO_2–heavy oil systems and pressure of nonequilibrium condition can be obtained.

As for the CH_4–heavy oil systems, the aforementioned procedure is followed. As for CO_2–C_3H_8–heavy oil systems, in Step #2, CO_2 is firstly injected into PVT cell and compressed into liquid CO_2, then liquefied C_3H_8 is introduced into the PVT cell. Once

the equilibrium is reached with the same procedure of Step #3 for CO_2–heavy oil systems, the pressure and concentration of each phase for CO_2–C_3H_8–heavy oil systems will be respectively determined, and then followed by Step #4.

Additionally, as for the procedures of equilibrium condition, Steps #1–3 are the same as those of nonequilibrium ones. In Step #4, except that the mixer in the liquid phase keeps stirring to ensure the equilibrium condition during entire experimental processes, other processes are kept the same as those of nonequilibrium conditions.

4.3 Mathematical Formulations

4.3.1 Volume of the evolved gas and the entrained gas

To describe the formation of gas phase processes, the following assumptions have been made:

1) The entrained gas in the oleic phase has the same properties as the free gas under the same pressure and temperature;
2) Compared with the external pressure of the alkane solvent(s)–CO_2–heavy oil systems, the Laplace pressure in the gas bubble is neglected (Gor *et al*., 2011); and
3) Foamy oil includes two components, i.e., the entrained gas and the mixture of dead oil and solution gas.

The typical feature of foamy oil is that the measured bubblepoint pressure is lower than the thermodynamic bubblepoint pressure (P_b) under equilibrium conditions, i.e.,

supersaturation (Chen *et al*., 2015). Physically, formation of gas phase in oil may be divided into the following three regimes, i.e., Regime #1: The first pressure decline; Regime #2: Rebound pressure; and Regime #3: The second pressure decline (Arora and Kovscek, 2003). More specifically, based on the instantaneous nucleation model associated with constant expansion rate experiments, all the gas bubbles are reasonably assumed to nucleate at the thermodynamic bubblepoint pressure of heavy oil (Kraus *et al*., 1993). In practice, the size of gas bubble cannot increase until the radius of gas bubble is large enough to surpass the nucleus size in Regime #1 (Kashchiev and Firoozabadi, 1993). Therefore, pressure of the entire system sharply decreases with an extremely small increase of the expanded volume on gas bubbles. In Regime #2, the growth of gas bubble volume and an increase in compressibility of the mixture usually lead to an increase in pressure when pressure decreases to a certain value, i.e., gas phase volume is sufficiently large to offset the effect of volume expansion on pressure. Finally, the oil withdrawal dominates the process of mass transfer so that pressure of the mixture system begins to decrease again (Arora and Kovscek, 2003). The gas bubble formation rate is found to be a function of the bubble growth (Kashchiev and Firoozabadi, 1993; Gor *et al*., 2011), while the volume of gas bubbles, in general, is a power function of time (Moulu, 1989; Kashchiev and Firoozabadi, 1993; Sheng *et al*., 1999a).

As mentioned previously, Sheng *et al*. (1995; 1997; 1999c) proposed a correlation to quantify the amount of the evolved gas as a function of time (Equation [2-6]). Due to the existence of different stages of gas exsolution, Equation [2-6] can be modified and expressed as follows,

$$n_{ev}(t)=\begin{cases} n_{eq}\left(t/t_{eq}\right)^{m_1} & t<t_{pb} \\ n_{eq}\left(t/t_{eq}\right)^{m_2} & t\geq t_{pb} \end{cases} \quad [4\text{-}1]$$

where t_{pb} is critical time that corresponds to the turning point pressure, i.e., pseudo-bubblepoint pressure; and m_1 and m_2 are bubble growth coefficients in different bubble growth regimes, respectively.

As for experiments with a constant expansion rate, the total volume of mixture, $V(t)$, at a given time is expressed as,

$$V(t)=V_l(t)+V_g(t) \quad [4\text{-}2]$$

where $V_l(t)$ and $V_g(t)$ are liquid and gas phase volume, respectively;

$$V_l(t)=V_{li}+c_t V_{li}\left[P_i-P(t)\right] \quad [4\text{-}3a]$$

where V_{li} is the initial liquid phase volume; c_t is compressibility of liquid under equilibrium conditions; P_i is initial pressure of the entire system; and $P(t)$ is pressure at time *t*.

Combining Equation [4-2] with real gas equation of state, i.e., $PV=znRT$, we can obtain,

$$\frac{\partial V_g}{\partial t}=\frac{\partial n}{\partial t}\frac{zRT}{P}-\frac{znRT}{P^2}\frac{\partial P}{\partial t} \quad [4\text{-}3b]$$

Substituting Equation [4-1] into Equation [4-3b], the relationship between pressure and expansion rate *q*, i.e., the volume increment of gas-liquid system per second, can be rewritten as follows,

$$\frac{\partial P}{\partial t}=\frac{\lambda zRT\dfrac{n_{eq}}{t_{eq}^{\lambda}}t^{\lambda-1}P}{\left[n_{eq}\left(\dfrac{t}{t_{eq}}\right)^{\lambda}zRT+P^2\gamma\right]}-\frac{P^2q}{\left[n_{eq}\left(\dfrac{t}{t_{eq}}\right)^{\lambda}zRT+P^2\gamma\right]}\quad\left(\lambda=m_1,t<t_{pb};\lambda=m_2,t\geq t_{pb}\right)$$

[4-4]

where $\gamma=c_tV_{li}$.

The ratio of the moles of the entrained gas to that of the evolved gas is used to determine the amount of the entrained gas in heavy oil. When pressure is larger than the pseudo-bubblepoint pressure (P_{pb}), there is no free gas phase in the system, indicating that all of the evolved gas remains entrained in the heavy oil, though pressure is lower than the thermodynamic bubblepoint pressure. Below P_{pb} , a portion of the evolved gas is released to be free gas from the oleic phase. It has been found that there exists a linear relationship between pressure and volume of free gas under equilibrium and nonequilibrium conditions when pressure is lower than the thermodynamic bubblepoint pressure or pseudo-bubblepoint pressure (Mastmann *et al*., 2001; Sahni *et al*., 2004; Chen *et al*., 2015). Thus, it is practical that the fraction of the entrained gas to the evolved gas can be expressed as follows (Chen *et al*., 2015),

$$\gamma\left(P\right)=\begin{cases}1, & P\geq P_{pb}\\ \dfrac{P-P_{ref}}{P_{pb}-P_{ref}}, & P_{ref}<P<P_{pb}\\ 0, & P\leq P_{ref}\end{cases}\qquad[4\text{-}5]$$

where P_{ref} is reference pressure (lower than P_{pb} , usually 101.325 kPa). Moles of the entrained gas, then, can be calculated as follows,

$$n_{en} = n_{ev}\gamma\left(P\right) \quad [4\text{-}6]$$

4.3.2 PR EOS

Similar to Chapter 3, PR EOS combined with the modified alpha function proposed by Li and Yang (2011) is selected to describe the equilibrium phase behaviour of alkane solvent(s)–CO_2–heavy oil systems in this study. The detailed expressions can be found in Chapter 3.

4.3.3 Properties of foamy oil

Since the volume and pressure of foamy oil can be theoretically calculated by using the newly proposed models, foamy oil compressibility can be directly determined according to its definition. In the literature, the foamy oil compressibility is the summation of that dead oil, dissolved gas, and entrained gas (Kraus *et al*., 1993; Sheng *et al*., 1999b). Simultaneous increase of volume and pressure for foamy oil may occur likely due to the increase of amount of entrained gas after the pseudo-bubblepoint pressure is reached. To ensure that the calculated compressibility is positive, the compressibility can be written as follows,

$$c_{fo} = \left| \frac{1}{V_{fo}} \frac{\partial V_{fo}}{\partial P} \right| \quad [4\text{-}7]$$

where c_{fo} and V_{fo} are the compressibility and volume of an alkane solvent(s)–CO_2–heavy oil system, respectively. The volume of foamy oil can be determined by,

$$V_{fo}\left(t\right) = V\left(t\right) - V_{free}\left(t\right) \quad [4\text{-}8]$$

where $V_{free}\left(t\right)$ is volume of the free gas.

The density of foamy oil can be directly calculated by using the mass and volume of foamy oil, and expressed as,

$$\rho_{fo} = \frac{m_{fo}}{V_{fo}} \qquad [4\text{-}9]$$

where m_{fo} is mass of the foamy oil, and calculated by

$$m_{fo} = m_t - n_{free} MW_{free} \qquad [4\text{-}10]$$

where m_t is total mass of mixture; n_{free} is moles of free gas; and MW_{free} is molecular weight of free gas. Also, densities of dead oil (heavy oil without solvents) can be computed by the following expressions (Li *et al*., 2013a),

$$\rho(T,P) = \frac{\rho_0(T,P_0)}{1-\eta \ln\left(\frac{G+0.001P}{G+0.1}\right)} \qquad [4\text{-}11]$$

where

$$\rho_0 = 784.0044 + 1.7217T - 3.3752\times10^{-3}T^2 \qquad [4\text{-}12a]$$

$$\eta = -6.1774 + 0.0213T \qquad [4\text{-}12b]$$

and

$$G = 3.7614\times10^{-4} - 1.8009\times10^{7}T^{-1} + 2.0605\times10^{9}T^{-2} \qquad [4\text{-}12c]$$

4.3.4 Numerical solution

Due to the nonlinearity of Equation [4-4], the Runge-Kutta fourth-order method is utilized to numerically solve the formulated mathematical matrix, assuming temperature

is constant. After discretizing the smooth pressure curve as an integration of a stepped curve with a fixed time step, Δt, Equation [4-4] can be rewritten as,

$$P^{t+1} = P^t + \Delta t \cdot \frac{\lambda z R T \frac{n_{eq}^t}{t_{eq}^{\lambda}} \Delta t^{\lambda-1} P^t - \left(P^t\right)^2 q}{\left[n_{eq}^t \left(\frac{\Delta t}{t_{eq}} \right)^{\lambda} z^t R T + \left(P^t\right)^2 \gamma \right]} \quad \left(\lambda = m_1, t < t_{pb}; \lambda = m_2, t \geq t_{pb} \right) \qquad [4\text{-}13]$$

The values of m_1 and m_2 are tuned with the particle swarm optimization (PSO) algorithm for every experimental run (i.e., each experimental process) to achieve the minimum deviation between the experimentally measured pressures and the theoretically calculated ones. The objective function can be expressed as,

$$O(P) = \sqrt{\frac{1}{N_m} \sum_{i=1}^{N_m} \left(\frac{P_i^{cal-} P_i^m}{P_i^m} \right)^2} \qquad [4\text{-}14]$$

where N_{m} is the number of measured pressure points during the experimental process; P_i^m is the i^{th} measured pressure point; P_i^{cal} is the calculated pressure point corresponding to P_i^m. It is worthwhile noting that the time step in Equation [4-13] cannot be larger than the minimum time interval of the measured pressure points used during the experiments which are normally ranged from 30 to 140 seconds, while it shall also satisfy the requirements of the objective function. Accordingly, the values of time step are selected to be 15 to 60 seconds for different cases to ensure a stable, converged, consistent, and accurate solution. Figure 4-2 shows the flowchart used to solve the mathematical model.

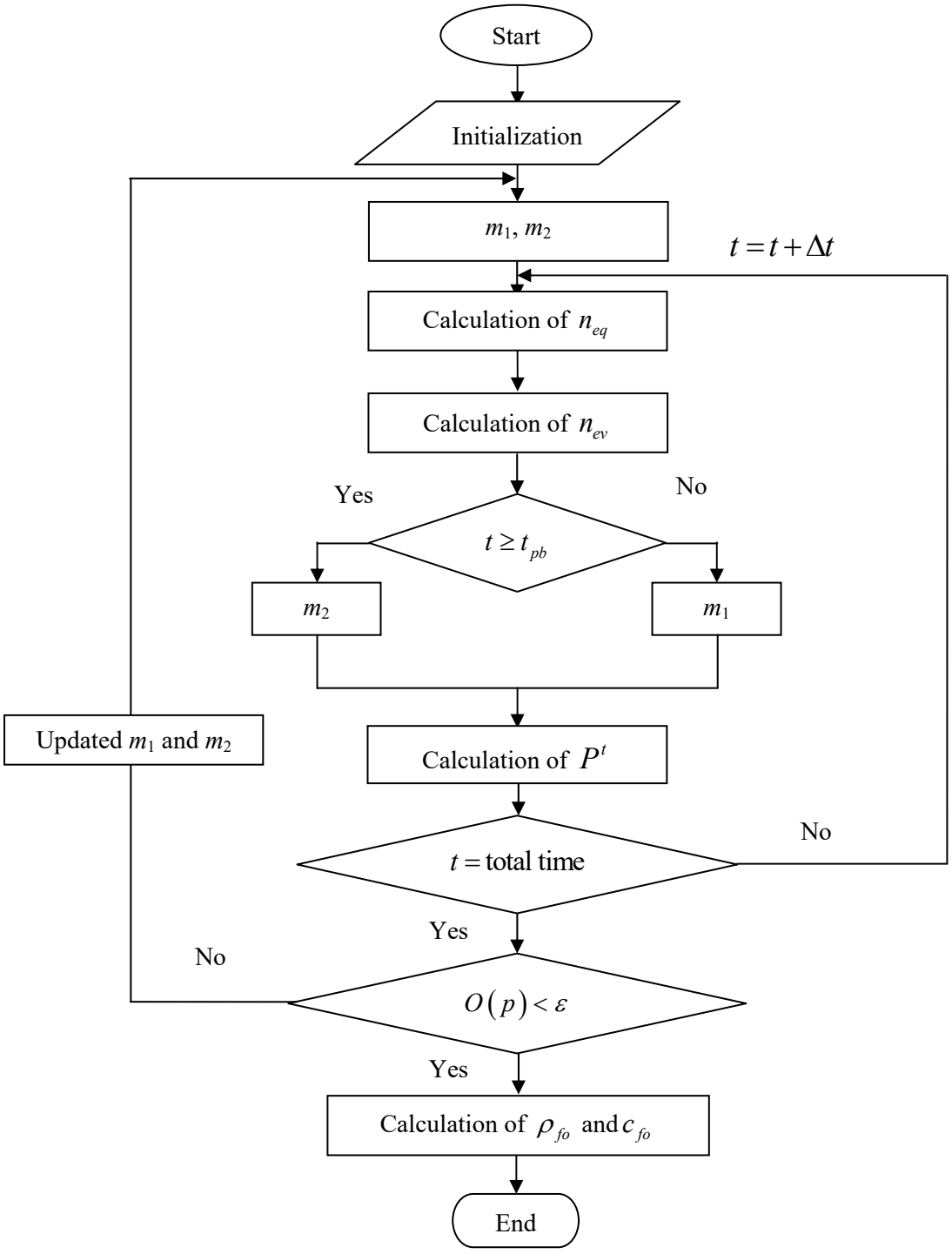

Figure 4-2 Flowchart for matching pressure profile with numerical method

4.4 Results and Discussion

In total, ten constant-composition expansion experiments under nonequilibrium conditions and seven constant-composition expansion experiments under equilibrium conditions have respectively been carried out for CO_2–heavy oil systems, CH_4–heavy oil systems, and CO_2–C_3H_8–heavy oil systems. The details of ten tests with nonequilibrium conditions are listed in Table 4-3, while the measured pressures and expansion volume (i.e., the volume difference between the volume measured at a given time and its initial volume) are depicted in Figures 4-3 to 4-5. Then, two parameters (i.e., apparent critical supersaturation pressure and rebound pressure) are evaluated based on the experimental measurements.

4.4.1 Apparent critical supersaturation pressure

Apparent critical supersaturation pressure (P_s) is defined as the pressure difference between thermodynamic bubblepoint pressure (P_b) and pseudo-bubblepoint pressure (P_{pb}) (Yortsos, 1997). Physically, the higher the apparent critical supersaturation pressure is, the more entrained gas will be contained in the heavy oil. Evidently, P_b can be located in the volume-pressure profiles of equilibrium state where the compressibility of mixture systems has changed sharply. As for pseudo-bubblepoint pressure, its value is essentially equal to the nucleation pressure as mentioned in literature (Sheng *et al*., 1999b) since the linear correlation between GOR and pressure is physically same as that of ratio of the entrained gas to the evolved gas. Also, during constant-composition expansion experiment processes, nucleation pressure can be determined by the turning point of

Table 4-3 Rebound pressures and apparent critical supersaturation pressures of alkane solvent(s)–CO_2–heavy oil systems

Test No.	Components	Temperature (K)	Expansion volume rate (cm^3/hr)	Rebound pressure (kPa)	P_b (kPa)	P_{pb} (kPa)	P_s (kPa)
1	CO_2–heavy oil	303.3	0.3	110	2172	1413	758
2		323.5	0.3	28	2661	2055	607
3		342.8	0.3	0	3351	2682	669
4	CO_2–C_3H_8–heavy oil	303.3	1.5	69	2220	1558	662
5		323.5	1.5	193	2972	2103	869
6		342.8	1.5	34	4054	3696	359
7		342.8	0.8	21	4054	3971	83
8	CH_4–heavy oil	342.8	0.2	0	4061	3061	1000
9		342.8	0.4	0	4061	2717	1344
10		342.8	0.8	0	4061	2392	1669

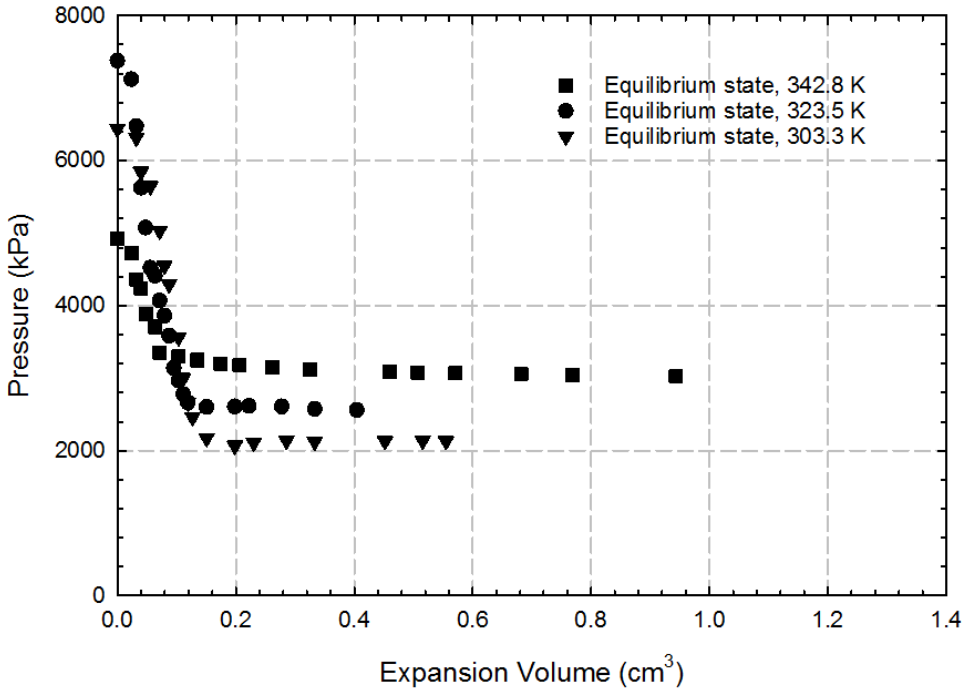

(a)

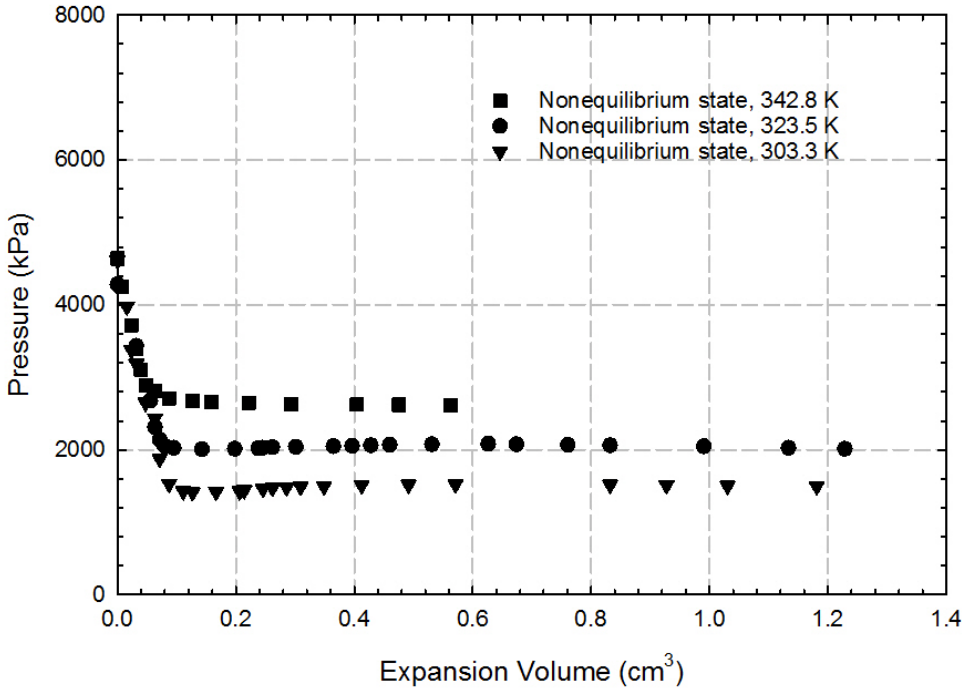

(b)

Figure 4-3 Measured pressure as a function of expansion volume for CO_2–heavy oil systems under **(a)** equilibrium conditions and **(b)** nonequilibrium conditions with expansion rate of 0.3 cm^3/hr

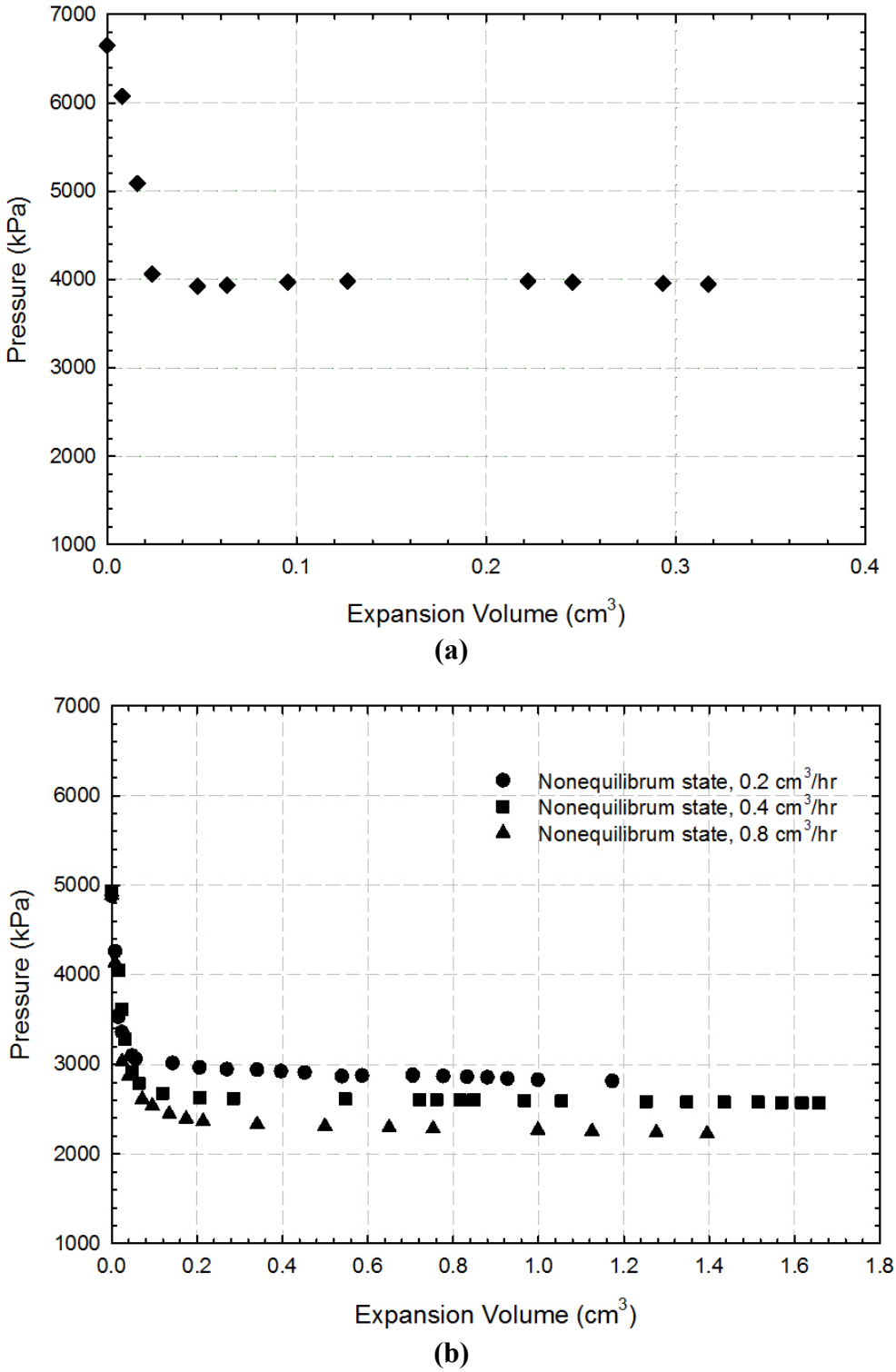

Figure 4-4 Measured pressure as a function of expansion volume at 342.8 K for CH_4–heavy oil systems under **(a)** equilibrium conditions and **(b)** nonequilibrium conditions with different expansion rates

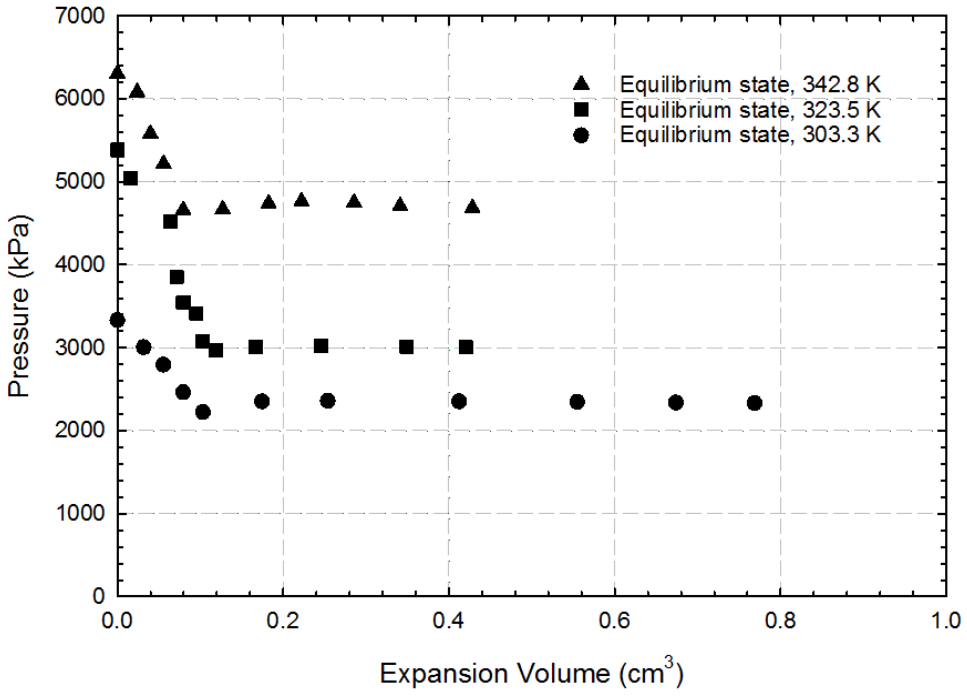

(a)

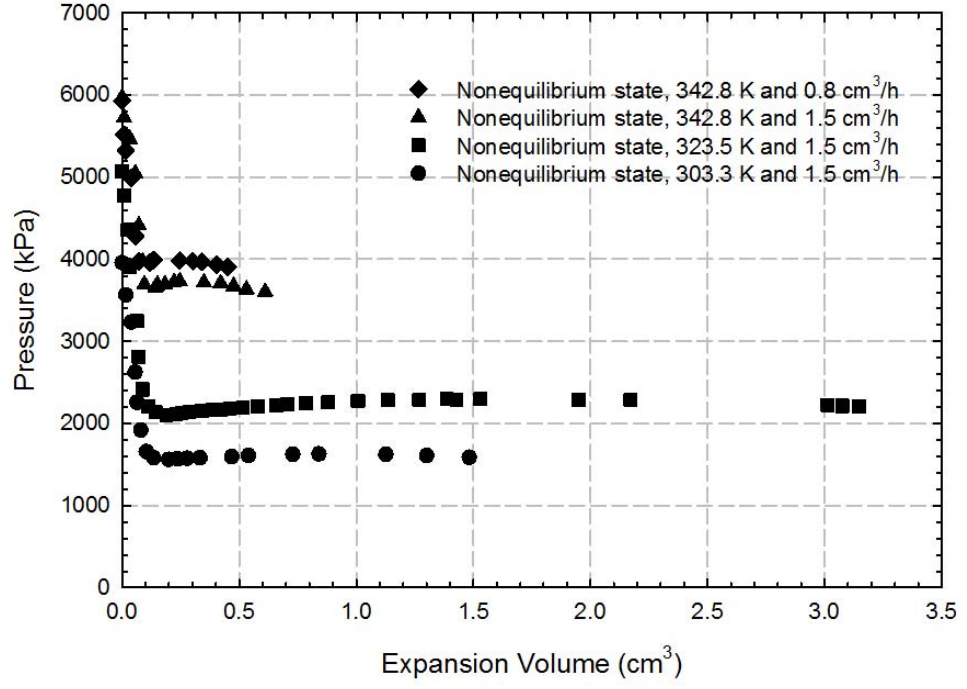

(b)

Figure 4-5 Measured pressure as a function of expansion volume for CO_2–C_3H_8–heavy oil systems under **(a)** equilibrium conditions and **(b)** nonequilibrium conditions with different expansion rates

compressibility of mixture (Firoozabadi *et al*., 1992). Therefore, the pseudo-bubblepoint pressure under nonequilibrium conditions can be located with the method similar to finding P_b in the volume-pressure profiles under equilibrium conditions (see Figures 4-3 to 4-5).

As can be seen from Table 4-3 and Figure 4-6, apparent critical supersaturation pressure monotonically increases with an increase in expansion rate for CH_4–heavy oil systems and CO_2–C_3H_8–heavy oil systems. This is in a good agreement with those reported in the literature (Firoozabadi *et al*., 1992; Bennion *et al*., 2003). Meanwhile, apparent critical supersaturation pressure is also found to be a function of mole fraction of alkane solvent(s) and CO_2. More specifically, the difference of apparent critical supersaturation pressure between Tests #7 and 10 is found to be 1585.79 kPa (see Table 4-3), though both tests are conducted at the same expansion volume rate. As for Test #7, a higher mole fraction of light components (i.e., solvents and CO_2) is considered as the main contribution to the relatively low apparent critical supersaturation pressure. A similar relationship has been found and formulated elsewhere (Sahni *et al*., 2004).

4.4.2 Rebound pressure

The difference between pseudo-bubblepoint pressure and the maximum pressure after the pseudo-bubblepoint pressure is defined as the rebound pressure in this study. In general, there is an increase in pressure after the pseudo-bubblepoint pressure is reached. The corresponding rebound pressures in Tests #1-10 are tabulated in Table 4-3. More

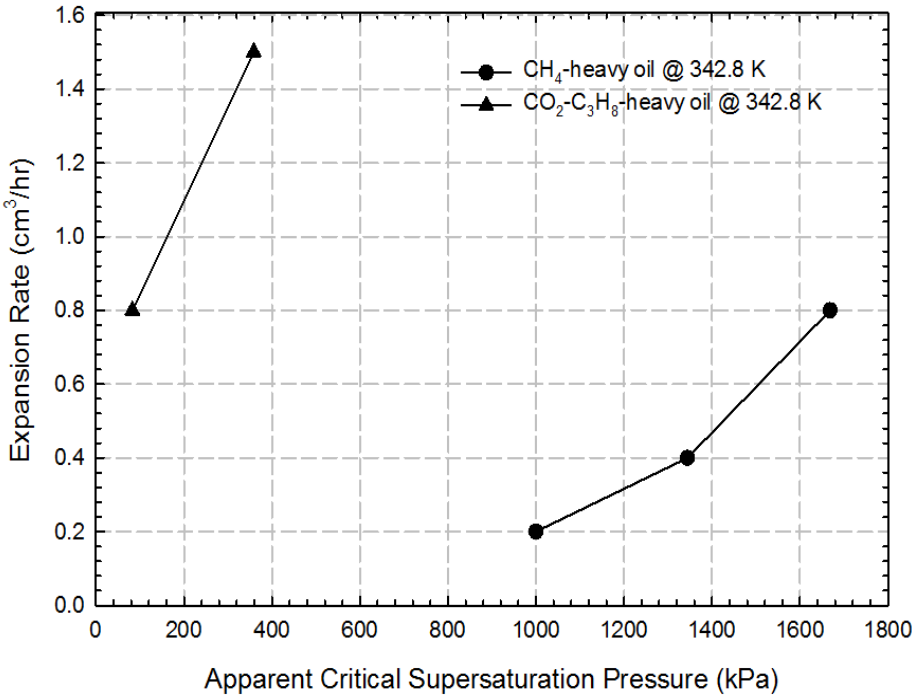

Figure 4-6 Expansion rate as a function of apparent critical supersaturation pressures for CH_4–heavy oil systems and CO_2–C_3H_8–heavy oil systems at 342.8 K, respectively

specifically, it is from Tests #6 and 7 found that a larger expansion volume rate causes a higher rebound pressure (see Figure 4-7). Compared to Test #7, the measured pressures of Test #6 are lower at the same volume (see Figure 4-5), indicating that the amount of the evolved gas from the oleic mixture with a lower expansion volume rate (Test #7) is larger than that with a higher expansion volume rate (Test #6). Such a difference results in a higher concentration gradient between gas bubble and liquid mixture in Test #6. Then, a relatively higher bubble growth rate can be generated to obtain a larger rebound pressure on the basis of diffusion-induced gas bubble growth theory (Rosner *et al*., 1972).

As for CO_2–heavy oil systems, the rebound pressures gradually and monotonically decline with an increase in temperature due to the increased mass transfer rate from liquid to gas, whereas, as for CO_2–C_3H_8–heavy oil systems, they can normally reach their respective peak values (see Figure 4-7). The latter may be ascribed to the fact that preferential diffusion of CO_2 and C_3H_8 in heavy oil systems (Li and Yang, 2016; Zheng *et al*., 2016a; Zheng and Yang, 2016). In addition, rebound pressures of CH_4–heavy oil system are found to be zero for three tests, implying that the amount of evolved CH_4 is too weak to impose a significant impact on the rebound pressure. This may be due to the fact that pressure increase from the cumulative volume of evolved gas cannot compensate the pressure decline caused by the expanded volume of the mixture. Therefore, a slow pressure-decline rather than a rebound pressure is generated under nonequilibrium conditions, compared with those of CO_2/CO_2–C_3H_8 heavy oil systems. Similar results for CH_4–*n*-$C_{10}H_{22}$ systems have been documented elsewhere (Firoozabadi *et al*., 1992).

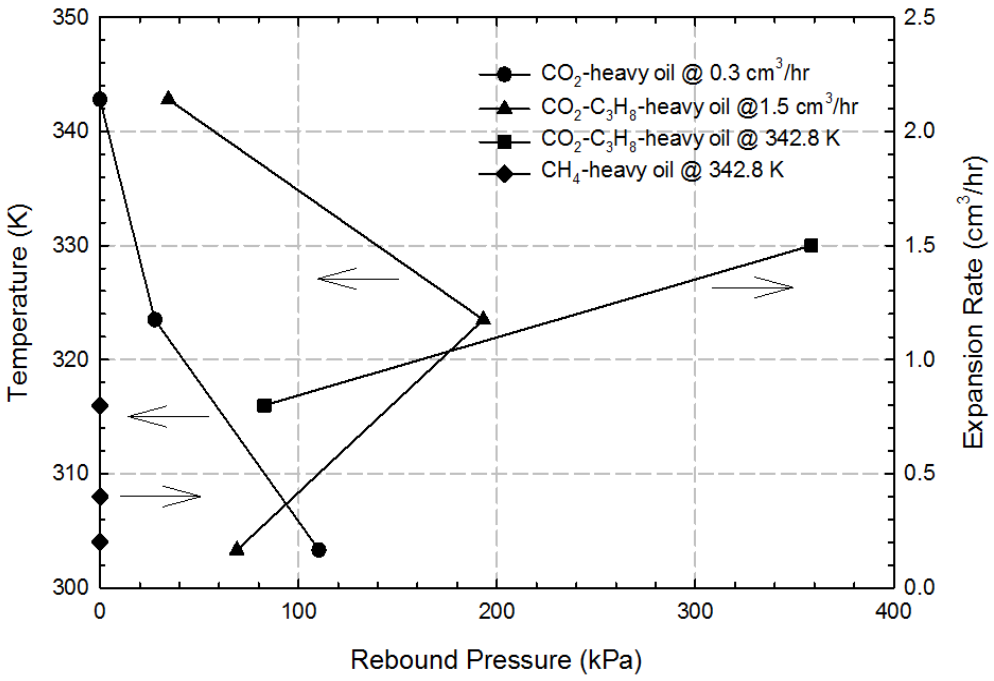

Figure 4-7 Rebound pressures at different expansion rates and temperatures for CH_4–heavy oil systems, CO_2–heavy oil systems, and CO_2–C_3H_8–heavy oil systems, respectively

It is noted that small pressure rebounds can also be observed in pressure-volume profiles under equilibrium conditions (Figure 4-5a). This may be caused by a relatively large withdrawal rate for the CO_2–C_3H_8–heavy oil systems, though an optimized withdrawal rate has been identified and utilized after several trial withdrawal rates.

4.4.3 Properties of foamy oil

Based on the matching results of experimental measurements (see Figures 4-8 to 4-10), properties (i.e., compressibility and density) of all alkane solvent(s)–CO_2–heavy oil systems are calculated. Also, the compressibility and density of CH_4–heavy oil systems have been compared under equilibrium and nonequilibrium conditions.

1) Compressibility

Three regimes can be observed in the pressure-compressibility profiles of foamy oil (see Figures 4-11 to 4-13), which are similar to those of conventional oil (Al-Mahrhoun, 2009). As for foamy oil, the pressure range of Regime #1, however, starts from its initial pressure to the pseudo-bubblepoint pressure. The value of compressibility is found to be 0.9×10^{-6} kPa^{-1}, which is in a good agreement with those reported in literature for similar heavy oils (Dusseault, 2001). This means that the compressibility in Regime #1 only represents characteristics of the liquid phase due to an extremely small volume of gas bubble, though gas starts to nucleate at the thermodynamic bubblepoint pressure (Arora and Kovscek, 2003). In Regime #2, a sudden change of compressibility is resulted from a quick expansion of the entrained gas on the pseudo-bubblepoint pressure. Similar finding has also been documented in the literature (Sheng *et al*., 1995). It is worthwhile noting

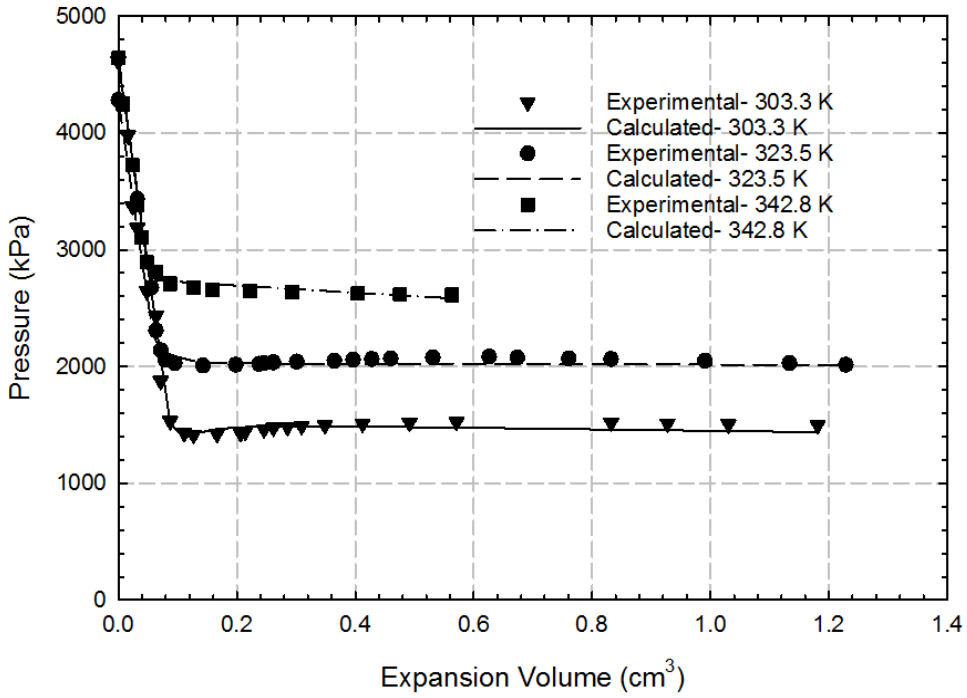

Figure 4-8 Measured and calculated pressure curves of CO_2–heavy oil systems as a function of expansion volume at an expansion rate of 0.3 cm^3/hr

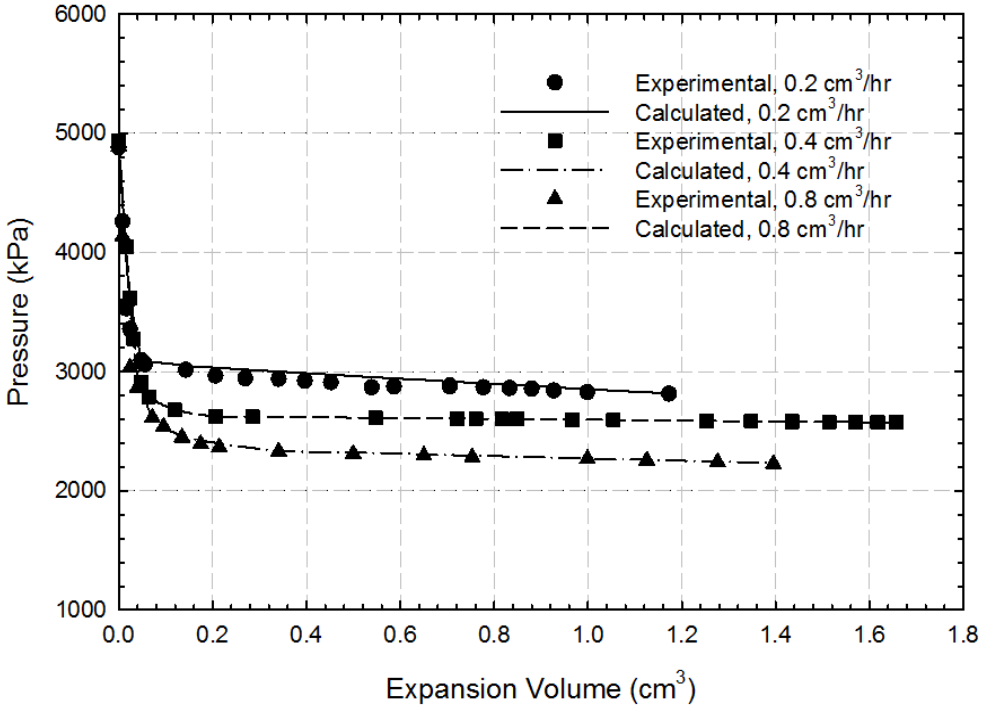

Figure 4-9 Measured and calculated pressure curves of CH_4–heavy oil systems at 342.8 K

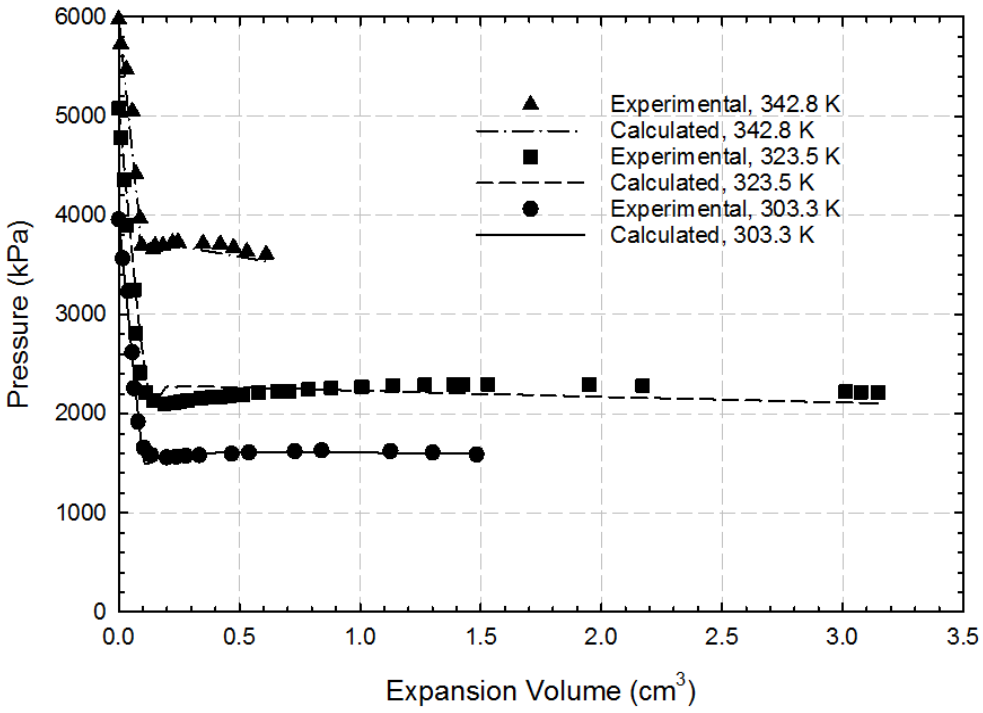

Figure 4-10 Measured and calculated pressure curves of CO_2–C_3H_8–heavy oil systems as a function of expansion volume at an expansion rate of 1.5 cm^3/hr

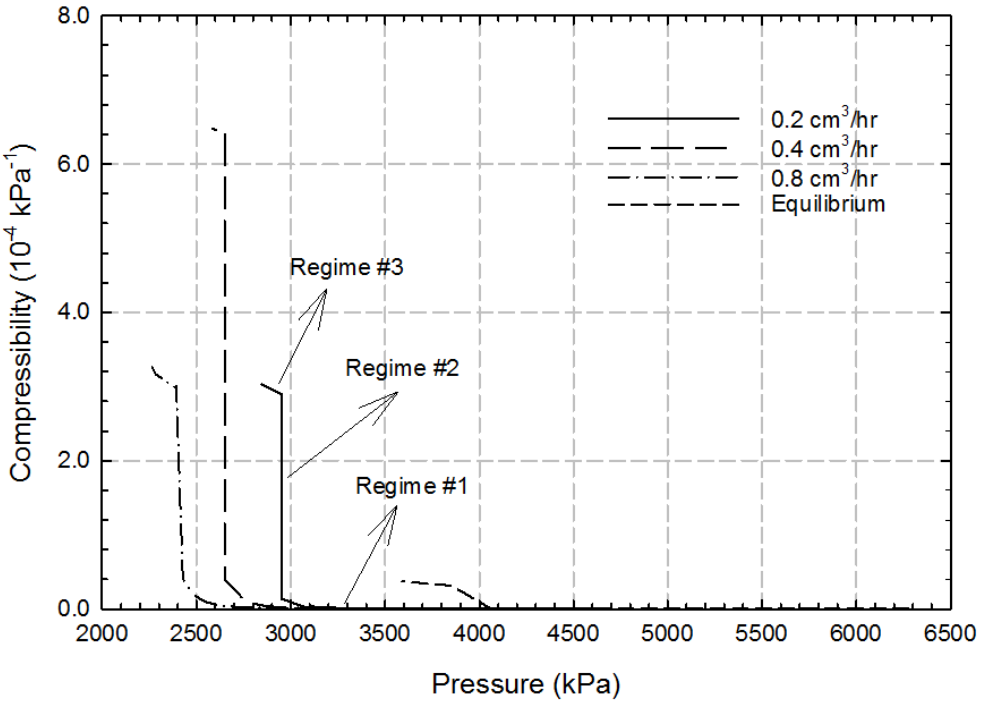

Figure 4-11 Foamy oil compressibility of CH_4–heavy oil systems as a function of pressure at 342.8 K

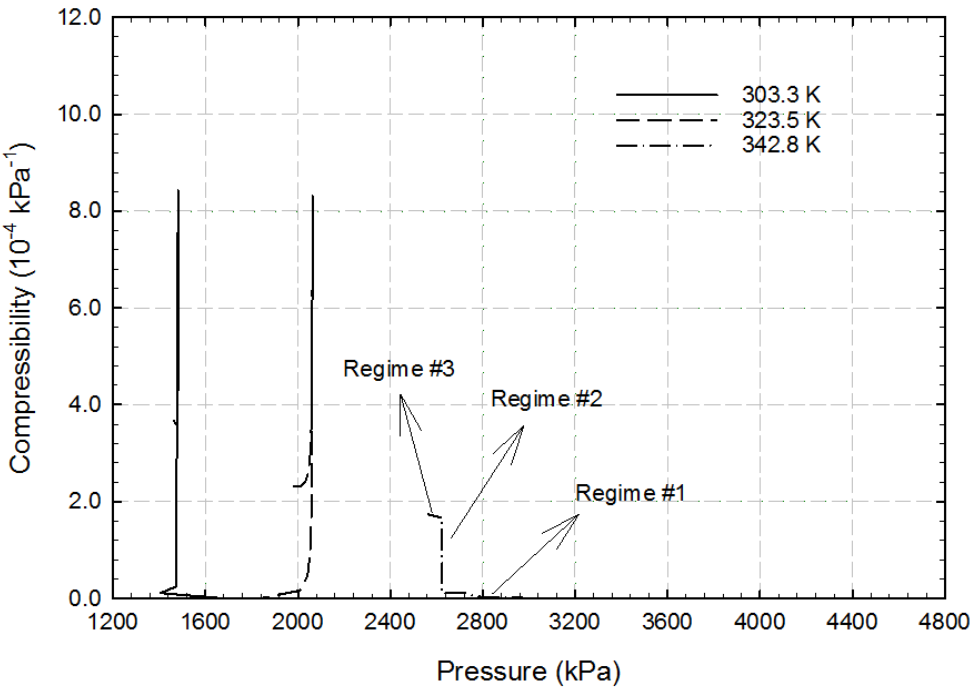

Figure 4-12 Foamy oil compressibility of CO_2–heavy oil systems as a function of pressure at an expansion rate of 0.3 cm^3/hr

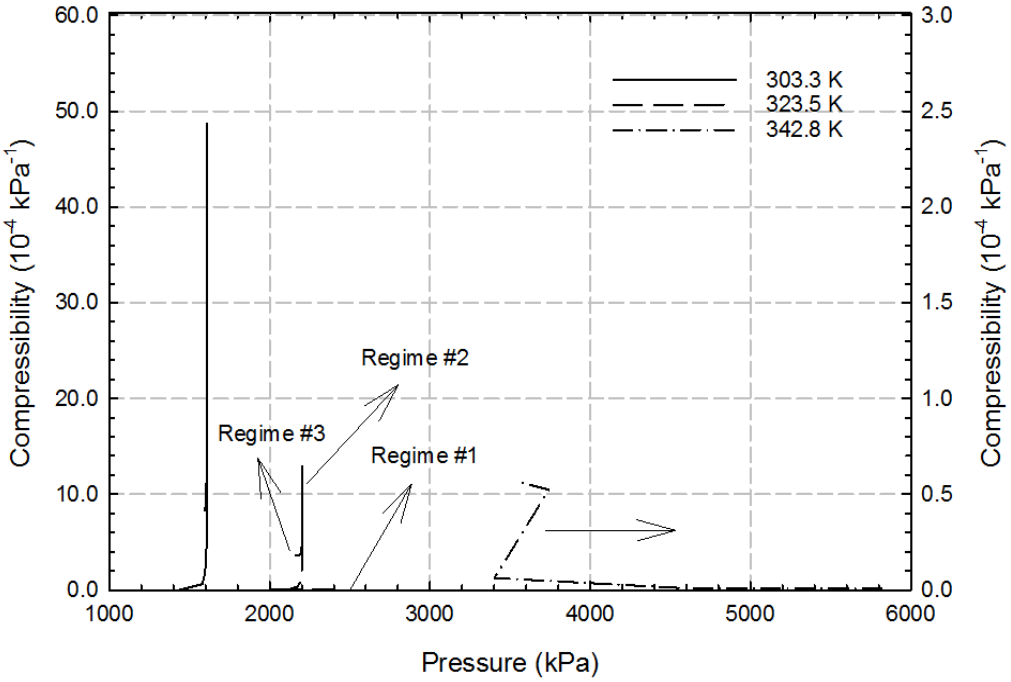

Figure 4-13 Foamy oil compressibility of CO_2–C_3H_8–heavy oil systems as a function of pressure at an expansion rate of 1.5 cm^3/hr

that rebound pressures in Tests #1–2 and Tests #4–7 cause a pressure reverse in the pressure-compressibility curve. There exists a sharp peak of compressibility in a range of 1.0–5.0×10^{-3} kPa^{-1}, depending on the pressure gradient that is gradually decreased with time during the occurrence of pressure rebounding. Subsequently, the pressure gradient is increased so that the compressibility is reduced to the values less than 8×10^{-4} kPa^{-1}, when pressure of the entire system begins to decrease again. In general, Regime #3 of foamy oil shows an increase in compressibility with a decrease in pressure since gas and oil coexist in the oleic phase. This finding is similar to that of the conventional oils (Adepoju, 2006). In particular, a decrease in temperature is found to cause an increase in compressibility in Regime #3 (see Figures 4-12 and 4-13). This may be attributed to the fact that the viscosity of heavy oil at a lower temperature is relatively larger so as to delay gas bubbles that are to be escaped from the oleic mixture during the experimental processes, resulting in a larger mole fraction of alkane solvent(s) or CO_2 and thus a higher compressibility of foamy oil.

2) Density

By only considering liquid compressibility of the saturated-heavy oil systems, density of foamy oil is found to gradually decrease when the pressure declines from its initial pressure to the pseudo-bubblepoint pressure. Subsequently, the density sharply declines because the volume of the entrained gas in the oleic phase is dramatically increased once the pseudo-bubblepoint pressure is reached. Similar phenomena are also observed for CH_4–heavy oil system (Mastmann *et al*., 2001; Bennion *et al*., 2003; Chen *et al*., 2015). It is noteworthy that some density-pressure profiles (see Figures 4-14 and 4-15) exhibit

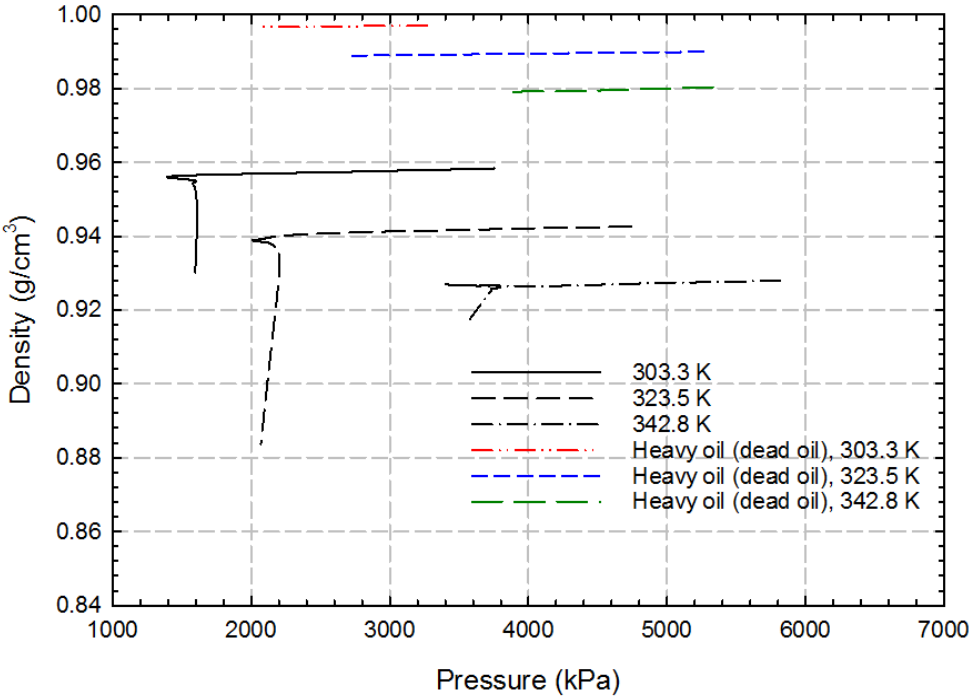

Figure 4-14 Foamy oil density of CO_2–C_3H_8–heavy oil systems at an expansion rate of 1.5 cm^3/hr and dead oil density as a function of pressure

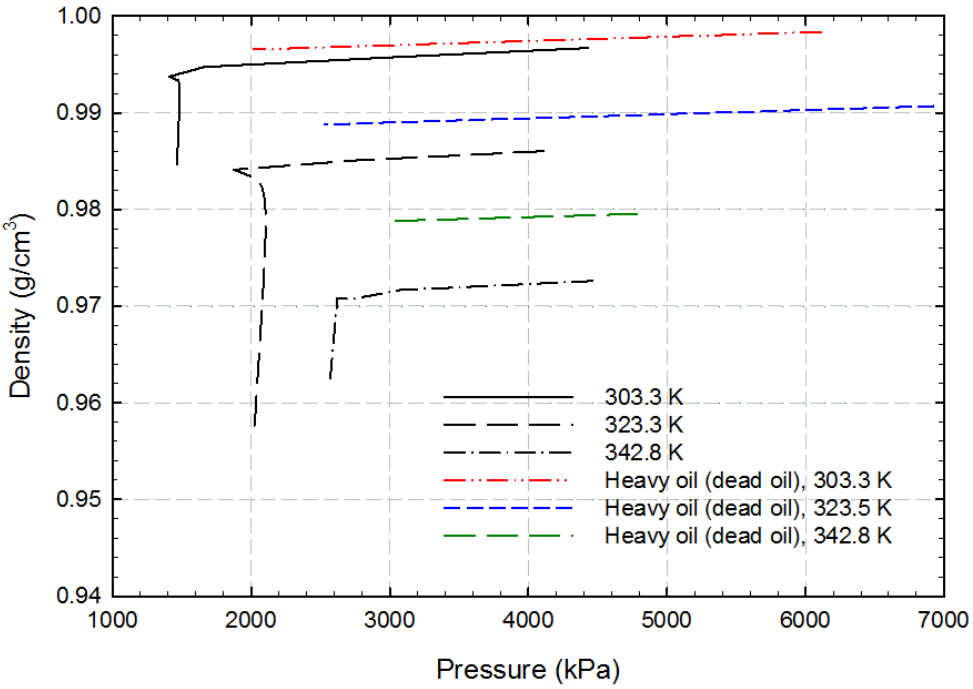

Figure 4-15 Foamy oil density of CO_2–heavy oil systems at an expansion rate of 0.3 cm^3/hr and dead oil density as a function of pressure

slight inward shapes at the turning points of the foamy oil density. This is mainly resulted from the rebound pressure after the pseudo-bubblepoint pressure.

Since the turning point of density occurs at the pseudo-bubblepoint pressure, either a high temperature or a low expansion volume rate leads to a large pressure pertaining to the density turning point. A higher temperature also results in less density at the same pressure during the experimental processes due mainly to a high pseudo-bubblepoint pressure and thermal expansion. In addition, the slopes of Tests #8–10 after the pseudo-bubblepoint pressure are found to be similar (see Figure 4-16), indicating that, once the pseudo-bubblepoint is reached at a certain temperature, the expansion rate does not impose a significant impact on the decline rate of density.

3) Comparison of properties under nonequilibrium and equilibrium conditions

In addition to being greatly affected by nonequilibrium conditions, foamy oil properties are a function of amount of the entrained gas, or essentially, time. Compared with those of equilibrium conditions, some characteristic phenomena are observed to be exclusively exhibited by foamy oil. Although similar three regimes for compressibility under equilibrium and nonequilibrium conditions can be observed (see Figure 4-11), three main differences do exist in all the regimes, i.e., a) ending-point pressure of Regime #1; b) shape of Regime #2; and c) the value of compressibility of Regime #3. Under equilibrium conditions, Regime #1 generally ends up at the thermodynamic bubblepoint pressure from its initial pressure rather than the pseudo-bubblepoint pressure of foamy oil (see Figure 4-11). The difference between two ending-points of equilibrium and non-

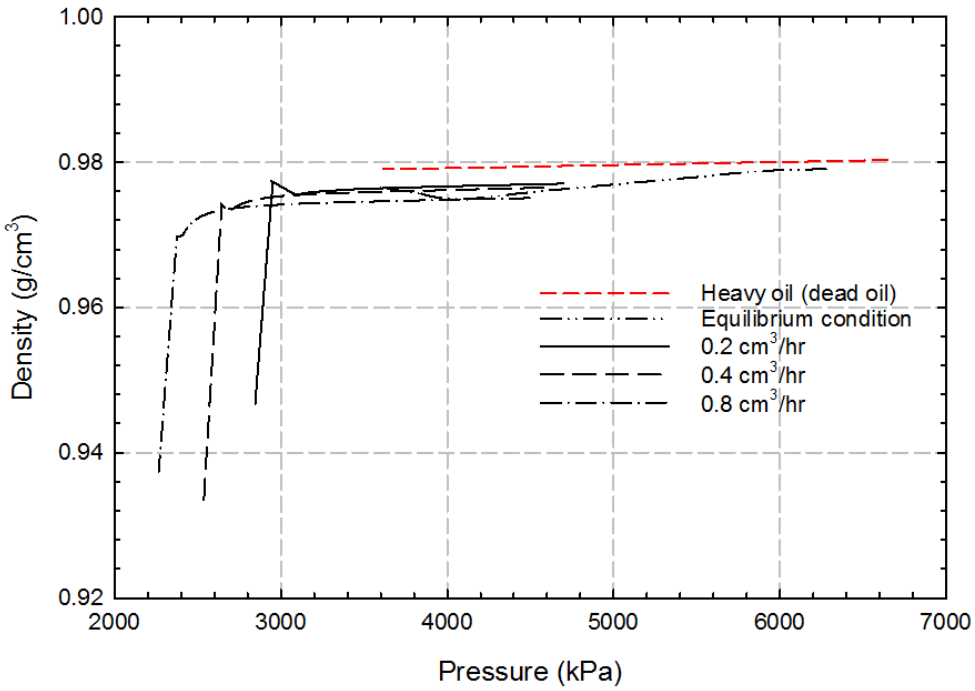

Figure 4-16 Foamy oil density of CH_4–heavy oil systems and dead oil density at 342.8 K as a function of pressure

equilibrium conditions is the so-called apparent critical supersaturation pressure as mentioned previously, because both ending-points are corresponding to P_b and P_{pb}, respectively. Also, a non-linear pressure reverse originated from the rebound pressure is observed at the beginning of Regime #2. Traditionally, such a non-linear pressure reverse under nonequilibrium conditions is replaced by a linear line under equilibrium conditions (see Figure 4-11). In Regime #3, compressibility under equilibrium conditions below bubblepoint pressure is found to be much larger than that above bubblepoint pressure because of the evolution of the first bubble of gas (Yortsos, 1997). As such, the nonequilibrium behaviour is enhanced by the increasingly entrained gas since foamy oil compressibility is mainly dependent on the amount of the entrained gas (Sheng, 1997). This may lead to the fact that the compressibility under nonequilibrium conditions after an abrupt increase in Regime #2 is much larger than that under equilibrium conditions (see Figure 4-11).

As for density, when pressure is higher than pseudo-bubblepoint pressure, density of foamy oil is essentially equal to its equilibrium value on account of negligible volume of gas bubbles. Meanwhile, both densities of equilibrium and nonequilibrium conditions are smaller than that of dead oil due to dissolution of solvent(s)/CO_2 into the heavy oil. The turning point of density for foamy oil, physically, is located in the pseudo-bubblepoint pressure rather than the thermodynamic bubblepoint pressure. It has been well recognized that density under equilibrium conditions begins to gradually increase when pressure is lower than P_b owing to the decline of mole fraction of light components. This is opposite to those under nonequilibrium conditions (see Figure 4-16). Effect of rebound pressure

on the density inevitably causes a slightly inward change to the turning points of foamy oil density, while, a simply monotonic decrease is evidently observed for dead oil because there is no phase change during the entire process.

4.5 Summary

A novel and pragmatic technique has been developed for experimentally and theoretically describing the nonequilibrium phase behaviour of alkane solvent(s)–CO_2–heavy oil systems under reservoir conditions. Based on the experimental results, it is found that a larger expansion volume rate causes a higher rebound pressure. Not only is the apparent critical supersaturation pressure increased with expansion rate, but also decreased with the mole fraction of either solvent or CO_2. There exist good agreements between the experimentally measured and theoretically calculated volume-pressure profiles under nonequilibrium conditions, indicating that the newly proposed mathematical models can be used to accurately quantify the nonequilibrium phase behaviour of the aforementioned systems. An inward shape in the pressure-density profiles is found due to the rebound pressure originated from the quick increase of the entrained gas after pseudo-bubblepoint pressure. Similarly, the rebound pressure also leads to a nonlinear pressure reverse in the sudden change on pressure-compressibility profiles, compared with the simple linear line which is expected for conventional oils. Such a sudden change in compressibility is located at the pseudo-bubblepoint pressure of foamy oils rather than the thermodynamic bubblepoint pressure.

CHAPTER 5 QUANTIFICATION OF NONEQUILIBRIUM PHASE BEHAVIOUR AND PHYSICAL PROPERTIES OF FOAMY OIL UNDER CONSTANT PRESSURE DECLINE RATE

5.1 Introduction

In this chapter, nonequilibrium phase behaviour under constant pressure decline rate is investigated (Shi and Yang, 2017a; 2017b; 2017c). Experimentally, a set of CCE experiments with constant pressure decline rate were implemented to scrutinize the nonequilibrium phase behaviour of solvent–CO_2–heavy oil systems. Theoretically, the amount of evolved gas formulated as a function of time is incorporated into the real gas equation to quantify the nonequilibrium phase behaviour of the aforementioned systems. Physical properties of foamy oil (i.e., compressibility and density) are determined, respectively, based on the attained dynamic amount of evolved gas and entrained gas. Also, the comparison of physical properties of foamy oil under constant pressure decline rate and constant volume expansion rate are analyzed and discussed.

5.2 Experimental

5.2.1 Materials

The dead heavy oil sample used in the CCE experiments with constant pressure decline rate is same as that in Chapter 4. Also, CO_2, CH_4, and C_3H_8 purchased from Praxair are employed to saturate heavy oil with stated purities of 99.998 mol%, 99.97 wt% and 99.5 wt%, respectively.

5.2.2 Experimental procedure

With the PVT setup as described in previous chapters, three feeds involving CO_2–heavy oil systems, CH_4–C_3H_8–heavy oil systems and CH_4–CO_2–heavy oil systems were tested with the equilibrium and nonequilibrium CCE experiments. The composition of each component in these three feeds can be seen in Table 5-1. The experimental procedure of CH_4–CO_2–heavy oil systems is introduced in details as an example for the implemented CCE tests in this chapter.

(1) The PVT cell and all the flow-tubes are completely cleaned and rinsed with kerosene before conducting experiment. Then, compressed air is used to flush the parts contacted with kerosene for at least one hour to get rid of the kerosene residuals;

(2) The vacuum pump is employed to evacuate the PVT cell and flow-tubes to eliminate the impurity effect of air;

(3) The pressurized methane flows into the PVT cell directly from the gas cylinder. Then, CO_2 contained in a gas cylinder would be injected into the PVT cell to form the gas mixture. The sample of CH_4-CO_2 mixture was collected with a pre-vacuumed gas sampler (Swagelok, Canada) for compositional analysis with gas chromatography (GC). Lastly, the heavy oil is slowly introduced into the PVT cell until the mole fraction of each component in the mixture satisfies the prespecified values;

(4) Once all the experimental fluids are contained in the PVT cell, the inlet valve is closed to isolate the CH_4–CO_2–heavy oil systems. Subsequently, the temperature and pressure of experimental fluids are increased to the prespecified values. Then, a mixer at the bottom of PVT cell starts to stir

Table 5-1 Compositions of alkane solvent(s)–CO_2–heavy oil systems

Feed No.	Compositions (%)			
	CO_2	CH_4	C_3H_8	Heavy oil
4	30.4	0.0	0.0	69.6
5	0.0	8.8	29.0	62.2
6	14.1	8.8	0.0	77.1

the mixture for more than 30 hours to ensure the establishment of equilibrium state;

(5) Prior to the measurement, the mixer is turned off to stop stirring. Then, the pressure is gradually decreased with a constant decline rate controlled by the slowly enlarged volume of experimental fluids. Then, the height and pressure of experimental fluids are simultaneously recorded. Consequently, the relationship between the volume of CH_4–CO_2–heavy oil systems and pressure under nonequilibrium condition can be obtained. Lastly, at the end of the experiment, the sample of free gas released from the liquid phase is collected with a vacuumed gas sampler for the GC compositional analysis

In addition, the procedures about equilibrium state are similar to those under nonequilibrium state, except that the mixer is kept on stirring the fluids during the experimental processes as described in Step #5. As for the CO_2–heavy oil systems and CH_4–C_3H_8–heavy oil systems, similar experimental procedures are followed, though GC compositional analyses of gas samples are not conducted for Feeds #4 and 5.

5.3 Theoretical Formulations

5.3.1 Mathematical model

The mathematical formulations in this chapter are similar as those introduced in Chapter 4. Based on the real gas equation, the volume of gas phase can be described as follows,

$$V_g = \frac{znRT}{P(t)} \qquad [5\text{-}1]$$

Substituting Equations [4-1], [4-3a] and [5-1] into Equation [4-2], the relationship between pressure and volume of experimental fluids with a constant pressure decline rate is derived as follows under the nonequilibrium conditions,

$$V = \frac{zRTn_{eq}}{P_i - d_p t}\left(\frac{t}{t_{eq}}\right)^{\lambda} + V_{li}\left(1 + d_p c_t t\right) \quad \left(\lambda = m_1, t < t_{pb}; \lambda = m_2, t \geq t_{pb}\right) \qquad [5\text{-}2]$$

where d_p is the pressure decline rate.

The amount of entrained gas can be attained with Equation [4-5] and [4-6]. Meanwhile, the details about PR EOS and properties of foamy oil can be seen in Chapter 3 and 4, respectively.

5.3.2 Numerical solution

The entire experimental duration is discretized into *n* time steps. The particle swarm algorithm (PSO) is employed to optimize the parameters required in Equation [5-2] in order to reduce the deviation between the calculated total volumes of experimental fluids and the measured ones. Then, the time-dependent physical properties are able to be attained by minimizing the deviation associated with the amounts of evolved and entrained gas. Figure 5-1 briefly depicts the aforementioned computational procedures. The specific procedures are detailed as follows,

(1) The physical parameters, such as temperature, pressure and volume at the beginning of experiments, are input to initialize the computation;

(2) The values of tuned parameters, m_1, m_2 and t_{eq}, are assigned by using the PSO algorithm. Then, the amount of evolved gas n_{eq} under equilibrium

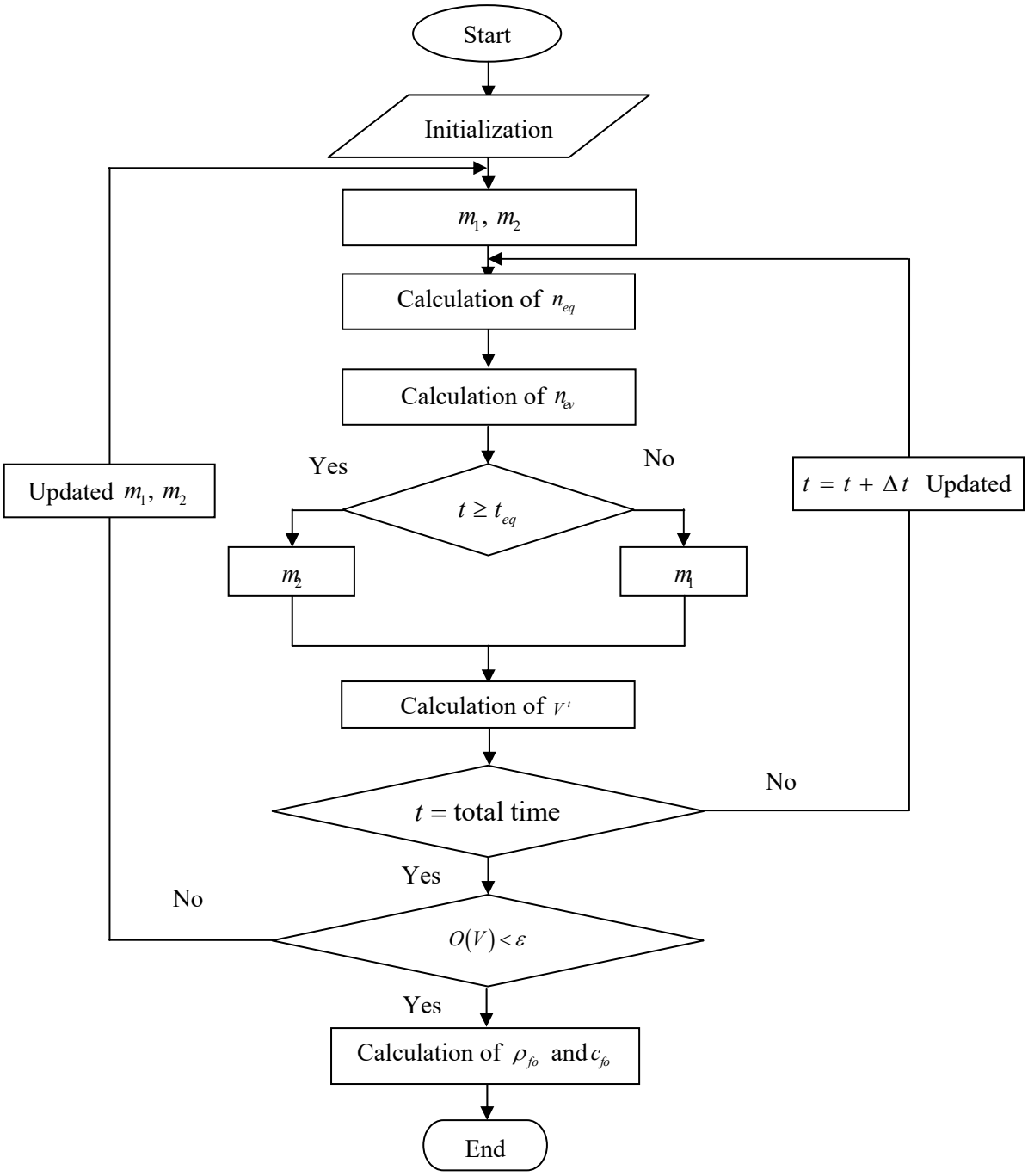

Figure 5-1 Flowchart for matching volume-pressure profile with numerical method

conditions is obtained by conducting two-phase flash calculation with PR EOS;

(3) The volume of fluids system is calculated with Equation [5-2], while the corresponding amounts of evolved and entrained gas are computed. The calculations are terminated once the time reaches the experimental duration;

(4) The objective function utilized to determine the acceptable matching criteria is defined as follows,

$$O(V)=\sqrt{\frac{1}{N_m}\sum_{i=1}^{N_m}\left(\frac{V_i^{cal}-V_i^m}{V_i^m}\right)^2} \qquad [5\text{-}3]$$

where N_m is the number of measured volume points during the experimental process; V_i^m is the i^{th} measured total volume point; V_i^{cal} is the calculated volume point corresponding to V_i^m. Once the objective function $O(V)$ is smaller than the pre-specified tolerance, the calculation will be terminated and thus the calculated results can be output as the optimal ones. Otherwise, iteration will be implemented by repeating Steps #2–4 till the updated value of objective function is less than the tolerance.

(5) The time-dependent compressibility and density of foamy oil are computed with Equations [4-7] and [4-9], respectively, when the amount of entrained gas is obtained on the basis of the optimal results in Steps #2–4.

5.4 Results and Discussion

The equilibrium and nonequilibrium phase behaviour of three alkane solvent–CO_2–heavy oil systems, i.e., CO_2–heavy oil, CH_4–C_3H_8–heavy oil, and CH_4–CO_2–heavy oil were

experimentally evaluated. To be more specific, prior to recording the nonequilibrium phase behaviour, five CCE experiments with constant volume expansion rate were performed under equilibrium conditions in order to measure the bubblepoint pressures for the aforementioned systems. Then, six CCE experiments with constant pressure decline rate are carried out under nonequilibrium conditions (Table 5-2). Also, the measured volume–pressure profiles of both equilibrium and nonequilibrium experiments are plotted in Figure 5-2. Subsequently, the newly proposed mathematical model is used to minimize the deviation between the measured total volume and its calculated value under nonequilibrium conditions. Good agreements have been accomplished for all the scenarios (see Figure 5-2). The parameters associated with nonequilibrium phase behaviour and physical properties of foamy oil are then analyzed.

5.4.1 Apparent critical supersaturation pressure

1) Effect of pressure decline rate

As can be seen in Table 5-2, pressure decline rate imposes a great impact on the apparent critical supersaturation pressure. Pressure decline rates of 20 kPa/min and 12 kPa/min result in a 900 kPa pressure difference of apparent critical supersaturation pressure in CO_2–heavy oil systems. In other words, the apparent critical supersaturation pressure increases with an increase in pressure decline rate. Similar findings were also found in CCE experiments with constant expansion rate. Such phenomenon may be explained by the fact that fewer nuclei with critical size and slower gas bubble growth rate with a higher pressure decline rate is generated, compared to those with a lower pressure decline rate under the same supersaturation pressure.

Table 5-2 Experimental results of CCE tests

Test No.	Components	Temperature (K)	Pressure decline rate (kPa/min)	P_b (kPa)	P_{pb} (kPa)	P_s (kPa)	Average gas exsolution rate (10^{-6} mol/kPa)	$\frac{P_{pb}-P_e}{P_{pb}}$
11	CO_2–heavy oil	303.3	12	2250	2100	150	0.852	0.40
12		303.3	20	2250	1200	1050	1.423	0.41
13		323.4	20	2750	2150	600	0.756	0.26
14	CH_4–C_3H_8–heavy oil	323.4	20	2900	2500	400	2.156	0.32
15		342.7	20	5000	4700	300	1.298	0.06
16	CH_4–CO_2–heavy oil	342.7	20	4978	3516	1462	2.298	0.64

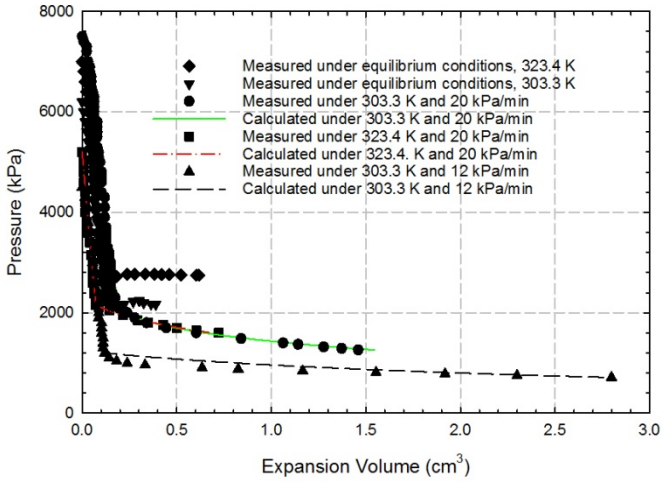

(a)

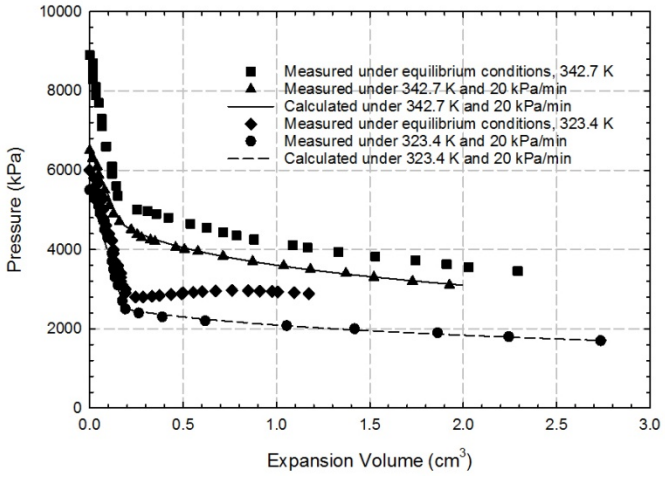

(b)

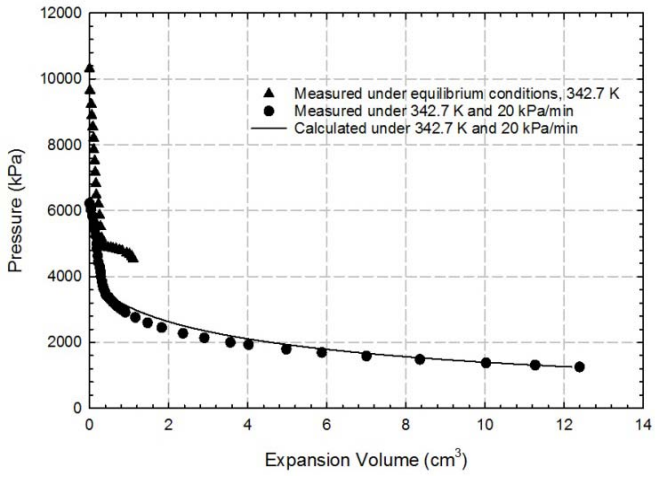

(c)

Figure 5-2 Pressure as a function of expansion volume for **(a)** CO_2–heavy oil systems, **(b)** CH_4–C_3H_8–heavy oil systems, and **(c)** CH_4–CO_2–heavy oil systems under equilibrium and nonequilibrium conditions

Based on the classical nucleation theory, when the supersaturation pressure and temperature are constant, the nucleation rate is time-independent (Bories and Prat, 2002; Delale *et al*., 2003; Chernov *et al*., 2014). The amounts of nuclei with critical size can be simply calculated with time and nucleation rate. Although a continuously increased supersaturation pressure (e.g., the operating conditions of the experiments in this study) makes the nucleation rate to be a complicated time-dependent variable, it still can be approximately calculated by a quasi-stationary nucleation rate related to the instantaneous supersaturation pressure (Bories and Prat, 2002), which is constrained by a limited slow pressure decline rate (i.e., $\ll 6\times10^{4}$ kPa/min : Kashchiev and Firoozabadi, 1993). Evidently, it takes a shorter time to achieve a certain supersaturation pressure with a faster pressure decline rate, implying that fewer amounts of nuclei with critical size are formed in the supersaturated heavy oil, compared to those generated with a slower pressure decline rate. On the other hand, theoretically, when the radius of a gas embryo in the liquid is increased to be the critical radius, the addition of only one molecule of dissolved gas to the gas embryo is enough to trigger a spontaneous growth of gas bubble (Jones *et al*., 1999). In general, coalescence as a result of collision from the Brownian motion and diffusion of dissolved gas are identified as two main mechanisms accounting for starting such gas bubble growth (Lillico *et al*., 2001). Fewer nuclei with critical size, as previously explained, mean a smaller density of gas bubbles in the heavy oil under the faster pressure decline rate. Hence, the probability of coalescence occurrence is correspondingly lowered due mainly to a large averaged spacing among gas nuclei with critical size (Lillico *et al*., 2001). Accordingly, the rate of phase transformation is decreased. However, a high supersaturation pressure can effectively decrease the

nucleation energy barrier and further increase the nucleation rate (Jones *et al*., 1999; Geilikman and Dusseault, 1999). This means that a high apparent supersaturation pressure is indispensable under a faster pressure decline rate in order to attain enough nucleated nuclei with critical size to achieve an explosive bubbling process.

2) Effect of temperature

Temperature of fluids system shows a consistent effect on the apparent critical supersaturation pressure. The decreased apparent critical supersaturation pressures are observed in both CO_2–heavy oil systems and CH_4–C_3H_8–heavy oil systems with a relatively high experimental temperature. Such a trend can be attributed to an accelerated nucleation rate and diffusion process, both of which are stemmed from a lower viscosity induced by a higher temperature.

It has been well recognized that the supersaturation pressure actually is the source of driving force, i.e., the excess energy, for the nucleation of gas bubbles in the supersaturated heavy oil. However, only a portion of such excess energy is spent on the generation of nucleated gas bubble surface and the remaining excess energy is expended by the viscous dissipation of heavy oil expansion (Lillico *et al*., 2001). The energy consumed by viscous dissipation is gradually decreased with a decrease in viscosity because all the excess energy is utilized for the nucleation of gas bubbles in the classical nucleation theory, which is suitable for the fluid systems with low viscosity, such as CO_2–water system (Katz and Blander, 1973; Ward and Levart, 1984). In other words, more

energy will be available for the nucleation of nuclei with critical size in the supersaturated liquid phase with a lower viscosity under the same conditions.

In addition, diffusion coefficient has been identified as a function of viscosity, or further, the temperature (Hayduk and Cheng, 1976). As a diffusion-controlled process, nucleation rate of gas bubbles has been theoretically found to be a proportional function of diffusion coefficient and temperature (Geilikman and Dusseault, 1999; Lillico *et al*., 2001). In addition to a large heat-induced diffusion coefficient, a high temperature of heavy oil can effectively boost the nucleation of gas bubbles. Meanwhile, the enhanced mass transfer rate resulted from the increased diffusion coefficient is capable of improving growth rate of gas bubbles on the basis of the kinetics of gas bubble growth (Lillico *et al*., 2001; Shi and Yang, 2017d). As mentioned in the previous section, a high density of nuclei with critical size and a large diffusion coefficient not only increase the amounts of nuclei with critical size, but also improve the probability of nuclei with critical size that can spontaneously grow to be larger gas bubbles, and subsequently, transform into a continuous phase.

3) Evolved gas and entrained gas

Both amounts of evolved gas and entrained gas are time-dependent. Essentially, they are closely associated with the nonequilibrium phase behaviour of gas–heavy oil systems. Figure 5-3 depicts the amounts of evolved gas and entrained gas with decline pressure rate at different temperatures for three alkane solvent–CO_2–heavy oil systems.

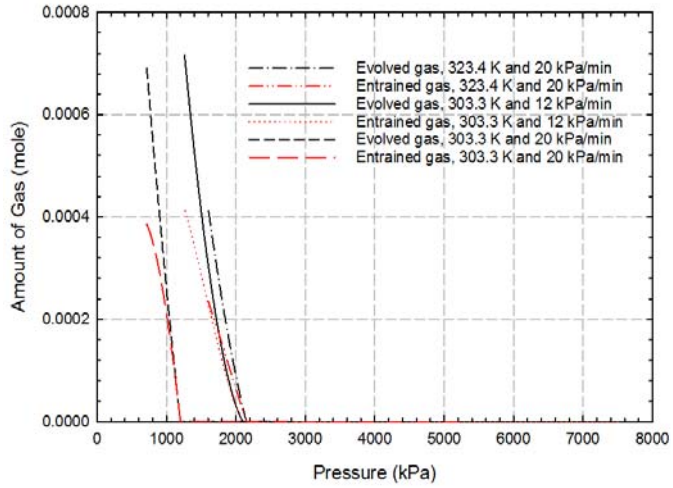

(a)

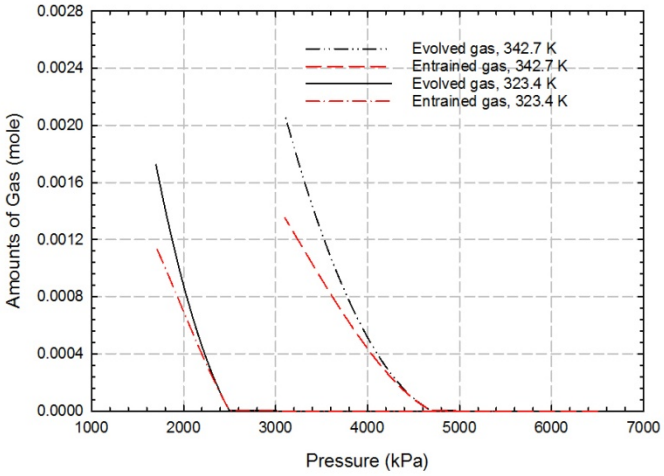

(b)

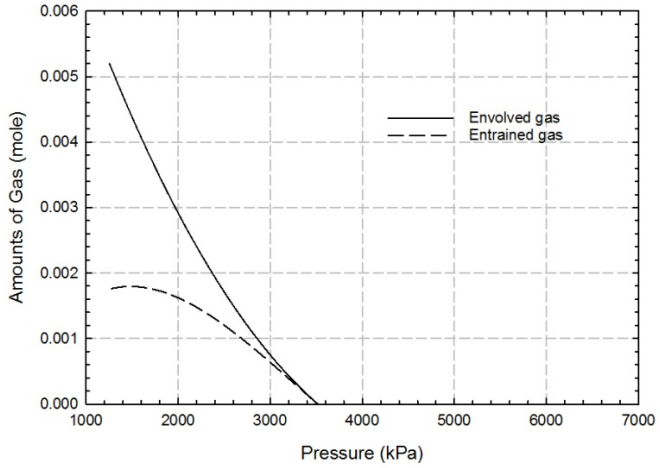

(c)

Figure 5-3 Amounts of evolved gas and entrained gas in **(a)** CO_2–heavy oil systems **(b)** CH_4–C_3H_8–heavy oil systems with pressure decline rate of 20 kPa/min, and **(c)** CH_4–CO_2–heavy oil systems with pressure decline rate 20 kPa/min at 342.7 K

One can find that the amount of evolved gas is a monotone decreasing function of pressure owing to a decreased solubility of gas in heavy oil, when pressure is lower than pseudo-bubblepoint pressure. It is worthwhile noting that the related slope gradually increases, implying that the gas exsolution rate, which is defined as the mole of evolved gas per unit of pressure drop, in heavy oil increases with a decrease in pressure under nonequilibrium conditions. Meanwhile, the average gas exsolution rates of six nonequilibrium experiments are tabulated in Table 5-2. Gas exsolution rate is found to increase with an increase in critical apparent supersaturation pressure for each alkane solvent–CO_2–heavy oil systems, which will be explained in the next chapter in details.

Regarding the amount of entrained gas, there is a maximum value with the decrease in pressure rather than a continuous rise similar to that of evolved gas (see Figures 5-3a and 5-3c). Physically, the evolved gas bubbles are formed in the supersaturated heavy oil, and then partially trapped in the viscous oleic phase. However, it is found from theoretical calculations that the amount of entrained gas, firstly, increases to a maximum point and then decreases to zero at the atmospheric pressure because the oleic phase is supposed to be dead oil without any dissolved gas and gas bubbles. The maximum amount of entrained gas in pressure-gas mole profile is determined by using the corresponding pseudo-bubblepoint pressure and the amount of evolved gas based on Equation [4-6]. As mentioned earlier, the amount of evolved gas is gradually increased with a decrease in pressure, while the ratio of entrained gas to evolved gas continuously decreases. When the positive effect (i.e., increasing amount of entrained gas) of the former is completely offset by the negative effect (i.e., reducing amount of entrained gas) of the latter, the

maximum amount of entrained gas is theoretically achieved. In a same solvent–CO_2–heavy oil systems, a low pseudo-bubblepoint pressure results in a low pressure corresponding to the maximum amount of entrained gas on account of a fixed amount of evolved gas. As for different solvent–CO_2–heavy oil systems with the same pseudo-bubblepoint pressure, a larger amount of dissolved gas usually means a higher amount of evolved gas, i.e., a larger maximum amount of entrained gas because of a greater positive effect. In particular, the reason why only Test #16 has reached the maximum amount of entrained gas among all the tests is that there is a large enough pressure drop below the pseudo-bubblepoint pressure at the end of Test #16. The corresponding ratio of pressure drop below the pseudo-bubblepoint pressure to the pseudo-bubblepoint pressure is 0.64, which is the highest one among six experiments (see Table 5-2).

5.4.2 Comparison of nonequilibrium CCE experiments with constant pressure decline rate versus constant volume expansion rate

Constant pressure decline rate and constant volume expansion rate are two major approaches to attain nonequilibrium conditions for the aforementioned systems, although field production constraints associated with foamy oil may be more complicated. A CCE experiment (i.e., Test #2) conducted in Chapter 4 is utilized to compare with Test #13 in this chapter because of the similar pseudo-bubblepoint pressure (Figure 5-4). The physical properties and corresponding comparable profiles are plotted in Figures 5-5 and 5-6.

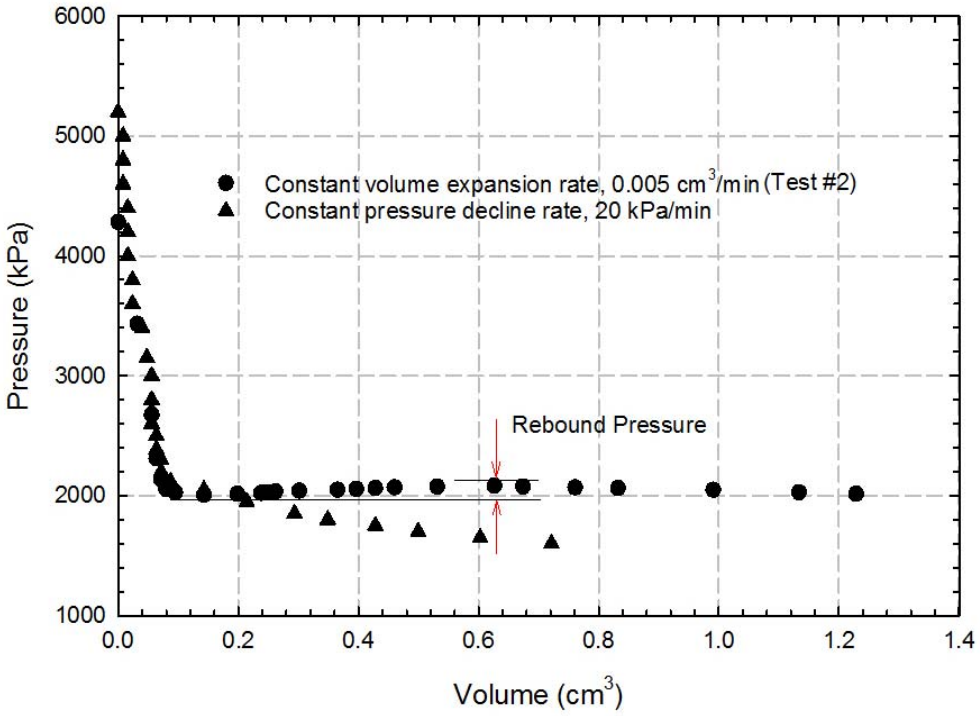

Figure 5-4 Pressure as a function of expansion volume for CO_2–heavy oil systems at 323.4 K

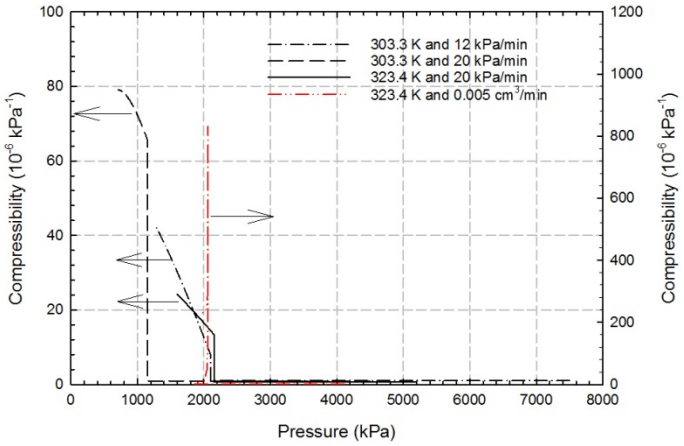

(a)

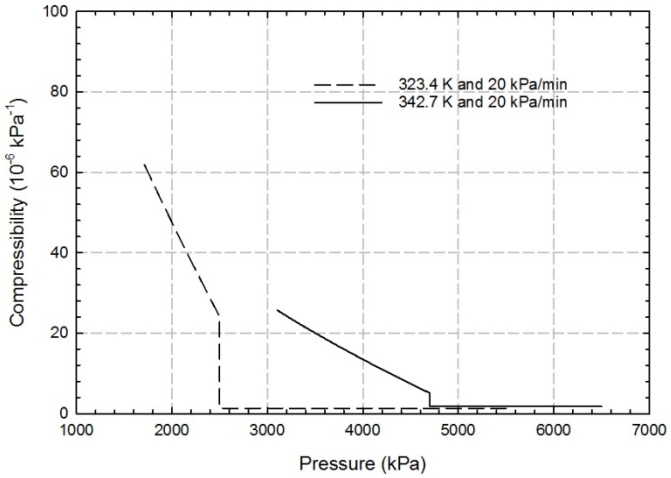

(b)

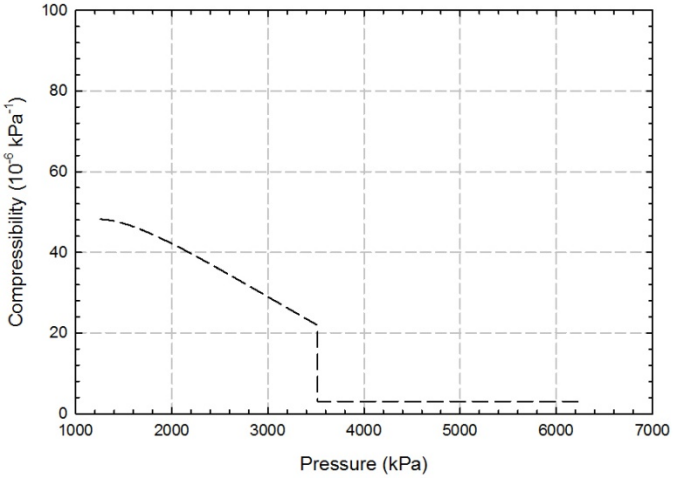

(c)

Figure 5-5 Compressibilities of oleic phase in **(a)** CO_2–heavy oil systems, **(b)** CH_4–C_3H_8–heavy oil systems, and **(c)** CH_4–CO_2–heavy oil systems at 342.7 K and pressure decline rate of 20 kPa/min

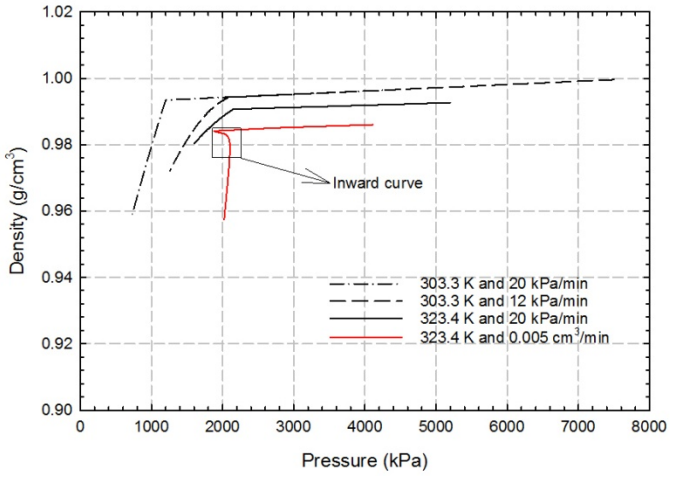

(a)

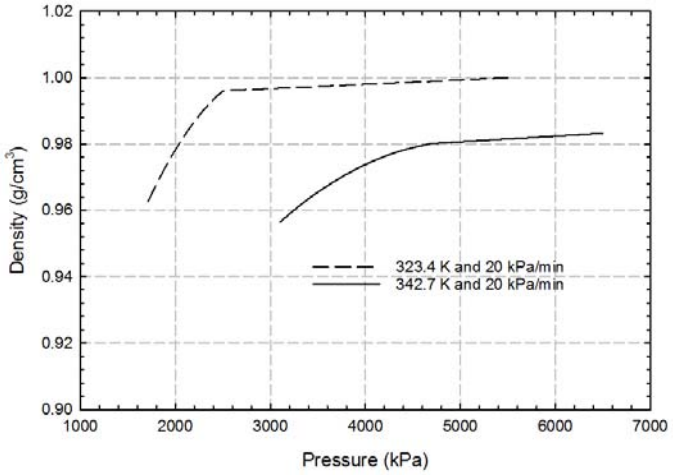

(b)

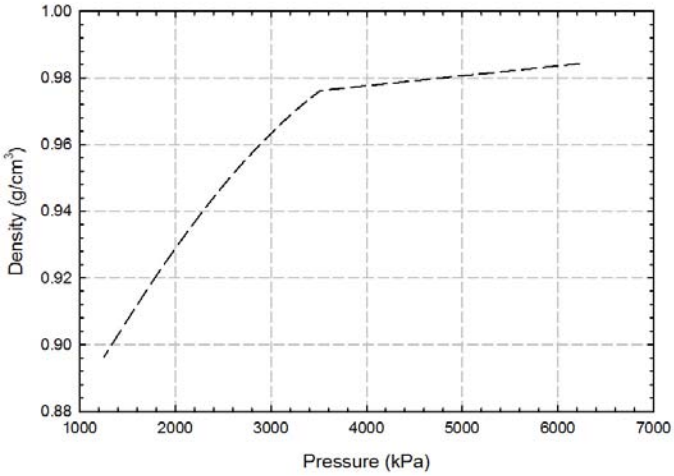

(c)

Figure 5-6 Densities of **(a)** CO_2–heavy oil systems, **(b)** CH_4–C_3H_8–heavy oil systems, and **(c)** CH_4–CO_2–heavy oil systems at 342.7 K and pressure decline rate of 20 kPa/min

Physically, both methods intend to induce a relatively fast pressure decline rate that does not allow all the evolved gas bubbles to escape from the viscous liquid during the process of pressure decline. Basically, when pressure is higher than pseudo-bubblepoint pressure, the difference between constant volume expansion rate and constant pressure decline rate is that the volume expansion rate of the latter is gradually increased instead of being constant in order to maintain a constant pressure decline rate. Such a difference leads to the disappearance of rebound pressure right after occurrence of the pseudo-bubblepoint pressure in the corresponding volume-pressure profiles for the CCE experiments with constant pressure decline rate, though such rebound pressure has been observed in the CCE experiments with constant volume expansion rates in Section 4.4.3. This, theoretically, means that the reservoir pressure can achieve a slight increase when the production rate of the heavy oil reservoir is controlled to be constant. In practice, a constant volume expansion rate or a constant production rate may be better for field operations than constant pressure decline rate because the rebound pressure is likely beneficial to the increase of recovery factor, while a constant pressure decline rate is more difficult to achieve.

As for the compressibility, one can find that there is a sharp peak and a pressure reverse in the pressure-compressibility profile of constant volume expansion rate in comparison to that of constant pressure decline rate because of the occurrence of pressure rebounding. Likewise, the disappeared rebound pressure leads to a direct decline of foamy oil density at the pseudo-bubblepoint pressure in the pressure-density profiles of constant pressure decline rate rather than a slight inward change (see Figures 5-4a and 5-5a), which is

caused by the rebound pressure, located at the turning point of pressure-density profiles with constant volume expansion rates.

5.5 Summary

A new and robust technique has been proposed to determine nonequilibrium phase behaviour of foamy oil and their corresponding physical properties during CCE experiments with constant pressure decline rates. Experimentally, nonequilibrium CCE experiments for three alkane solvent–CO_2–heavy oil systems show that apparent critical supersaturation pressure increases with an increase in pressure decline rate and a decrease in temperature. A low density of nuclei with critical size and a slow diffusion process with a fast pressure decline rate and low temperature are expected in comparison to those with a slow pressure decline rate and high temperature under the same pressure based on the classical nucleation theory. This may be the underlying mechanism for the enlarged critical apparent supersaturation pressure as mentioned previously.

The amount of evolved gas keeps increasing along with the decline of pressure, while there is a maximum value for the amount of entrained gas during the same process of pressure decline. In general, the trends of physical properties under a constant pressure decline rate are similar as those attained under a constant volume expansion rate. However, the rebound pressure extensively found in CCE experiments with a constant volume expansion rate cannot be observed in CCE experiments with a constant pressure decline rate due to a gradually increased volume expansion rate for the maintenance of a constant pressure decline rate. As such, no pressure reverse and a slight inward change

can be observed around the pseudo-bubblepoint pressure in the compressibility-pressure profile and density-pressure profile, respectively, a constant pressure decline rate.

CHAPTER 6 QUANTIFICATION OF A SINGLE GAS BUBBLE GROWTH FOR ALKANE SOLVENT(S)–CO_2–HEAVY OIL SYSTEMS WITH CONSIDERATION OF MULTICOMPONENT DIFFUSION UNDER NONEQUILIBRIUM CONDITIONS

6.1 Introduction

In this chapter, a mechanistic model has been developed and validated to quantify a single gas bubble growth with considering multicomponent gas diffusion in alkane solvent(s)–CO_2–heavy oil systems under nonequilibrium conditions (Shi and Yang, 2017d). The classical continuity equation, motion equation, diffusion-convection equation, real gas equation, and PR EOS are integrated into an equation matrix to dynamically predict a single gas bubble growth. Also, the viscous term of motion equation on the gas phase pressure is included due mainly to the viscous nature of heavy oil. Combining with the experimental measurements, the critical nucleus radius and gas bubble growth are quantitatively predicted with the newly proposed model. Effects of mass transfer, supersaturation pressure, mole concentration of each component, liquid cell radius, and pressure decline rate on the gas bubble growth are examined and analyzed for a total of 23 scenarios.

6.2 Mathematical Formulations

To accurately simulate and analyze the growth of a gas bubble in supersaturated heavy oil, consideration of the limited volume of liquid phase should be included so as to more closely approximate the actual conditions of gas exsolution. The well-known liquid cell assumption is regarded as an appropriate scheme to quantify such a gas evolving process (Amon and Denson, 1984; Leung *et al*., 2006). More specifically, the liquid cell

assumption postulates that a gas bubble is surrounded by a liquid concentric shell with a finite thickness and a certain amount of the dissolved gas. Figure 6-1 depicts the schematic of a cell model where r_{b0} is radius of an initial gas bubble, i.e., critical nucleus radius; $r_b(t)$ is radius of the gas bubble at time *t*; r_e is outer boundary radius of liquid shell; and $c(r,t)$ is the gas concentration at radius *r* and time *t*.

6.2.1 Assumptions

To quantify the transient growth of an isolated gas bubble under nonequilibrium conditions, the mathematical model is developed based on the following assumptions:

(1) The entire system is considered to be isothermal;

(2) The gas bubble boundary and liquid shell boundary are assumed to be spherically symmetric during the gas bubble growth processes (Rosner and Epstein, 1972);

(3) The liquid is incompressible (Scriven, 1959);

(4) The liquid pressure is equal to the applied system pressure due to thermodynamic equilibrium;

(5) Inertial force is negligible (Gor and Kuchma, 2009); and

(6) The diffusion coefficient is constant during the gas bubble growth processes (Leung *et al*., 2006);

(7) The properties of evolved gas phase are same as those under equilibrium conditions.

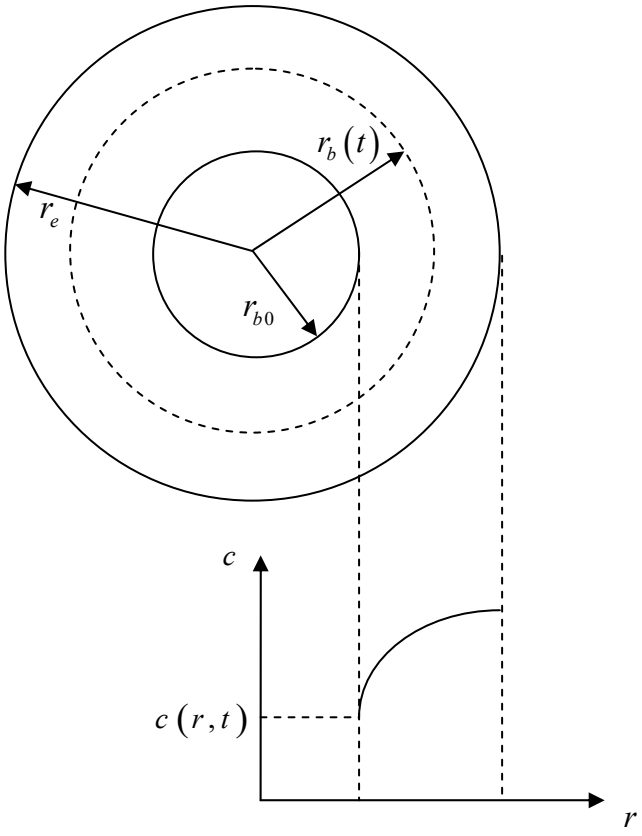

Figure 6-1 Schematic of the cell model

6.2.2 Continuity equation

The continuity equation for the flow of an incompressible liquid around an expanding gas bubble can be expressed as,

$$u_r r^2 = u_r\left(r_b\right) r_b^2 \qquad r_b\left(t\right) \le r \le r_e \tag{6-1}$$

where u_r is radial fluid velocity.

6.2.3 Equation of motion

Combined with Equation [6-1], the equation of motion can be simplified as follows (Gor and Kuchma, 2009),

$$p_g = p_l + \frac{2\sigma}{r_b} + 4\mu\frac{\dot{r}_b}{r_b} \tag{6-2}$$

where $\dot{r}_b$ is the change of r_b over time, i.e., $\frac{dr_b}{dt}$; p_l is pressure of liquid phase; p_g is the pressure of gas bubble; μ is viscosity of liquid phase; and σ is interfacial tension (IFT) between gas and liquid. Generally, the third term of the right-hand side in Equation [6-2] has been neglected due mainly to the low viscosity of liquid phase in previous work (Scriven, 1959; Rosner and Epstein, 1972; Payvar, 1987). Since heavy oil is featured by its high viscosity, this term is included in this chapter to quantitatively capture the viscosity effect on the gas bubble growth, especially during the early bubble growth stage.

In addition, a specific parachor model for alkane solvent(s)–CO_2–heavy oil systems is employed to determine the dynamic IFT of multicomponent gas phase and heavy oil in this study at a constant temperature (Li *et al*., 2012),

$$\sigma = \left(\frac{D_{og}}{D_{go}} \right)^{-0.448} \left(\rho^L \sum_{i=1}^{n} x_i P_{pi} - \rho^V \sum_{i=1}^{n} y_i P_{pi} \right)^4 \quad [6\text{-}3]$$

where x_i is mole composition of the i^{th} component in liquid phase; y_i is mole composition of the i^{th} component in gas phase; P_{pi} is parachor of the i^{th} component, ρ^L and ρ^V is the molar densities of liquid and gas phases, respectively; and D_{og} and D_{go} are the diffusion coefficients of heavy oil in gas solvent and gas solvent in heavy oil, respectively.

The specific viscosity correlation for dead and diluted heavy oil proposed by correlation Yarranton *et al*. (2013) is utilized for the prediction of mixture viscosity. More details can be found in Section 3.2.2.

6.2.4 Mass transfer equation

The mass transfer of diffusing gas in the liquid shell of the proposed model is governed by the diffusion-convection equation as follows,

$$\frac{\partial c_i}{\partial t} + u_r \frac{\partial c_i}{\partial r} = \frac{D}{r^2} \frac{\partial}{\partial r} \left(r^2 \frac{\partial c_i}{\partial r} \right) \quad [6\text{-}4]$$

where c_i is mole concentration of the i^{th} component and D_i is the diffusion coefficient of the i^{th} component of gas phase.

At the interface of gas-liquid phase, the mass transfer of diffusing gas from the liquid phase to vapour phase must be equal to the mass increment of diffusing gas in the gas bubble. Specifically, for multicomponent gas diffusion, the equation can be expressed as,

$$\frac{\partial}{\partial t}\left(\frac{p_g r_b^3}{zRT}\right) = 3r_b^2 \sum_{i=1}^{n} D_i \left(\frac{\partial c_i}{\partial r}\right)\Bigg|_{r=r_b} \qquad [6\text{-}5]$$

where R is the universal gas constant; z is compressibility factor of the gas mixture; T is temperature of gas phase. It is worthwhile noting that Equation [6-5] considers the gas mixture as one component rather than multicomponents, which is different with previous work (e.g., Cable and Frade, 1987). This is mainly attributed to the fact that the classical bubble growth models usually treat the diffusing gas evolved from the liquid phase as an ideal gas (Scriven, 1959; Rosner and Epstein, 1972; Cable and Frade, 1987; Leung *et al*., 2006; Wong and Maini, 2007). Such an assumption allows that the partial pressure of each gas component is proportional to its mole fraction, and then the mass balance equation at the gas-liquid interface can be respectively formulated for each component of the diffusing gas (Cable and Frade, 1987). Due to high pressures and temperatures in a reservoir, it actually makes the behaviour of the evolved gas greatly deviate from that of ideal gas. A generalized mass balance equation for multicomponent diffusing gas at the gas-liquid interface, i.e., Equation [6-5], not only attains the prediction of real gas properties, but also avoids the complex procedures to determine the partial pressures in a real gas system.

6.2.5 Initial and boundary conditions

The initial concentration of each individual component in a mixture is assumed to be a known input,

$$c_i(r) = c_{i0}, \qquad t = 0, \qquad r_b < r \le r_e \qquad [6\text{-}6]$$

where c_{i0} is the initial concentration of the i^{th} dissolved component. Since the gas bubble is assumed to grow in a limited volume liquid shell without mass transfer at the outer boundary, the amount of gas in the liquid shell is constant. The concentration gradients of the diffusing gases at the outer boundary of the liquid shell are zero and can be expressed as follows,

$$\left.\frac{\partial c_i}{\partial r}\right|_{r=r_e} = 0 \qquad [6\text{-}7a]$$

At the inner boundary of liquid cell, i.e., the gas-oil interface, Henry's law is usually used to relate concentration of the diffusing gas to its pressure with strict constraint of sufficiently dilute solution (Rosner and Epstein, 1972; Arefmanesh *et al*., 1992). Evidently, it is difficult to constrain the conditions of gas bubble growth under the pressure and temperature of heavy oil reservoirs within the narrow applicable range of the Henry's law. The quasi-equilibrium condition has been validated to be an appropriate boundary condition during the mass transfer processes for solvent(s)–heavy oil systems (Tharanivasan *et al.*, 2004; Sun *et al*., 2014; Li and Yang, 2016; Zheng and Yang, 2016). Therefore, it is acceptable to assume that the following quasi-equilibrium boundary condition shall be able to satisfy the requirement of determining the relationship between the concentration and pressure.

$$c_i = c_{i,sat}\left[p_g(t)\right]\Big|_{r=r_b} \qquad [6\text{-}7b]$$

Since the Peng-Robinson equation of state (PR EOS) has been extensively utilized to predict phase behavior in petroleum and chemical industries owing to its recognized accuracy and robustness, it is employed to compute the two-phase flash calculation for determining the concentration of diffusing gas in Equation [6-7b]. Also, it is noteworthy

that the recently proposed alpha function (Li and Yang, 2011) is used to improve the prediction accuracy of phase behavior for alkane solvent(s)–CO_2–heavy oil systems.

6.2.6 Numerical solution

The equation matrix comprising Equations [6-1], [6-2], [6-4], and [6-5] governs the solitary bubble-growth dynamics in alkane solvent(s)–CO_2–heavy oil systems under nonequilibrium conditions. Numerical methods shall be applied for solving the coupled equations mainly owing to the nonlinearity caused by the variable properties of fluids and velocity of gas-liquid interface associated with the mass transfer of the diffusing gases. An implicit finite difference scheme, i.e., the Crank-Nicolson method, is utilized to numerically solve the aforementioned equation matrix to ensure the convergence of the developed simulation algorithm. The computational procedure (see Figure 6-2) is briefly described as follows:

(1) The physical parameters are firstly inputted, while the initial conditions are given. Especially, a guessed critical nucleus radius (the starting gas bubble radius for a stable bubble growth) for the first time step is assumed.

(2) Calculating the concentration of each gas, $c_i\big|_{r=r_b}$, at the gas-liquid interface based on Equation [6-7b];

(3) Comparing the calculated gas concentrations in Step #2 with initial dissolved gas concentration in the liquid. Once the minimum concentration difference as defined in Equation [6-8] is smaller than prespecified accuracy and larger than zero, namely,

$$0 < \min\left(c_i - c_i\big|_{r=R}\right) < \varepsilon \qquad [6\text{-}8]$$

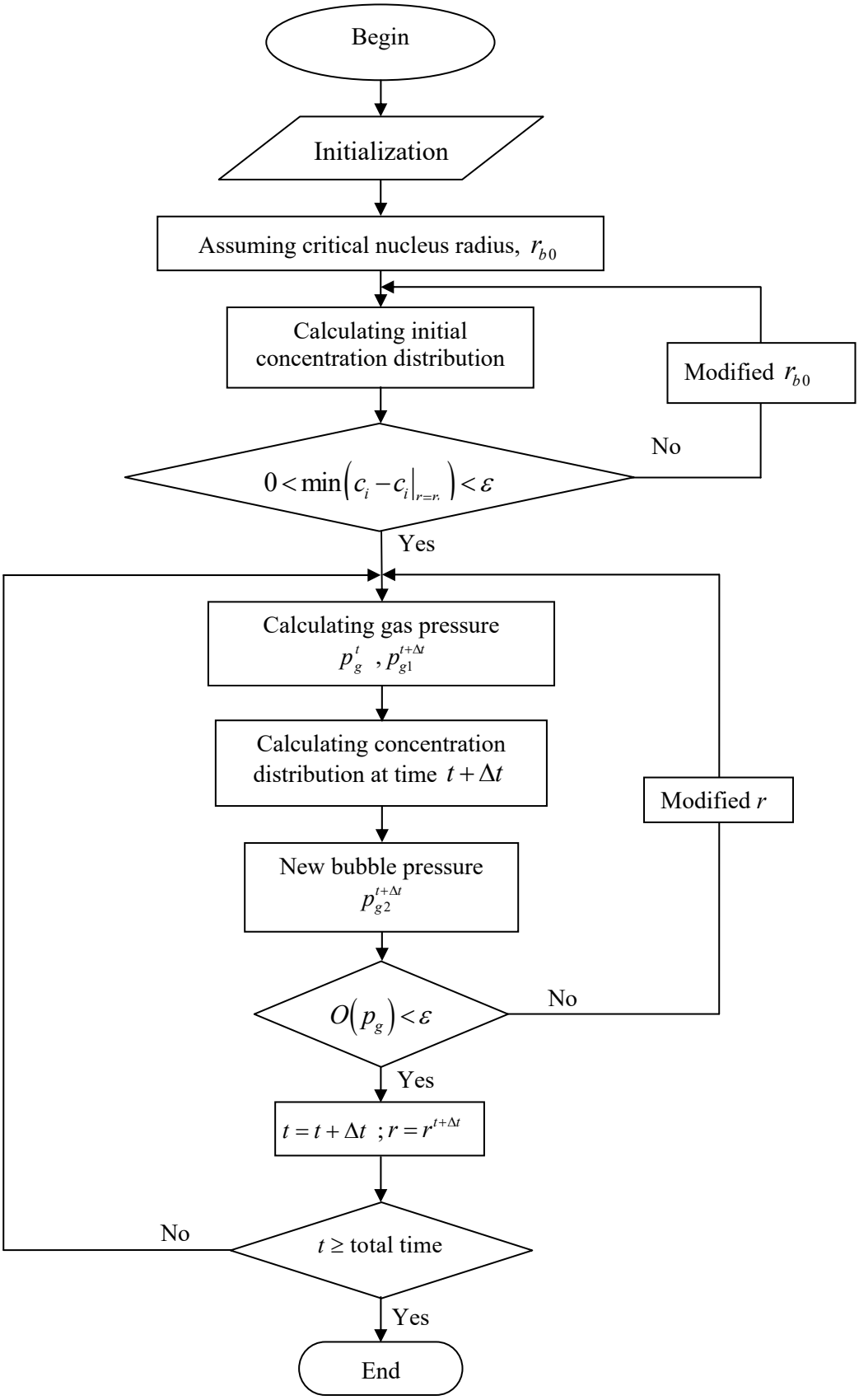

Figure 6-2 Flowchart of numerically solving the equation matrix

(4) The pressures of gas bubble, p_g^t and $p_{g1}^{t+\Delta t}$, at time t and $t+\Delta t$ are calculated with Equation [6-2] and the gas bubble radius, respectively. Then, velocity of the gas-liquid interface is computed with Equation [6-1];

(5) Two-phase flash calculation with PR EOS is conducted to determine the boundary concentration of each solvent component at time $t+\Delta t$;

(6) The concentration distribution of each diffusing gas component in the liquid cell is attained with Equation [6-4];

(7) A new pressure, $p_{g2}^{t+\Delta t}$, of gas bubble at time $t+\Delta t$ is then obtained with Equation [6-5];

(8) The objective function pertaining to the gas bubble pressures at time $t+\Delta t$ is defined as follows,

$$O\left(p_g\right)=\sqrt{\left(\frac{p_{g2}^{t+\Delta t}-p_{g1}^{t+\Delta t}}{p_{g1}^{t+\Delta t}}\right)^2} \qquad [6\text{-}9]$$

Once the objective function $O\left(p_g\right)$ is less than the prespecified accuracy (i.e., 10^{-5} in this chapter), the pressure and radius of gas bubble at time $t+\Delta t$ are considered to be the true values, and then the calculation proceeds to the next time step. Otherwise, the radius of gas bubble at time $t+\Delta t$ shall be adjusted so as to reduce the value of $O\left(p_g\right)$ to be smaller than the prespecified tolerance by repeating Steps #4–8.

6.2.7 Model validation

Limited experimental measurements of a single gas bubble growth in heavy oil system have been made available in the literatures. Szekely and Martins (1971) reported that

growth of a solitary gas bubble is photographed, while the gas bubble radius is recorded as a function of time in binary *n*-pentane–*n*-tetradecane (*n*-C_5H_{12}–*n*-$C_{14}H_{30}$) systems. As can be seen in Figure 6-3, there exists an excellent agreement between the measured gas bubble radii and those calculated with the newly proposed model, indicating that the newly proposed model can be used to effectively account for the underlying mechanisms of gas bubble growth in gas-liquid alkane solvent(s) systems. The detailed parameters used in the calculation are tabulated in Table 6-1. It is worthwhile noting that the original alpha function of the PR EOS instead of the recently modified one (Li and Yang, 2011) is employed to calculate fluids compositions under quasi-equilibrium boundary conditions (i.e., Equation [6-7b]) because this is a binary component system. Also, such experimental measurements collected from the literature are not sufficient to determine the critical nucleus radius which is defined as the initial value of gas bubble radius during the period of a stable bubble growth, though the newly model has been validated with the measured bubble radius.

6.3 Results and Discussion

Two CCE experiments (Test #4 in Table 4-3 and its corresponding equilibrium CCE experiment) in Section 4.4 are utilized for the calculation of single gas bubble growth. Correspondingly, the bubblepoint pressure and pseudo-bubblepoint pressure are measured to be 2220 kPa and 1558 kPa at 303.3 K, respectively. Based on the experimental results, the gas bubble growth in a CO_2–C_3H_8–heavy oil mixture is quantified and discussed. Then, a total of 23 scenarios simulating bubble-growth behaviour in heavy oil with two diffusing gas components are designed and calculated to

Table 6-1 Physical and correlated properties of *n*-C_5H_{12}–*n*-$C_{14}H_{30}$ systems (Szekely and Martins, 1971) and CO_2–C_3H_8–heavy oil systems

Parameter	*n*-C_5H_{12}–*n*-$C_{14}H_{30}$ systems	CO_2–C_3H_8–heavy oil systems
Temperature (K)	298.15	303.3
Pressure (kPa)	2.67×10^{-2}	1558
Coefficient A of heavy oil viscosity	–	9.4669
Coefficient B of heavy oil viscosity	–	3.5861
Initial bubble radius (μm)	100.0	1.0
Liquid shell radius (μm)	50000.0	100.0

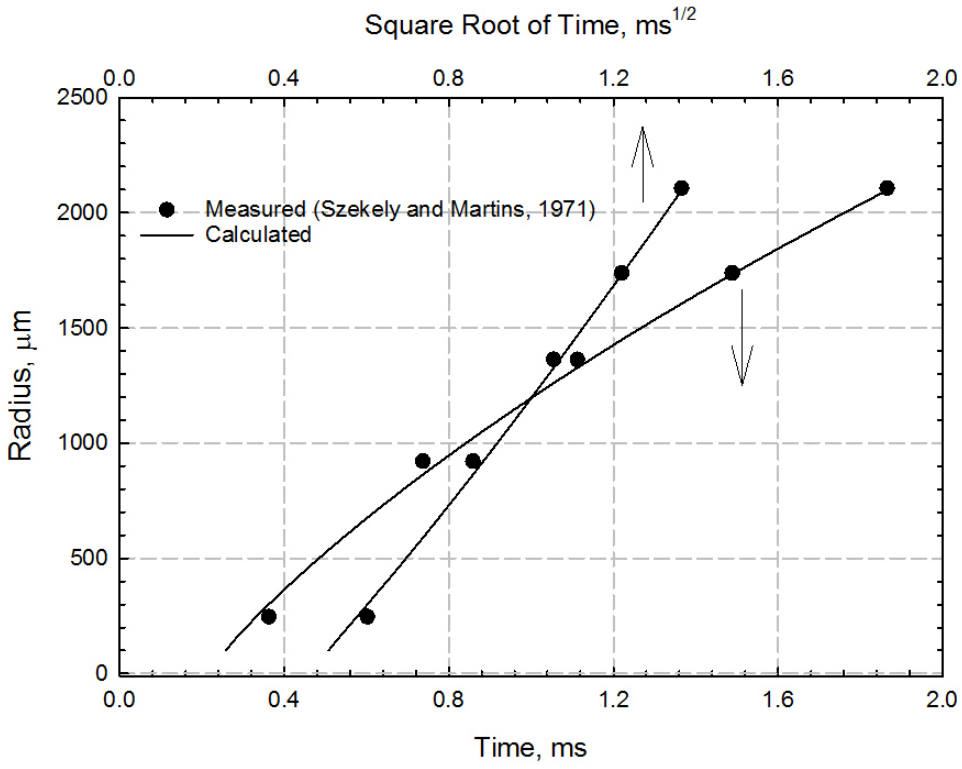

Figure 6-3 Comparison of the measured and calculated bubble radius for *n*-C_5H_{12}–*n*-$C_{14}H_{30}$ systems

perform sensitivity analysis on the factors involved in the gas bubble growth. These factors mainly include supersaturation pressure, mole fraction of gas component, liquid cell radius, and pressure decline rate on the gas bubble radius. Physical parameters used in the model are tabulated in Tables 6-1 and 6-2, respectively.

6.3.1 Gas bubble growth of CO_2–C_3H_8–heavy oil systems

Although the experiment is operated with a constant expansion volume rate, the system pressure before pseudo-bubblepoint pressure is still basically decreased with a constant depletion rate. It is calculated to be 10.0 kPa/s by using the measured pressures and time. Figure 6-4 shows the profile of gas bubble radius over time with the pressure decline rate of 10.0 kPa/s. One can find that the bubble growth rate gradually decreases with time. This can be explained by the decline of mass transfer rate caused by gradually approaching equilibrium state of gas solvent distribution in the oleic phase.

In this chapter, the critical nucleus radius is computed to be 0.19 μm with the measured pseudo-bubblepoint pressure. Physically, the first portion of gas phase is formed on the pseudo-bubblepoint pressure in the foamy oil, implying that the stable gas bubble growth is triggered when the liquid pressure declines to the pseudo-bubblepoint pressure. On the other hand, when the concentration of each gas in the vicinity of gas bubble is larger than that at the gas-liquid interface, a stable explosive gas bubble growth can likely occurs. Based on Equation [6-2], gas pressure is strongly related to the critical nucleus radius which is usually small enough to impose a great impact on the gas pressure, when the nucleated gas bubble begins to grow. According to the concentration requirement at the

Table 6-2 The 23 scenarios designed for sensitivity analysis

Scenario No.	D_{CO_2} (referred to original value)	$D_{C_3H_8}$ (referred to original value)	Supersaturation pressure (kPa)	CO_2 mole concentration (referred to original value)	C_3H_8 mole concentration (referred to original value)	Liquid shell radius (μm)	Pressure decline rate (kPa/s)
1	100%	100%	–*	–*	–*	–*	–*
2	80%	80%	–*	–*	–*	–*	–*
3	120%	120%	–*	–*	–*	–*	–*
4	120%	100%	–*	–*	–*	–*	–*
5	80%	100%	–*	–*	–*	–*	–*
6	100%	120%	–*	–*	–*	–*	–*
7	100%	80%	–*	–*	–*	–*	–*
8	100%	100%	–*	–*	50%	–*	–*
9	80%	100%	–*	–*	50%	–*	–*
10	100%	80%	–*	–*	50%	–*	–*
11	–*	–*	500	–*	–*	–*	–*
12	–*	–*	600	–*	–*	–*	–*
13	–*	–*	700	–*	–*	–*	–*
14	–*	–*	–*	110%	110%	–*	–*
15	–*	–*	–*	90%	90%	–*	–*
16	–*	–*	–*	110%	100%	–*	–*
17	–*	–*	–*	90%	100%	–*	–*
18	–*	–*	–*	100%	110%	–*	–*
19	–*	–*	–*	100%	90%	–*	–*
20	–*	–*	–*	–*	–*	50	–*
21	–*	–*	–*	–*	–*	200	–*
22	–*	–*	–*	–*	–*	–*	10.0
23	–*	–*	–*	–*	–*	–*	5.0

*Note: Parameter is same as original input value.

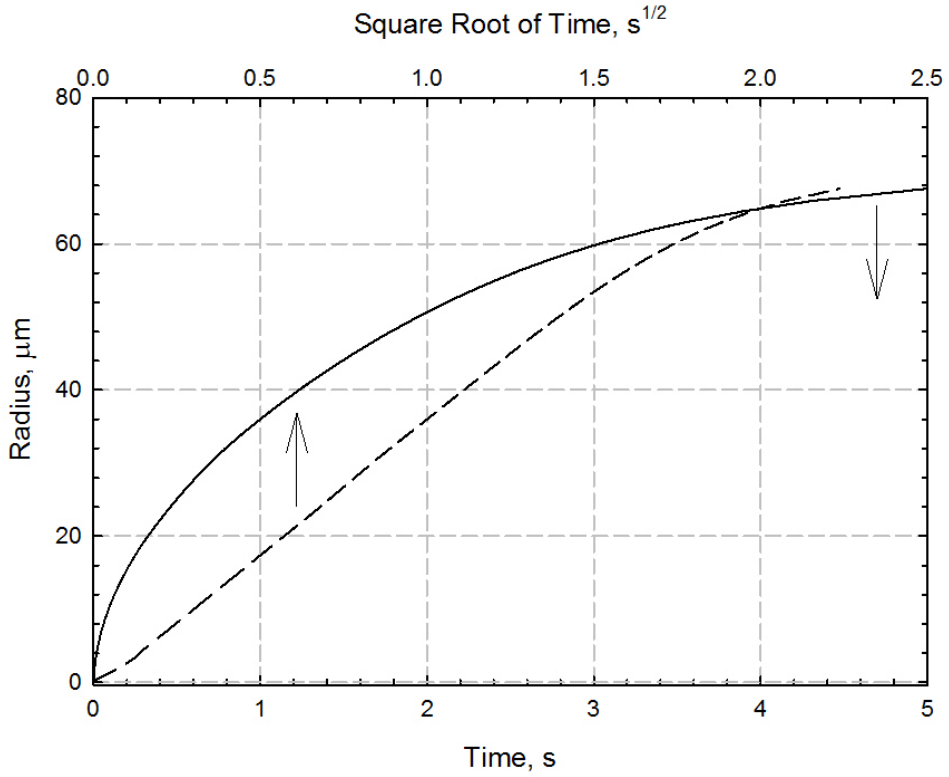

Figure 6-4 The calculated radius of a gas bubble for CO_2–C_3H_8–heavy oil systems

gas-liquid interface for a stable bubble growth, the related gas bubble pressure can be obtained. Furthermore, the critical nucleus radius can be determined with the corresponding gas bubble pressure and Equation [6-2]. The detailed procedure is listed as the first three steps in Section 6.2.6.

Physically, the critical nucleus radius for homogeneous nucleation is in the order of a few nm, which is corresponding to a supersaturation pressure of several thousand psi (Yortsos and Parlar, 1989; Kashchiev and Firoozabadi, 1993). Several researchers (Smith, 1988; Claridge and Prats, 1995) proposed that the nucleation process in bulk heavy oil is affected by the asphaltene content which acts as dispersed nucleation sites. Such phenomenon may lead to a heterogeneous nucleation occurring in bulk heavy oil (Ward and Levart, 1984), implying that the critical nucleus radius in bulk heavy oil shall be much larger than a few nm because the supersaturation pressure of the heterogeneous nucleation usually is much lower than that of the homogeneous nucleation (Yortos and Parlar, 1989). Thus, the critical nucleus radius determined by the proposed procedure in this chapter, 0.19 μm, should be in an appropriate range.

Although the critical nucleus radius can be obtained with the aforementioned procedure, this value is not used for the following sensitivity analysis (Sections 6.3.2–6.3.7). This is because the parameters affecting the gas bubble growth must be varied in a certain range in order to perform appropriate sensitivity analysis; however, such varied parameters could change the pseudo-bubblepoint pressures of the mixtures to some extent. This means that the aforementioned critical nucleus radius calculated with actual experimental

measurements may be unequal to the ones in those designed scenarios with the changed parameters. It would lead to an unstable bubble growth process since such a value is physically constrained to the experimental measurements in this study if the calculated critical nucleus is still employed for performing sensitivity analysis. Consequently, an assumed critical nucleus radius (1.0 μm) is utilized in the sensitivity analysis only aiming to avoid the possible unstable bubble growth processes in those designed scenarios and benefit the comparison among different results as well. In the literature, the initial critical nucleus radius is usually assumed to be 1.0 μm (Arefmanesh *et al*., 1992; Kumar, 1999) because it is difficult to experimentally determine the critical nucleus radius. On the other hand, the assumed value of 1.0 μm is much larger than the calculated value of 0.19 μm in this study, ensuring that the concentration gradient from liquid to gas bubble is positive, i.e., the gas bubble growth is a stable process.

6.3.2 Mass transfer

Effect of mass transfer is examined by varying diffusion coefficients of both diffusing gas (i.e., CO_2 and C_3H_8). Two types of evaluating methods are designed in the simulations. Type I: Diffusion coefficients of both diffusing gases are simultaneously varied with the same proportions referred to their initial input values. Type II: Diffusion coefficient of only one diffusing gas is changed for assessing the corresponding effect. More specifically, for Type I, both diffusion coefficients are varied in the range of 80% to 120% of their original values (Scenarios #1–3). For Type II (Scenarios #1, 4–7), diffusion coefficient of one diffusing gas (CO_2 or C_3H_8) changed from 80% to 120% of

its original value, while diffusion coefficient of the other diffusing gas (C_3H_8 or CO_2) remains unchanged. The results are shown in Figures 6-5 and 6-6, respectively.

For Type I, it can be found that diffusion coefficients impose a great influence on the bubble growth rate. A higher diffusion coefficient leads to a larger gas bubble radius. Similar finding was documented in literature as well (Leung *et al*., 2006). For Type II, a similar trend of gas bubble growth is also attained. Effects of the varied CO_2 and C_3H_8 diffusion coefficients on bubble growth are quite close. In other words, the contributions of CO_2 and C_3H_8 gas diffusion to the gas bubble formation are almost the same in this specific scenario possibly due to the similar mass transfer rate. Although the diffusion coefficient of C_3H_8 is about 4 times larger than that of CO_2, the mole concentration gradient of the former on the gas-liquid interface is about 1/5 of the latter. In fact, once the mole concentration of C_3H_8 is assumed to be the half of its original value (Scenarios #8–10), effects of diffusion coefficient of CO_2 and C_3H_8 on bubble growth are different (see Figure 6-6c).

6.3.3 Supersaturation pressure

Supersaturation pressure is defined as the pressure difference between thermodynamic bubblepoint pressure (P_b) and actual pressure of liquid phase in the saturated oil that is lower than P_b (Kamath and Boyer, 1995). It is usually utilized to indicate the degree that the amounts of the dissolved gas at the actual pressure and temperature exceed that of gas dissolved under equilibrium conditions (Kennedy and Olson, 1952).

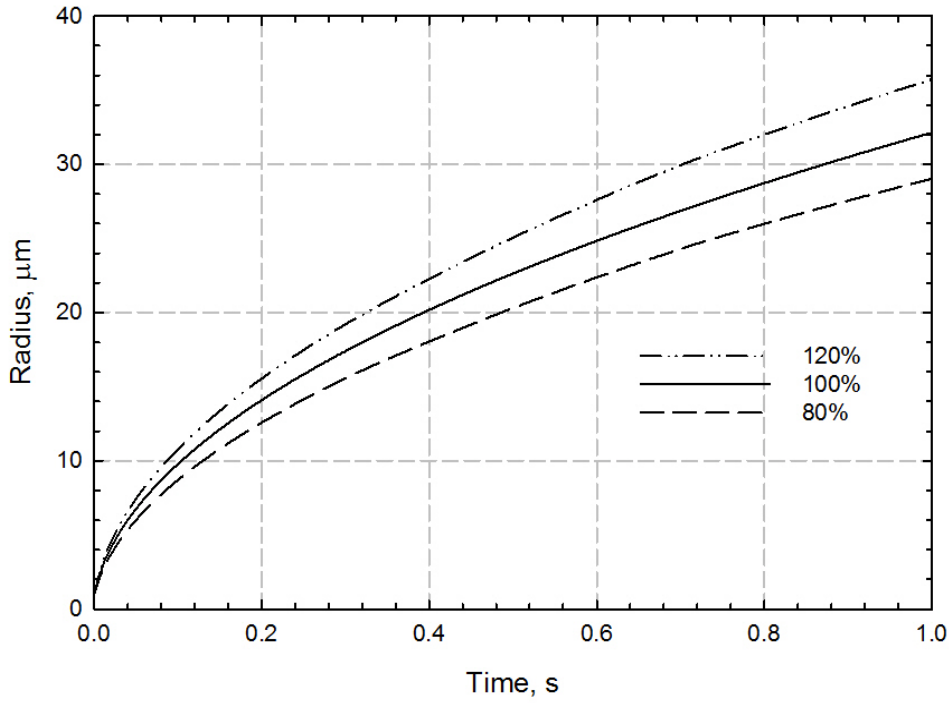

Figure 6-5 Bubble radius as a function of time with varying two gas diffusion coefficients

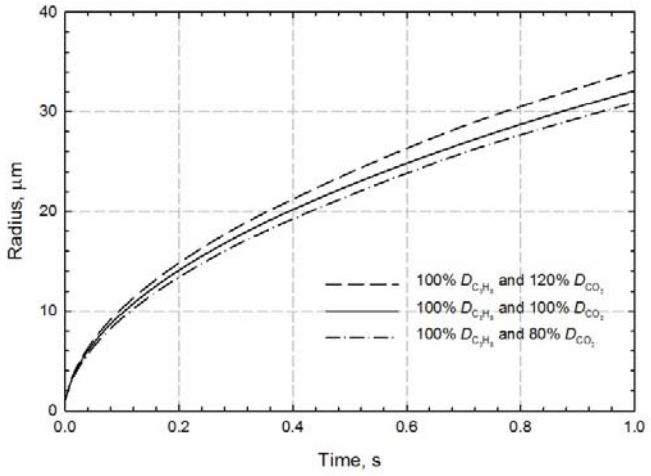

(a)

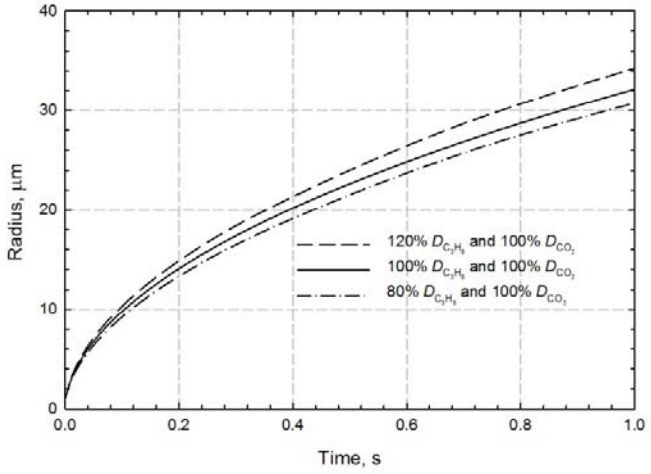

(b)

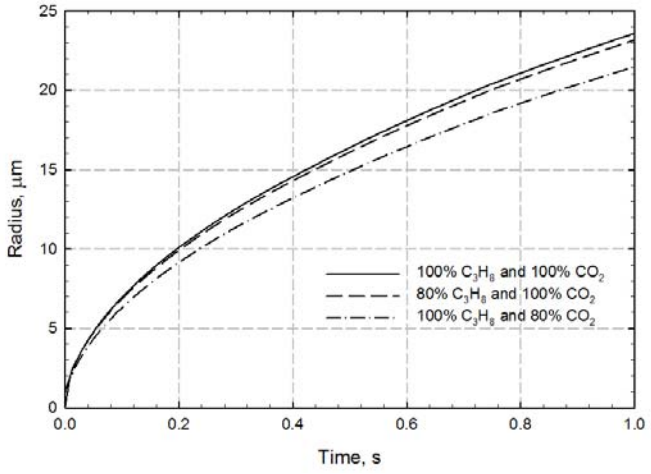

(c)

Figure 6-6 The relationship between the bubble radius and time with varying individual diffusion coefficient of **(a)** CO_2, **(b)** C_3H_8 with the 100% original mole concentration of both gases, and **(c)** CO_2 and C_3H_8 with 50% C_3H_8 original mole concentration

Three scenarios (Scenarios #11–13) are schemed with the supersaturation pressures assumed to be 500, 600, and 700 kPa in this chapter. As can be seen in Figure 6-7, both gas bubble size and bubble growth rate are increased with an increase in supersaturation pressure. This is ascribed to the fact that a high supersaturation pressure leads to high concentration gradients of both diffusing gases at the gas-liquid interface and interior of the liquid shell surrounding the gas bubble. Accordingly, mass transfer rates of the diffusing gases from liquid to gas bubble are accelerated further to enhance the bubble growth rate. Similar results are also documented elsewhere (Kashchiev and Firoozabadi, 1993).

6.3.4 Mole concentration of diffusing gas

Two types of evaluating methods are introduced, which are similar to those used in Section 6.3.2. Type III: both mole concentrations of diffusing gases are simultaneously changed with same proportion (90%, 100%, and 110%). Type IV: Only one diffusing gas mole concentration (90%, 100%, and 110% of CO_2 or C_3H_8) is varied, meanwhile, the other one is kept to be its original value. The calculated bubble radii as a function of time under different mole concentrations of diffusing gases are illustrated in Figure 6-8.

In general, higher mole concentrations of the diffusing gas result in both a larger gas bubble radius and a higher growth rate (see Figure 6-8a). The high mole concentration gradient is regarded as the main mechanism to account for the improvement of the mass transfer rate of both diffusing gases. However, for Type IV, it is worthwhile noting that effects of mole concentration of CO_2 and C_3H_8 on size and growth rate of gas bubble are

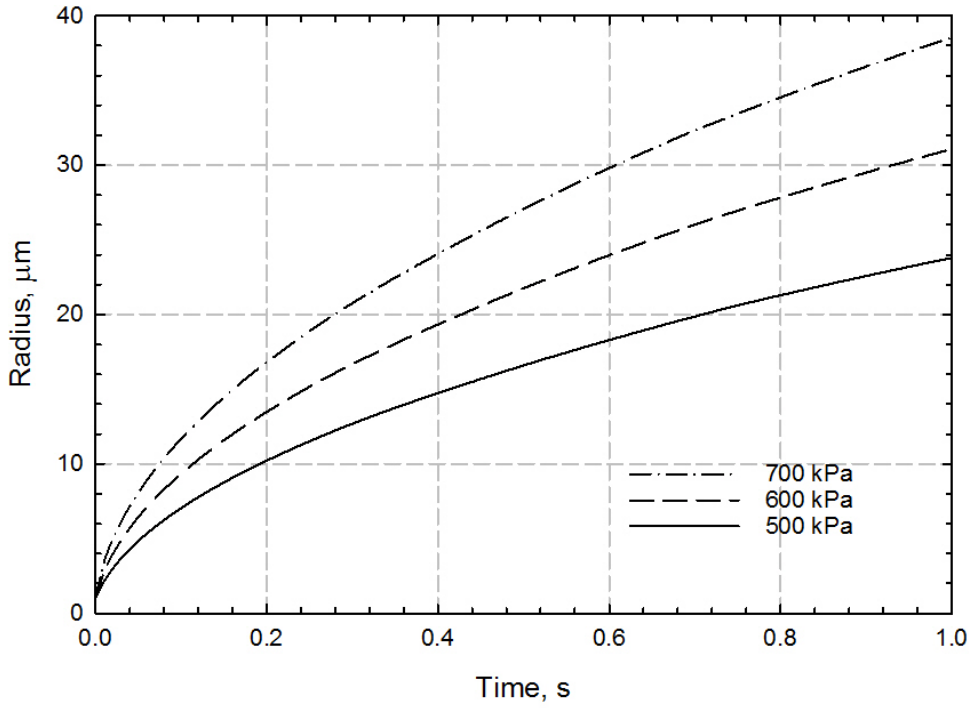

Figure 6-7 The relationship between the bubble radius and time with different supersaturation pressures

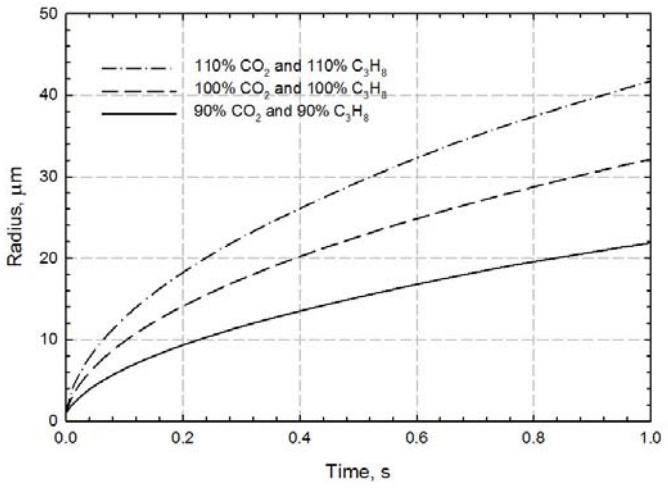

(a)

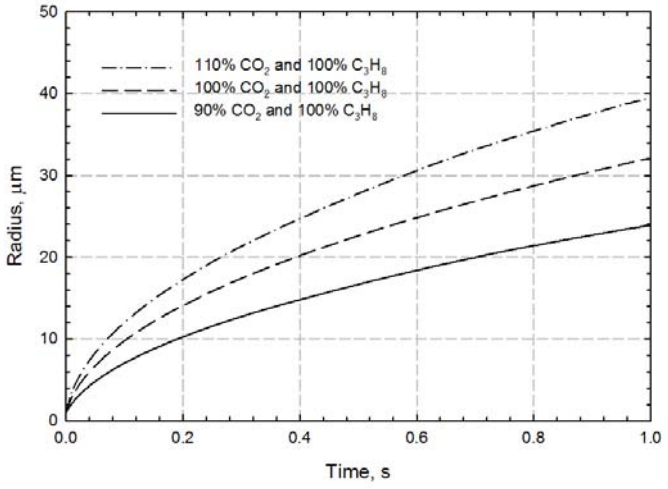

(b)

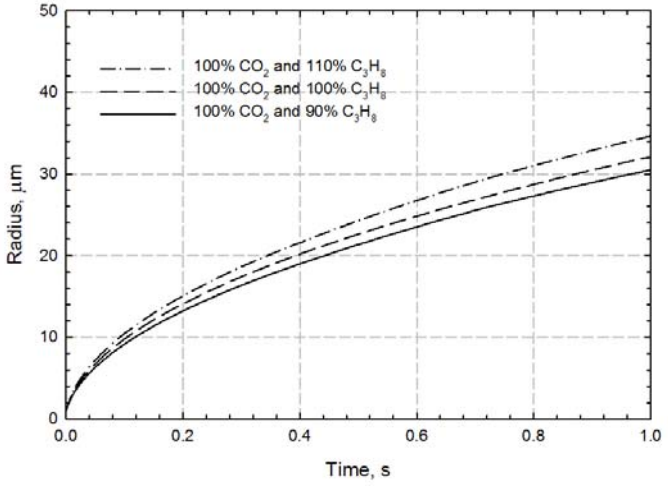

(c)

Figure 6-8 The relationship between the bubble radius and time with varying **(a)** both two gases mole concentrations, **(b)** CO_2 mole concentration, and **(c)** C_3H_8 mole concentration

different, while the individual mole concentration of CO_2 and C_3H_8 vary with the same percentage change with respect to their initial values (see Figures 6-8b and 6-8c).

Effect of CO_2 mole concentration shows a greater impact on the bubble growth than that of C_3H_8. The underlying reason is because the change of mole concentration of the dissolved gas in the oleic phase is capable of affecting the thermodynamic bubblepoint pressure. Thus, the supersaturation pressure is actually changed when the liquid pressures of Scenarios #16–19 utilized in simulation are still equal to the pressure of Scenario #1. More specifically, the original thermodynamic bubblepoint pressure is measured to be 2220 kPa. Also, when the mole concentration of CO_2 is varied to be 90% and 110% of the original mole concentrations, the thermodynamic bubblepoint pressures of the mixture are calculated to be 2354 kPa and 2063 kPa, respectively. The corresponding supersaturation pressures are respectively determined to be 754 kPa and 463 kPa. Likewise, the thermodynamic bubblepoint pressures of 90% and 110% C_3H_8 mole concentrations are calculated to be 2235 kPa and 2186 kPa, respectively, while the corresponding supersaturation pressures are found to be 635 kPa and 586 kPa. Compared with the original supersaturation pressure of 620 kPa, the changed CO_2 mole concentrations lead to larger deviations of supersaturation than those of C_3H_8 and further a greater influence on the bubble growth rate based on the discussion of Section 6.3.3.

6.3.5 Radius of liquid shell

Figure 6-9 illustrates three profiles on gas bubble radius with varied liquid cell radius ranged from 50–200 μm (Scenarios #1, 20, and 21). Although it can be observed that the

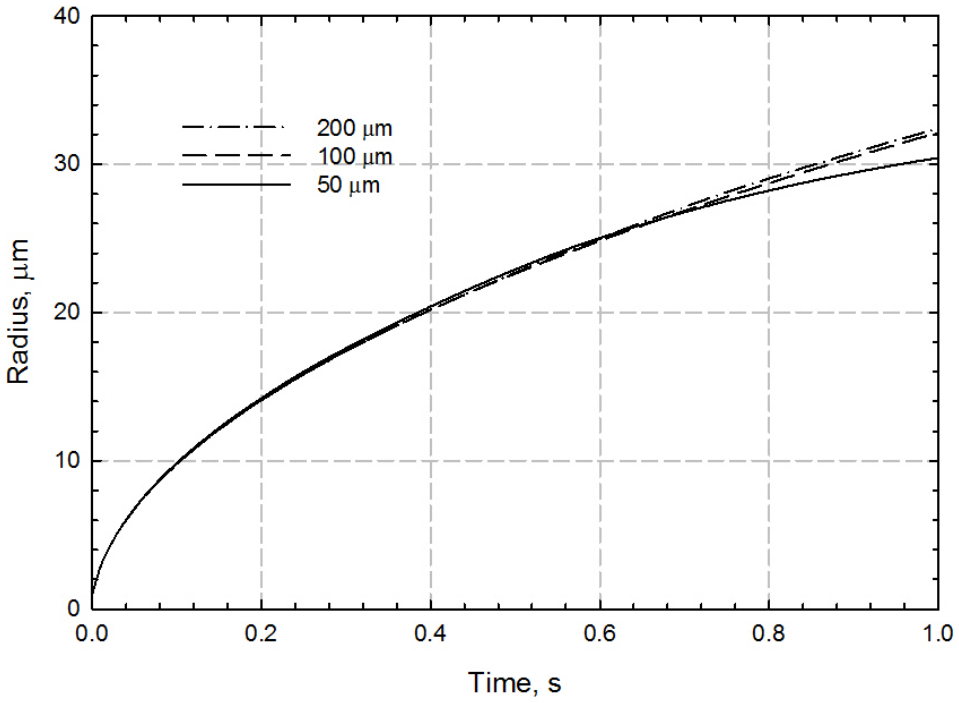

Figure 6-9 The relationship between the bubble radius and time with different liquid cell radius

gas bubble radius generally increases with an increase in liquid cell size, there is no large difference between 100 μm and 200 μm in comparison to that between 50 μm and 100 μm. Physically, at early stage of gas bubble growth, the decline of mole concentration of the dissolved gas in the liquid cell only occurs in the vicinity of gas bubble. As for the liquid shells with a radius of 100 μm and 200 μm, the decline of mole concentration caused by the mass transfer on the gas-liquid interface has not spread to the outer boundaries of the liquid shell during the period of simulation. In contrast, when the liquid shell radius is 50 μm, the mole concentrations of CO_2 and C_3H_8 have been 88.8% and 94.9% of their initial values at the end of the simulation, respectively.

Also, the relationship between liquid shell radius and bubble growth can be employed to interpret the better stability of foamy oil generated with a faster pressure decline rate. Both theoretical analysis and experimental observation have shown that bubble density increases as an increase in the pressure decline (Firoozabadi and Kashchiev, 1996). Meanwhile, radius of liquid shell actually is a parameter closely associated with gas bubble density. Physically, the lower gas bubble density is, the larger the liquid cell will be. Therefore, a smaller liquid cell, further a smaller gas bubble, should be expected under a higher pressure decline rate. On the other hand, Geilikman *et al*. (1995) categorized gas bubbles of heavy oil into a rigid (small) bubble and a soft (large) bubble, indicating that the large bubble is less stable than the small bubble. All the aforementioned findings imply that a small liquid cell stemmed from a high pressure decline rate can lead to a stable foamy oil system.

6.3.6 Pressure decline rate

In practice, the nonequilibrium conditions inducing the formation of gas bubble are always generated by the gradually enlarged system volume or decreased system pressure. Two scenarios (Scenarios #22 and 23) are designed to examine the impact of decline rate of system pressure on the bubble growth. Figure 6-10 illustrates the profiles of gas bubble radius over time. In particular, the system pressures of both Scenarios #22 and 23 begin to decrease from 1800 kPa. The pressure decline rate of Scenario #22 (i.e., 10.0 kPa/s) is two times as large as that of Scenario #23 (i.e., 5.0 kPa/s). It can be found that the gas bubble radius of former is gradually larger than that of the latter. The different supersaturation pressures are the primary cause of such phenomenon, that is, the supersaturation pressure of Scenario #22 is gradually higher than that of Scenario #23 with time because of a larger pressure decline rate of the former. Correspondingly, the gas bubble radius of the former increases faster.

6.3.7 Relationship between bubble growth rate and time

Sheng *et al*. (1999c) concluded that the gas bubble radius should be a linear function of the square root of time for diffusion-controlled gas bubble growth. To examine the relationship between gas bubble radius and time, Scenarios #1, 11, 15, 20, and 22 are chosen to represent the bubble growth processes under different conditions in this study. Figure 6-11 depicts the profiles of bubble radius over the square root of time.

It is noteworthy that gas bubble radius is observed to be a linear function of square root of time, i.e., $r \propto t^{1/2}$, in a specific range of time except for Scenario #22 (see Figure 6-11).

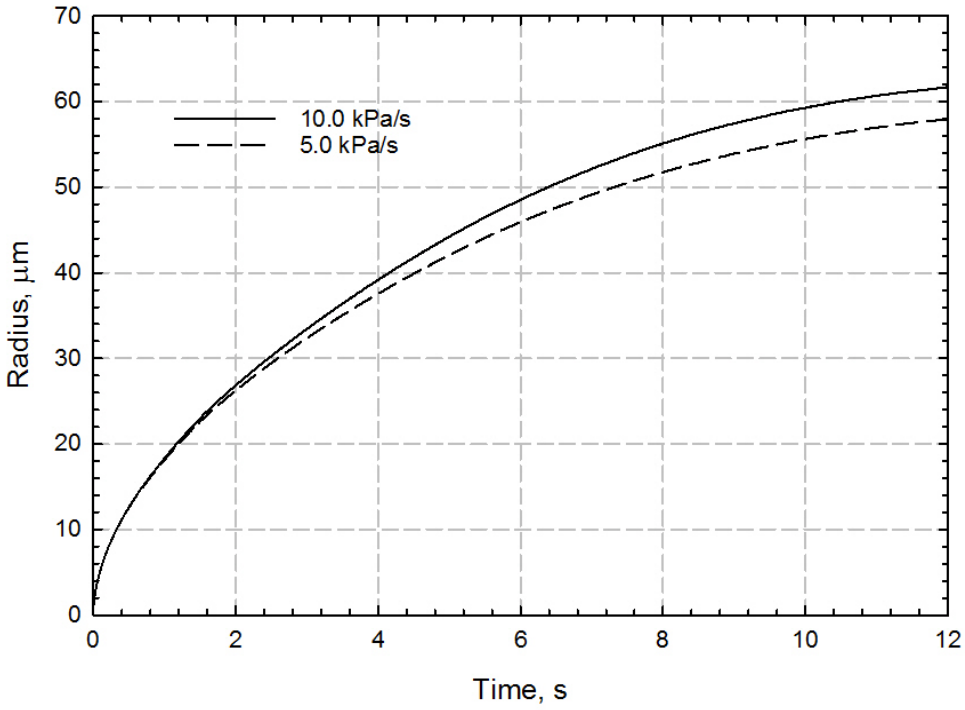

Figure 6-10 The relationship between the bubble radius and time with different pressure decline rates

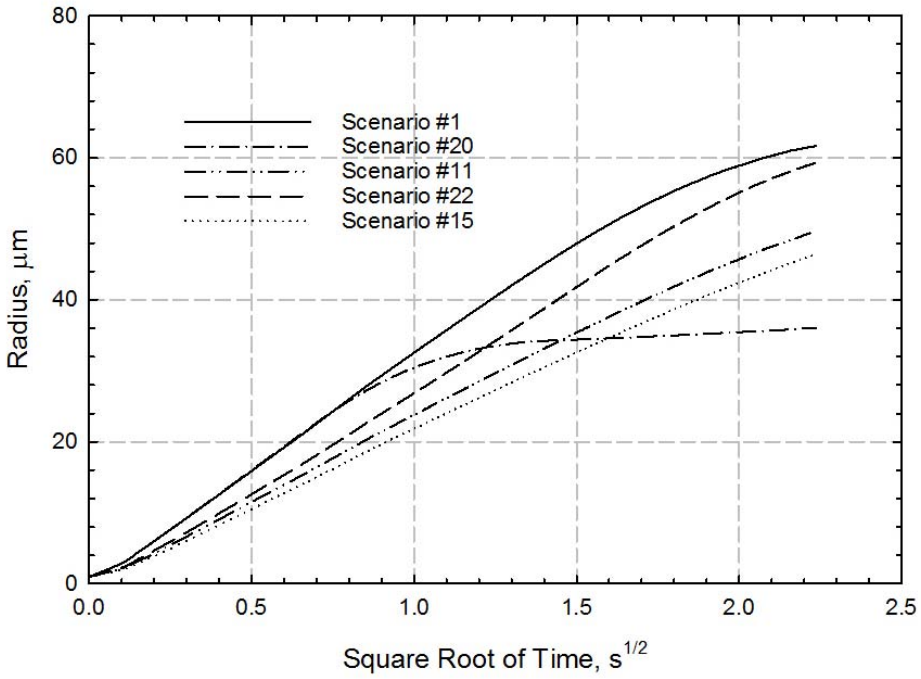

Figure 6-11 The relationship between the bubble radius and square root of time

Although the starting points of such linear relationship are almost same, the ending points are different for Scenarios #1, 11, 15, 20. Such difference is actually caused by the limited volume of the liquid cell. According to the discussion in Section 6.3.5, the gas bubble growth rate is going to be slowed down, when the decline of dissolved gas concentration spreads to the outer boundary of the liquid cell. Further, the decreased bubble radius growth rate results in the deviation of the relationship between the radius and square root of time from the straight line. Meanwhile, the difference of conditions between Scenario #22 and Scenarios #1, 11, 15, and 20 is that the system pressures of the latter are decreased to the designed pressure by one-step pressure drop (constant supersaturation pressure) rather than a gradual pressure decline. Such findings imply that only the two conditions (infinite surrounding liquid volume and one-step pressure drop) are met, the linear relationship between the gas bubble radius and the square root of time may be expected. Otherwise, the bubble growth rate is a changeable parameter over the square root of time because of the limited amount of diffusing gas in the liquid cell and the varying supersaturation pressures from the gradual pressure depletion.

6.4 Summary

A mechanistic model has been proposed and validated to quantify the process of a solitary gas bubble growth with multicomponent gas in the alkane solvent(s)–CO_2–heavy oil systems. Especially, utilization of the real gas equation and the quasi-equilibrium condition is verified to effectively attain the simulation of a gas bubble growth under the reservoir conditions. Based on the CCE experiments conducted under equilibrium and nonequilibrium conditions, a gas bubble growth process in CO_2–C_3H_8–heavy oil systems

is illustrated with the newly proposed model, while a method for determining the critical nucleus radius has also been developed. Five factors strongly related to the gas bubble growth, i.e., mass transfer, supersaturation pressure, mole concentration, liquid cell radius and pressure decline rate, are evaluated and discussed. It can be concluded that a higher diffusion coefficient is able to result in a larger bubble growth rate. However, when the diffusion coefficient of only one gas component theoretically varied, the changed range of the bubble growth rate is actually dependent on the combined effect of mole concentration and diffusion coefficient of individual diffusing gas. Also, a larger supersaturation pressure and pressure decline rate can effectively enhance the bubble growth rate owing to the generated higher concentration gradient. The effect of the changed mole concentration of each diffusing gas does not impose a similar effect on the bubble growth despite the similar changing range of mole concentration. This is because the same range of the varied composition of each gas component is not capable of having the same impact on the thermodynamic bubblepoint pressure, and further the supersaturation. In addition, a large liquid cell leads to a large gas bubble after the decline of mole concentration in the liquid phase spreads to the boundary of the liquid cell. The linear relationship between gas bubble radius and square root of time may only be found under conditions of an unlimited surrounding liquid volume and one-step pressure drop.

CHAPTER 7 QUANTIFICATION OF DYNAMIC VOLUME OF FOAMY OIL FOR ALKANE SOLVENT(S)–CO_2–HEAVY OIL SYSTEMS WITH CONSIDERATION OF PREFERENTIAL DIFFUSION UNDER NONEQUILIBRIUM CONDITIONS

7.1 Introduction

Based on the mechanistic model of a single-gas bubble growth developed in Chapter 6, a novel and robust technique has been developed to determine the dynamic volume growth of multi-component gas bubbles with consideration of preferential mass transfer of each gas component in alkane solvent(s)–CO_2–heavy oil systems under nonequilibrium conditions. Combined with the newly proposed mechanistic model, a volume equation is incorporated into an equation matrix to theoretically describe the kinetics of multi-component gas bubbles growth. Such an equation matrix is then solved to match the pressure-volume as a function of time measured with CCE tests under nonequilibrium conditions, allowing for determining the dynamic volume of gas bubbles by taking the preferential diffusion of each component in a gas mixture into account. Subsequently, dynamic composition and volume of evolved gas in foamy oil can be quantified and analyzed. On the basis of the matched experimental measurements, sensitivity analysis has been performed to numerically examine supersaturation pressure, pressure decline rate, and amount of each gas component on the growth of gas bubbles.

7.2 Theoretical Formulations

7.2.1 Mathematical model

The mathematical formulations and the corresponding assumptions in this chapter are similar as those introduced in Chapter 6. The total volume of experimental fluids, which

is calculated as a sum of the liquid phase volume and the gas phase volume during the CCE tests with a constant pressure-decline rate, can be written as follows,

$$V(t) = V_l(t) + V_g(t) \quad [7\text{-}1a]$$

where $V_l(t)$ and $V_g(t)$ are the volume of liquid and gas phase, respectively. The liquid volume can be formulated with the following equation under the experimental conditions of a constant pressure-decline rate,

$$V_l(t) = V_{li}\left(1 + c_t d_p t\right) \quad [7\text{-}1b]$$

where V_{li} is the initial liquid phase volume; c_t is compressibility of liquid; P_i is initial pressure of the entire system; and d_p is the pressure-decline rate. Since the gas phase is generated in a form of bubbles during the entire CCE tests based on the assumption, the gas volume can be readily expressed as,

$$V_g(t) = \frac{4\pi r_b(t)^3}{3} N_b \quad [7\text{-}1c]$$

where N_b is total number of gas bubbles in oleic phase.

The continuity equation, equation of motion, mass transfer equation and the related boundary conditions are detailed in Sections 6.2.2 to 6.2.5.

7.2.2 Numerical solution

It is notable that it is extremely difficult to obtain an analytical solution for such an equation matrix because of the strongly non-linear relationship between properties of gas and liquid and velocity of the growing gas bubble radius. Accordingly, an implicit finite difference scheme (i.e., Crank-Nicolson method) is employed to discretize the non-linear

equation matrix to achieve a numerical solution due to its recognized stability. The equation-solving procedures are detailed as follows:

(1) The required parameters about the physical properties of gas and liquid phase, e.g., composition of each component are firstly input, and then the initial conditions are assigned;

(2) The guessing values of a total amounts of gas bubbles and individual diffusion coefficients are given;

(3) A gas bubble radius at time $t+\Delta t$ is assumed. Then, the gas bubble pressures, p_g^t at time t and $p_g^{t+\Delta t}$ at time $t+\Delta t$ are calculated based on Equation [6-2], respectively. Also, velocity of the gas-liquid interface is obtained with Equation [6-1];

(4) The gas concentration is determined based on the quasi-equilibrium boundary condition. Then, the concentration distribution of each gas component in the liquid cell is computed with Equation [6-5]. Lastly, the amount of each gas component diffusing into a gas bubble is accomplished;

(5) The gas bubble pressure at time $t+\Delta t$, $p_g^{t+\Delta t*}$, is also calculated on the basis of mass balance of each gas component in the liquid and gas bubble;

(6) Theoretically, once $p_g^{t+\Delta t}$ in Step #3 is equal to $p_g^{t+\Delta t*}$ in Step #5, the assumed gas bubble radius in Step #3 is considered as the actual value and the calculation can proceed to the next time step. Otherwise, an adjusted gas bubble radius at time $t+\Delta t$ will replace the original one assumed in Step #3 and repeat Steps #3-6 until the objective function, i.e., Equation [6-9], satisfies the prespecified accuracy.

(7) The calculation is continuously conducted from Step #3 to Step #6 at each time step till the total experimental time is reached. Then, the volume of fluids at each time step is computed with Equations [7-1a]-[7-1c]. The objective function associated with the dynamic volume of experimental fluid and composition of evolved gas is respectively defined as follows,

$$O(V,c) = O(V) + O(c) \quad [7\text{-}2a]$$

$$O(V) = \sqrt{\frac{1}{N_m}\sum_{t=0}^{N_m}\left(\frac{V_T^c - V_T^m}{V_T^m}\right)^2} \quad [7\text{-}2b]$$

$$O(c) = \sqrt{\frac{1}{N_g}\sum_{i=1}^{N_g}\left(\frac{y_{\exp}^i - y_{cal}^i}{y_{\exp}^i}\right)^2} \quad [7\text{-}2c]$$

where V_T^c is the calculated volume of experimental fluids; V_T^m is the measured volume of experimental fluids; N_m is the amount of measured points of volume; $y_{\exp}$ is the measured mole fraction; y_{cal} is the calculated mole fraction; N_g is the number of gas component; When Equation [7-2a] reaches the prespecified accuracy, individual diffusion coefficient for each component in a gas mixture and the corresponding amounts of gas bubbles are viewed as the actual ones for the alkane solvent(s)–CO_2–heavy oil systems under nonequilibrium conditions. On the contrary, the guessing values in Step #2 will be adjusted to lessen the deviation between the measured volume and diffusion coefficients and calculated ones with repeating the calculation from Step #2 to Step #7. The flowchart of solving procedure is presented in Figure 7-1.

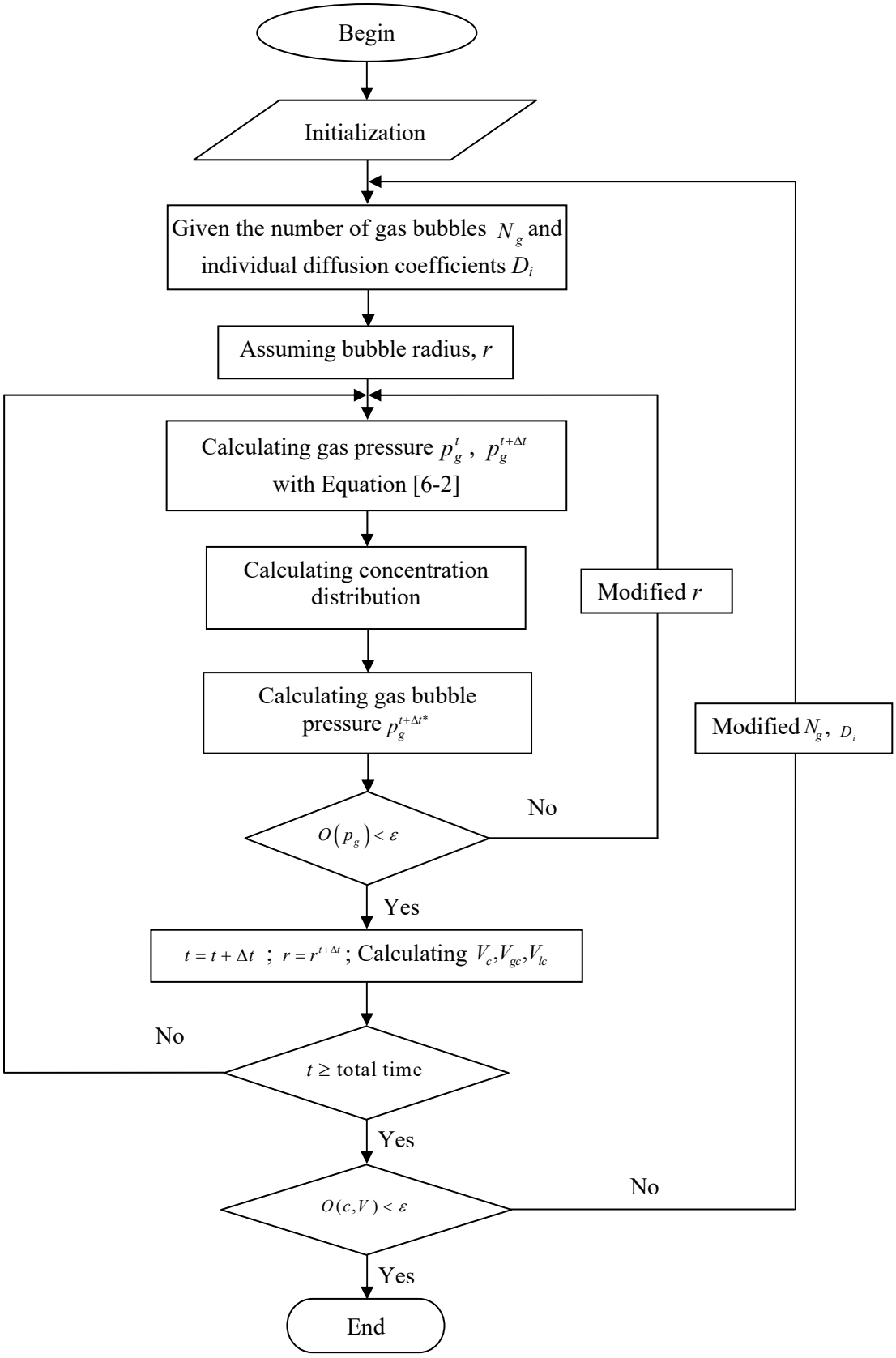

Figure 7-1 Flowchart of numerically solving the mathematical models

7.3 Results and Discussion

Two CCE tests conducted for CH_4–C_3H_8–heavy oil systems (Test #14 in Table 5-2) and CH_4–CO_2–heavy oil systems (Test #16 in Table 5-2) were matched with the newly proposed model in this chapter. It can be observed that the experimental duration of CH_4–CO_2–heavy oil systems is much longer than that of CH_4–C_3H_8–heavy oil systems because a sufficient amount of free gas can be collected for performing GC analysis (Figure 5-2). Also, both the individual diffusion coefficient of each gas component and the amount of evolved gas are calculated and analyzed. Subsequently, supersaturation pressure, pressure decline rate, and mole concentration of gas component are evaluated with 10 designed scenarios based on CH_4–C_3H_8–heavy oil systems to identify the underlying mechanisms affecting the dynamic volume of foamy oil. The corresponding input parameters in the mathematical model are detailed in Tables 7-1 and 7-2. It is worthwhile noting that the diffusion coefficients of CH_4 and C_3H_8 in CH_4–C_3H_8–heavy oil systems are 1.2×10^{-10} m^2/s and 6.8×10^{-10} m^2/s, respectively, which are measured in pure gas–heavy oil systems (Yang and Gu, 2006c).

7.3.1 Dynamic volume and preferential diffusion

The measured bubblepoint pressures and pseudo-bubblepoint pressures of two experimental fluids are listed in Table 5-2. In addition, the volume of free gas in the CH_4–CO_2–heavy oil systems at pressure of 1930 kPa was measured to be 1.90 cm^3 under non- equilibrium conditions. As depicted in Figure 7-2, there exist excellent agreements between the measured volume-pressure profiles and calculated ones with the newly proposed models. The compositions of CH_4 and CO_2 in evolved gas at the end of

Table 7-1 Physical and correlated properties of CH_4–CO_2–heavy oil systems and CH_4–C_3H_8–heavy oil systems

Parameter	CH_4–CO_2–heavy oil systems	CH_4–C_3H_8–heavy oil systems
Temperature (K)	342.7	323.4
Pressure (kPa)	3516	2500
Coefficient *A* of heavy oil viscosity	9.4669	9.4669
Coefficient *B* of heavy oil viscosity	3.5861	3.5861
Initial bubble radius (μm)	1.0	1.0
Number of gas bubbles	104	1010

Table 7-2 The 10 scenarios designed for sensitivity analysis

Scenario No.	Supersaturation pressure (kPa)	Pressure decline rate (kPa/min)	C_3H_8 mole concentration (referred to original value)	CH_4 mole concentration (referred to original value)
24	400	–*	–*	–*
25	600	–*	–*	–*
26	–*	10	–*	–*
27	–*	30	–*	–*
28	–*	–*	110%	110%
29	–*	–*	90%	90%
30	–*	–*	110%	100%
31	–*	–*	90%	100%
32	–*	–*	100%	110%
33	–*	–*	100%	90%

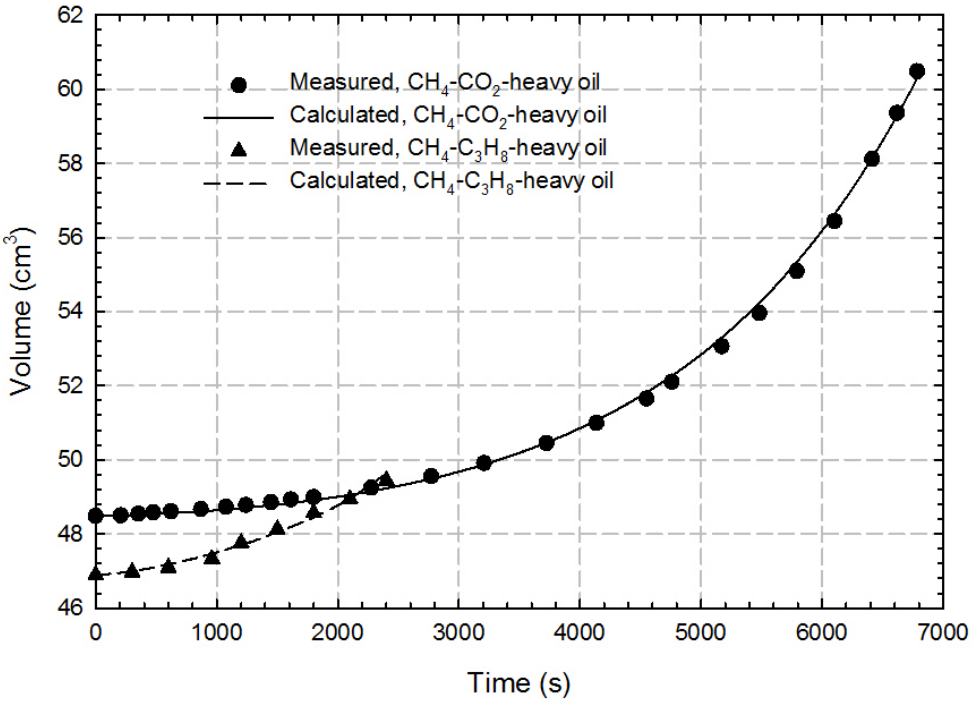

Figure 7-2 Measured and calculated liquid volumes of CH_4–CO_2–heavy oil systems and CH_4–C_3H_8–heavy oil systems below the pseudo-bubblepoint pressure under nonequilibrium conditions

experimental duration are calculated to be 45.9 mol% and 54.1 mol%, respectively, which is very close to their corresponding experimental measurements of 47.2 mol% and 51.6 mol% with a respective deviation of 2.8% and 4.8%. Both of the aforementioned results confirm that the newly developed model can be used to effectively and accurately capture the essentially time-dependent volume of foamy oil. Furthermore, such GC compositional analysis also validated the feasibility of Assumption #5 in Section 3.2 since no C_{2+} components are detected in the free gas. Based on the total volume of evolved gas bubbles calculated by the newly proposed model, amount of the free gas in the CH_4–CO_2–heavy oil systems can be computed to be 1.64 cm^3 with a relative deviation of 13.7% from the measured volume (i.e., 1.90 cm^3). Such a relatively large difference is probably caused by the assumption that properties of evolved gas during the mass transfer process can be quantified with real gas equation, which is generally utilized to describe the properties of gas phase under equilibrium conditions. The corresponding computation needs an additional equation related to the amounts of entrained gas and evolved gas (Equation [4-6]) since the proposed model in this chapter mainly focuses on examining the individual mass transfer of each component in a gas mixture in the viscous oleic phase under nonequilibrium conditions.

The diffusion coefficients of CH_4 and CO_2 during the nonequilibrium CCE tests for CH_4–CO_2–heavy oil systems are determined to be 7.81×10^{-10} m^2/s and 9.96×10^{-10} m^2/s, respectively. It can be found that both of them are larger than the ones obtained with pure gas in the literature (Table 7-3). Such a difference on diffusion coefficient for both CO_2 and CH_4 may be mainly attributed to the fact that a relatively high temperature and a low

Table 7-3 Comparison of diffusion coefficients for CO_2 and CH_4 in different heavy oils

Gas system	Sources	Heavy oil	Viscosity (cP)	Pressure (kPa)	Temperature (K)	Diffusion coefficient (10^{-10} m^2/s)
CO_2: 38.5 mol% CH_4: 61.5 mol%	This study	Lloydminster heavy oil	12854 @ 294.55 K	3516-1255	342.7	9.96 (CO_2) 7.81 (CH_4)
CO_2	Yang and Gu (2006c)	Lloydminster heavy oil	23000 @ 297.05 K	2000-6000	297.05	2.0-5.5
CO_2	Li and Yang (2016)	Lloydminster heavy oil	12854 @ 294.55 K	3741-3371	294.55	8.24
CH_4	Yang and Gu (2006c)	Lloydminster heavy oil	23000 @ 297.05 K	6000-14000	297.05	1.2–1.9
CH_4	Upreti and Mehrotra (2002)	Athabasca Bitumen	821000 @ 298.15 K	4000	298.15-363.15	0.810-4.315
				8000		0.582-2.029

viscosity of heavy oil are able to result in relatively large diffusion coefficient. The reason is that, physically, a low viscosity of heavy oil can cause an increase in diffusion coefficient based on Equation [3-7]. Meanwhile, a higher concentration of dissolved gas should be found in a supersaturated alkane solvent(s)–CO_2–heavy oil systems oil system under comparable conditions. This can lead to a larger diffusion coefficient on the basis of experimental work (Yang and Gu, 2008), and further, enhance the mass transfer rate. This likely is another underlying reason why a larger diffusion coefficient can be found and determined.

7.3.2 Growth rate of evolved gas

As can been seen in Figure 7-2, the growth rate for the volume of CH_4–C_3H_8–heavy oil systems, or essentially, the volume of evolved gas because of the minor contribution of pure liquid expansion to the total volume, is much higher than that of CH_4–CO_2–heavy oil systems. Such a difference can mainly be ascribed to both a faster mass transfer rate and a lower experimental pressure during the CCE tests. The gas exsolution rate is introduced to characterize the mass transfer rate of a gas solvent, which is directly calculated from the amount of evolved gas and the corresponding pressure drop, although the volume growth rate of evolved gas actually is not a constant. In particular, gas exsolution rates during the entire experimental processes for CH_4–C_3H_8–heavy oil systems and the same time period (0 to 40 min) for CH_4–CO_2–heavy oil systems are calculated to be 2.31×10^{-6} mol/kPa and 0.96×10^{-6} mol/kPa, respectively. As listed in Table 5-2, the pseudo-bubblepoint pressure of the former is only 2500 kPa, which is 1016 kPa less than that of the latter during the gas exsolution process (see Figure 7-2) that

takes the same pressure-decline rate used in both CCE tests into account. Such a large pressure difference inevitably results in a large volume difference between two CCE tests, not to mention a faster gas exsolution rate occurring in CH_4–C_3H_8–heavy oil systems.

7.3.3 Concentration and composition of evolved gas

Concentration profiles of gas in a liquid cell for both experimental fluids are plotted in Figures 7-3 and 7-4, respectively. As can be found, concentration of each component in the gas mixture is gradually decreased with time. Furthermore, the decreasing rate of concentration of each component at the gas-oil interface is determined by the pressure decline rate based on Equation [6-7b] since gas solubility in oleic phase, physically, decreases with a decrease in pressure, provided that temperature remains constant. On the other hand, the concentration of each component gradually declines with a decrease along the distance to the interior boundary of the liquid shell, i.e., the gas-oil interface, which sustains the bubble growth. Although the liquid cell is only an assumed liquid sphere containing the gas bubble, such concentration profile of each gas component in the liquid surrounding the gas bubble is similar to those documented elsewhere (Moulu, 1989).

Accordingly, the dynamic mole compositions of evolved gas in CH_4–CO_2–heavy oil systems and CH_4–C_3H_8–heavy oil systems can be obtained on the basis of the computed concentration distribution in the liquid phase (see Figure 7-5). It is worthwhile noting that, as for CH_4–CO_2–heavy oil systems, the calculated compositions of two gases are very close to the measured ones at the end of the experiment, which further confirms the

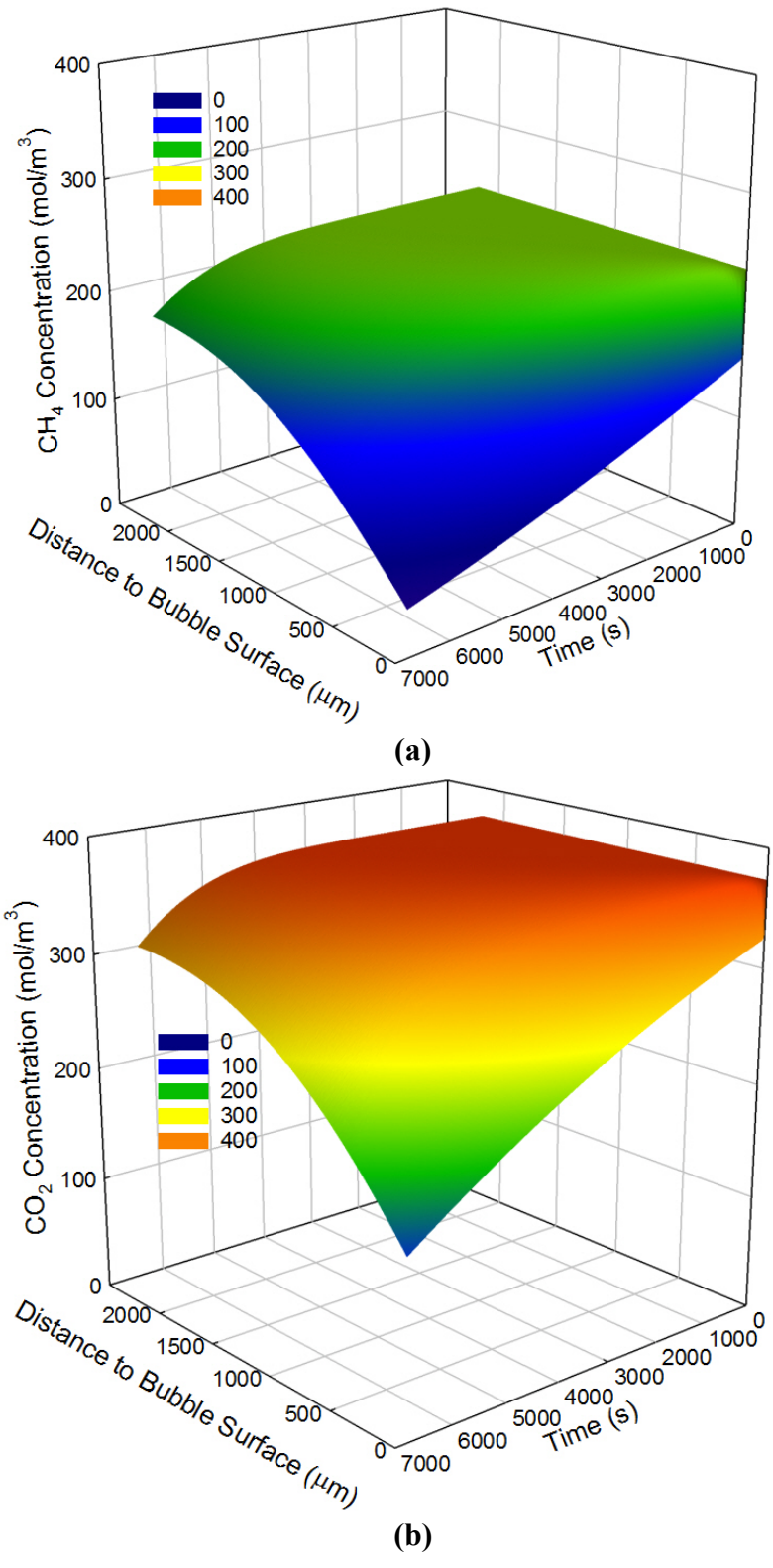

Figure 7-3 Concentration distributions of **(a)** CH_4 and **(b)** CO_2 in liquid shell of CH_4–CO_2–heavy oil systems

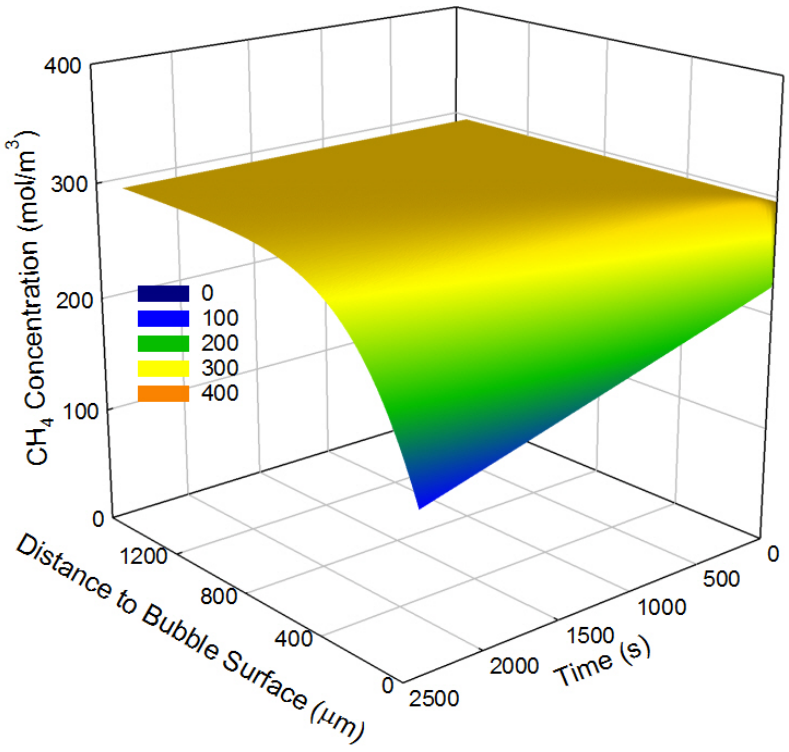

(a)

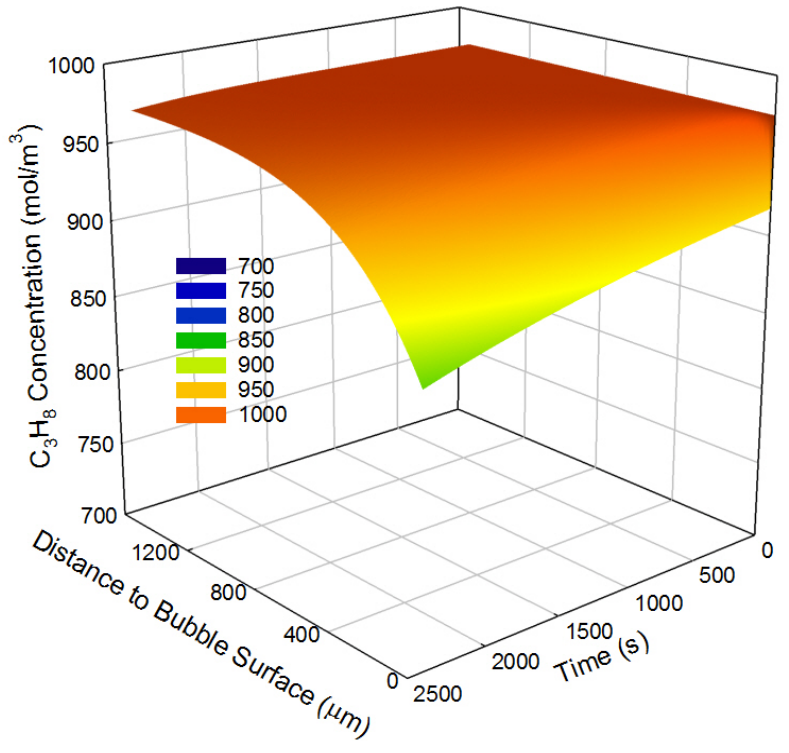

(b)

Figure 7-4 Concentration distributions of **(a)** CH_4 and **(b)** C_3H_8 in liquid shell of CH_4–C_3H_8–heavy oil systems

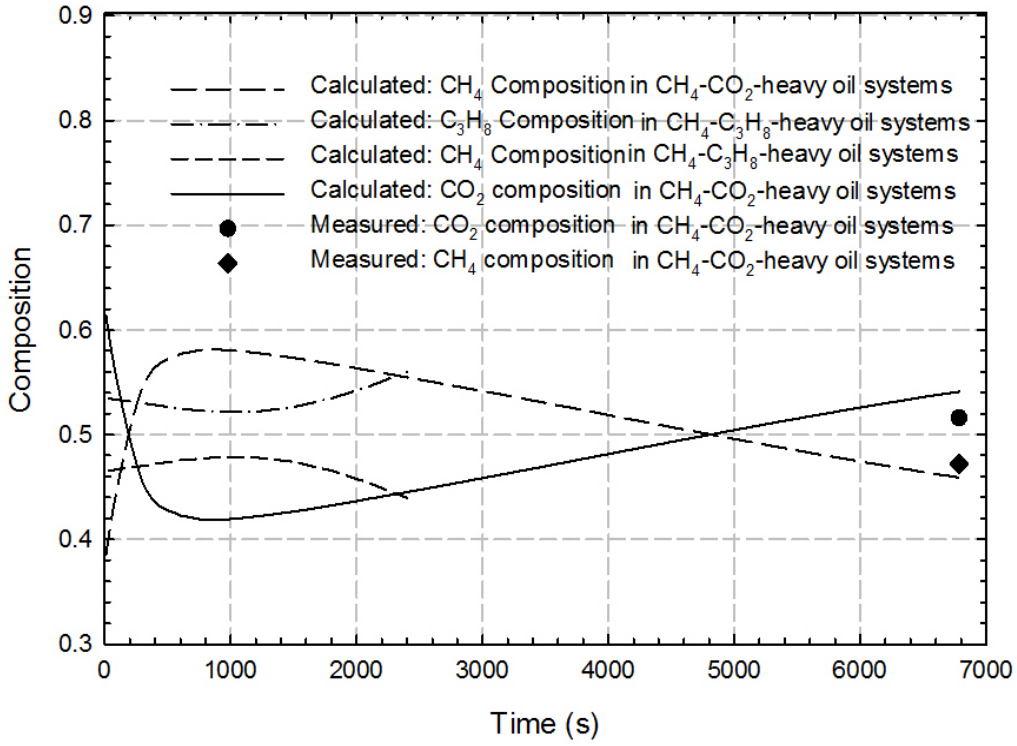

Figure 7-5 Measured and calculated dynamic composition of each gas component in evolved gas for CH_4–CO_2–heavy oil systems and CH_4–C_3H_8–heavy oil systems, respectively

reliability of the newly developed technique for determining dynamic compositions of the aforementioned systems. Meanwhile, it can be found that CH_4 mole compositions reach maximum at the early stage of gas exsolution and then gradually decreases in CH_4–CO_2–heavy oil systems and CH_4–C_3H_8–heavy oil systems. Correspondingly, inverse trends are observed about both CO_2 mole composition and C_3H_8 mole composition. Such a phenomenon is essentially stemmed from the mass transfer rate of each gas component. At the beginning, a large concentration gradient of CH_4 greatly contributes to the mass transfer of CH_4 from liquid to gas, while the diffusion coefficient of CH_4 is less than those of CO_2 and C_3H_8. Particularly, the average concentration difference of CH_4 between the gas-oil interface and the outer boundary of the liquid cell is found to be 85.2 mol/m^3 in the first 500 seconds, compared with 53.3 mol/m^3 of CO_2 during the same time period in CH_4–CO_2–heavy oil systems. Likewise, such concentration differences are 94.7 mol/m^3 and 67.3 mol/m^3 for CH_4 and C_3H_8 during the first 1200 seconds, respectively, in CH_4–C_3H_8–heavy oil systems. However, such concentration difference is gradually decreased with time, though liquid pressure is still continuously declined with a constant rate, resulting in a decrease in the mole concentration at the gas-liquid interface. Therefore, the contribution of the relatively large diffusion coefficient of either C_3H_8 or CO_2 on the mass transfer rate is greater than those of the relatively high concentration gradient of CH_4 after a certain time. This implies that the compositions of evolved gas are actually dominated by the mass transfer rate of each gas component, which is consistent with the Fick's law. At the end, however, the composition of evolved gas will be predictably close to the initial gas composition since all the dissolved gas will be released from the oleic phase at the atmospheric pressure.

7.3.4 Sensitivity analysis

1) Supersaturation pressure

Supersaturation pressure is the pressure difference between the bubblepoint pressure and actual pressure in a supersaturated liquid system (Kamath and Boyer, 1995) and usually employed to represent the supersaturated degree. Figure 7-6 plots the volume growth curves of foamy oil under supersaturation pressures of 400, 600 kPa (Scenarios #24 and 25) and experimental case of CH_4–C_3H_8–heavy oil systems (500 kPa), respectively. The growth rate of foamy oil volume is found to accelerate with an increase in supersaturation pressure. The newly proposed model reveals that a high supersaturation pressure is able to result in a large concentration gradient of each gas solvent both at the gas-liquid interface and within the liquid. Hence, a fast mass transfer rate can be expected based on the Fick's law. In other words, more dissolved gas in the heavy oil saturated with alkane solvent(s) and CO_2 is able to diffuse into gas bubbles during the same time frame.

2) Pressure decline rate

Generally, a high pressure decline rate has been experimentally validated to cause a low pseudo-bubblepoint pressure, i.e., a large critical supersaturation pressure (Kumar *et al*., 2002). Also, as mentioned in Section 6.3.5, a more stable foamy oil system can be generated because of the smaller gas bubbles resulting from a higher pressure decline rate.

In addition to the experimental case (i.e., pressure decline rate: 20 kPa/min), two scenarios (Scenarios #26 and 27) with different pressure decline rates are simulated so as to examine the corresponding effects. Figure 7-6 presents the relationship between the

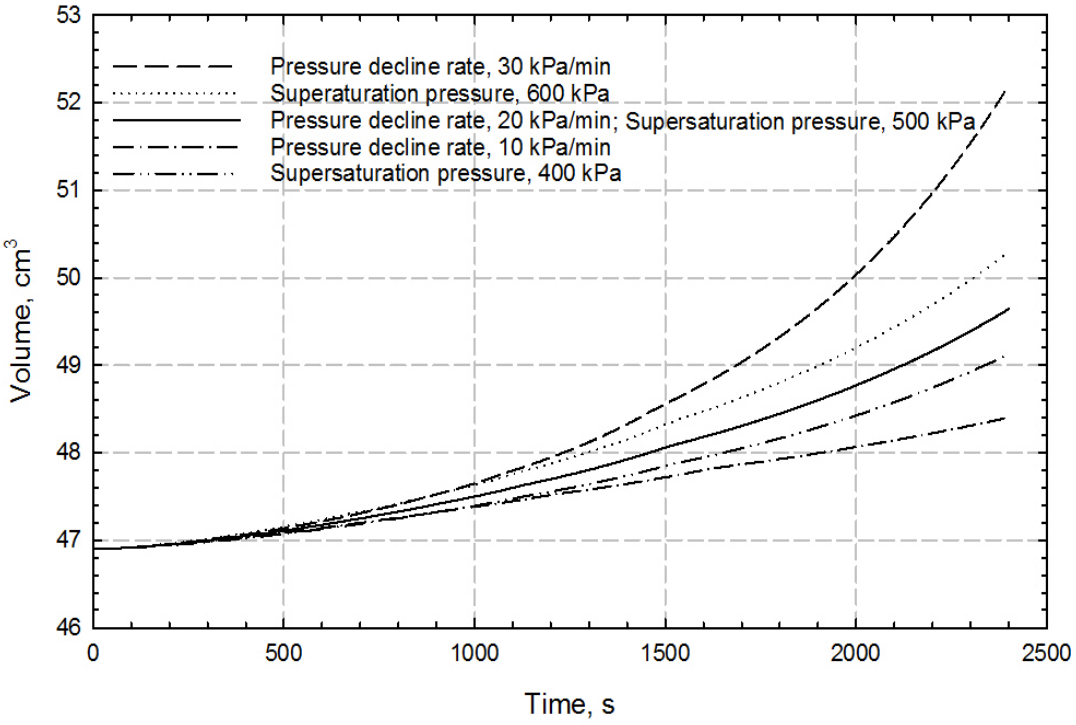

Figure 7-6 Volume of foamy oil under different supersaturation pressures and pressure decline rates, respectively

volume of foamy oil and pressure decline rate. It reveals that a high pressure decline rate is beneficial to the volume growth of foamy oil. Physically, gas solubility is decreased with a decrease in fluid pressure. A higher pressure decline rate means that the fluids pressure is lower after certain time, when the other operating conditions remain the same. Therefore, a stronger supersaturation degree is established because more dissolved gases are waiting for being released from the oleic phase to be evolved gas, which is caused by a lower solubility. Hence, as mentioned previously, a faster volume growth of foamy oil can be attained by an enhanced the mass transfer rate.

3) Gas concentration

Two types of scenarios are designed and simulated, which are respectively featured by changing individual concentration of each gas and both. More specifically, both mole concentrations of CH_4 and C_3H_8 are varied with ±10% on the basis of actual experiment ones in Type I (Scenarios #28 and 29). Likewise, the individual mole concentrations of CH_4 and C_3H_8 are changed to be 90% and 110% of their original ones, respectively, in Type II (Scenarios #30–33).

Figure 7-7 depicts the relationships between the foamy oil volume and time with various mole concentrations. As can be seen from Figure 7-7a, the mole concentration of dissolved gas imposes a great effect on the growth of foamy oil volume, although the range of mole concentration is only changed to be ±10% of their original ones. Supersaturation and mass transfer rate may be the underlying reasons accounting for such a phenomenon. It is well recognized that the thermodynamic bubblepoint pressure is greatly affected by the compositions and components of fluids mixture (Ahmadi *et al*.,

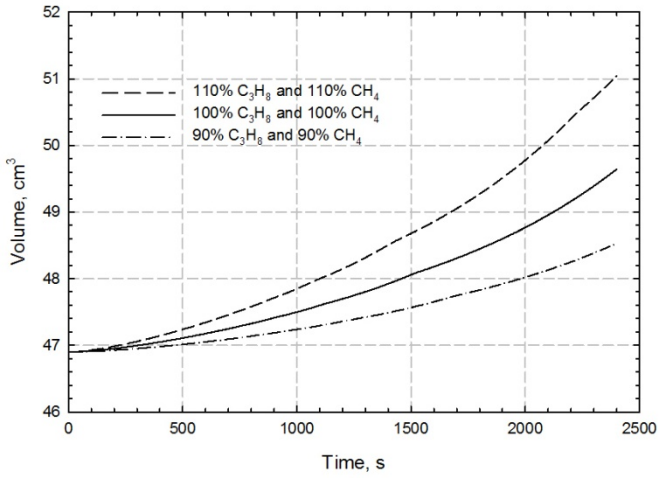

(a)

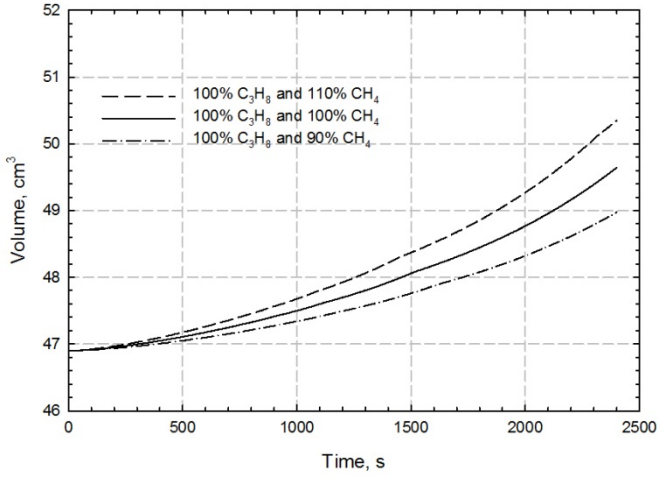

(b)

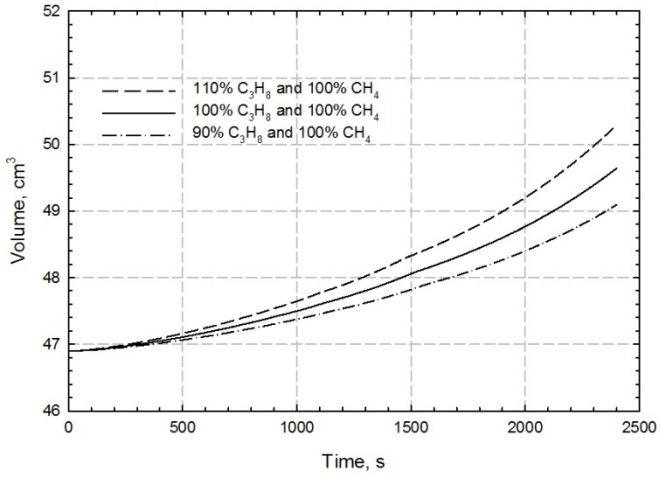

(c)

Figure 7-7 The relationship between the foamy oil volume and time with various mole concentrations for **(a)** both gases, **(b)** CH_4, and **(c)** C_3H_8

2014). When the mole concentrations of gas components are varied, it physically means the changes of either composition in the entire fluids system or thermodynamic bubblepoint pressure. In particular, the bubblepoint pressures of Scenarios #28 and 29 are calculated to be 3126 kPa and 2716 kPa, respectively, rather than 3000 kPa of Scenarios #24. Consequently, the corresponding supersaturation pressures of Scenarios #28 and 29 are computed to be 626 kPa and 216 kPa, respectively. As discussed previously, it is inevitably to change the growth rate of foamy oil volume as a function of supersaturation in Scenarios #28 and 29 since it is a monotonic increasing function of supersaturation pressure.

On the other hand, a larger mole concentration of dissolved gas is found to lead to a larger concentration gradient and a faster mass transfer rate under the same conditions based on the Fick's law. It can be concluded that a high mole concentration of dissolved gas in Scenario #28 can cause an increased volume growth rate owing to an accelerated mass transfer rate of gas components.

Meanwhile, it can be found that the variation of CH_4 mole concentration shows a greater effect on the growth rate of foamy oil volume than that of C_3H_8 (see Figures 7-7b and 7-7c). It is mainly ascribed to the compound influence of changed bubblepoint pressure and individual mole concentration of gas component, which is basically same as those for Scenarios #28 and 29. To be more specific, the bubblepoint pressures of Scenarios #30 and 31 related to C_3H_8 mole concentration are calculated to be 2897 kPa and 2960 kPa which are quite close to its original value of 3000 kPa. The bubblepoint pressures of

Scenarios #32 and 33 can reach 3160 kPa and 2692 kPa, respectively. Bubblepoint pressures for the former, evidently, make the corresponding supersaturation pressures less than those of the latter. It is worthwhile pointing out that a high mole concentration of C_3H_8 (Scenario #30) results in low bubblepoint pressure and supersaturation pressure rather than large ones like CH_4. However, a faster growth rate of foamy volume is still able to be observed, although a reduced supersaturation pressure has been stated to theoretically decrease the volume growth rate. This is because of the offset of an increase in C_3H_8 amount on the impact caused by a small supersaturation pressure.

7.4 Summary

A novel and pragmatic technique has been proposed to quantify the dynamic volume of foamy oil for alkane solvent(s)–CO_2–heavy oil systems under nonequilibrium conditions by considering preferential diffusion of each component in a gas mixture. The quasi-equilibrium boundary condition combined with PR EOS is employed at the interface of gas bubble and adjacent liquid instead of the Henry's law to represent the relationship of the gas pressure and the concentration of gas under high pressures and elevated temperatures on the basis of the classical gas bubble growth model. Such modification has been validated to be reliable for describing mass transfer processes of gas from liquid to gas bubbles based on the CCE tests with CH_4–C_3H_8–heavy oil systems and CH_4–CO_2–heavy oil systems under nonequilibrium conditions. Accordingly, individual diffusion coefficient and dynamic composition of gas component as well as the volume of evolved gas in foamy oil can be quantified with the newly proposed model. A relatively large diffusion coefficient of each gas component can be expected due to a high mass transfer rate stemmed from nonequilibrium conditions. Meanwhile, a higher volume-growth rate

of evolved gas is found for CH_4–C_3H_8–heavy oil systems compared to CH_4–CO_2–heavy oil systems owing to a faster mass transfer rate between gas and liquid phases as well as a lower pressure of gas phase in the former system. Preferential diffusion and concentration gradient are found to be the main mechanisms that affect the dynamic composition of evolved gas. The gas component with a faster mass transfer rate has a greater effect on the volume growth rate. In addition, a larger supersaturation pressure and a faster pressure decline rate are found to be beneficial to the volume growth of foamy oil due mainly to an enhanced mass transfer rate.

CHAPTER 8 CONCLUSIONS AND RECOMMENDATIONS

8.1 Conclusions

The major contributions of this research are listed as follows:

(1) A novel and pragmatic technique has been developed and validated to accurately determine the individual diffusion coefficient of each component in the alkane solvent(s)-assisted recovery processes under high pressure and elevated temperature with consideration of natural convection induced by the heated and diluted heavy oil.

(2) Novel theoretical formulations have been developed to quantify the nonequilibrium phase behaviour of alkane solvent(s)–CO_2–heavy oil systems under either a constant volume expansion rate or a constant pressure decline rate. Meanwhile, mathematical models are respectively established to determine compressibility and density of the oleic phase mixed with the entrained gas (i.e., foamy oil).

(3) A mechanistic model has been proposed and validated to describe a single gas bubble growth process with considering multicomponent gas diffusion in alkane solvent(s)–CO_2–heavy oil systems under nonequilibrium conditions. This enables us to not only examine the effects of each component in a gas mixture and operating conditions, such as mole fraction, diffusion coefficient

and pressure decline rate, on the gas bubble growth, but also determine the critical nucleus radius.

(4) A pragmatic and robust technique has been developed and validated to determine the dynamic volume of foamy oil by considering preferential diffusion of individual components in a gas mixture for the alkane solvent(s)–CO_2–heavy oil systems. Such newly developed technique allows us to determine individual diffusion coefficient of each gas component in the gas mixture during the mass transfer processes of foamy oil formation.

Accordingly, the main conclusions of this research work can be summarized as follows:

(1) The individual diffusion coefficient of each diffusing gas in an alkane solvent(s)–CO_2–heavy oil mixture determined with the newly proposed model is found to be higher than the one calculated by using the conventional method. This can be explained by the fact that a molecular diffusion process is slowed down by the natural convection induced by the volume expansion of a diluted and heated oleic phase due to its opposite movement direction.

(2) The apparent critical supersaturation pressure is increased with either an increase in expansion rate of the mixture volume or an increase in pressure decline rate because a higher pressure decline rate leads to fewer nuclei with critical size and slower gas bubble growth. A high temperature usually results

in a decrease in critical supersaturation pressure owing to an accelerated nucleation rate and diffusion process.

(3) Both density and compressibility of foamy oil are a function of time, or essentially, the amount of the entrained gas. The density of foamy oil is found to sharply decrease at the pseudo-bubblepoint pressure due mainly to the dramatic increase in the volume of the entrained gas in heavy oil. Meanwhile, compressibility under nonequilibrium conditions below bubblepoint pressure is enhanced by the increasingly entrained gas and found to be much larger than that under equilibrium conditions. The difference of physical properties between a constant pressure decline rate and a constant volume expansion rate lies in the effect of rebound pressure which only can be observed under constant volume expansion rates.

(4) Combined effect of mole concentration and diffusion coefficient of each gas component dominates not only the mass transfer rate of each gas component, but also the contribution of each gas component on the gas bubble growth rate since a large mass transfer rate is found to essentially result in a high gas bubble growth rate. In particular, the same variation of mole concentration of different gas components usually cannot impose the same effect on the gas bubble growth rate. This is attributed to the fact that such variation leads to both changes of the concentration of corresponding gas component and variation of supersaturation of the entire fluid systems to different extents.

(5) The increased supersaturation pressure and pressure decline rate are capable of improving the bubble growth rate because of the increase in concentration gradient at the gas-liquid interface. In addition, a large liquid cell leads to a large gas bubble after the decline of mole concentration spreads to the boundary of a liquid cell. The linear relationship between gas bubble radius and square root of time may only be found under the conditions of the unlimited surrounding liquid volume and one-step pressure drop.

(6) Individual diffusion coefficient of each gas component during the mass transfer of foamy oil formation is found to be relatively large because of a high mass transfer rate occurring under nonequilibrium conditions. Meanwhile, the mass transfer rate between gas bubbles and oleic phase as well as the low pressure of gas bubble generation (i.e., pseudo-bubblepoint pressure) is able to impose a great effect on the volume growth of evolved gas, or in other words, foamy oil. The dynamic composition of evolved gas is dominated by preferential diffusion and concentration.

8.2 Recommendations

The nonequilibrium phase behaviour of foamy oil and the corresponding mass transfer processes are strongly associated with its flow performance in heavy oil reservoirs. In this study, comprehensive evaluation has been performed for the alkane solvent(s)–CO_2–heavy oil systems. In general, it is of practical and fundamental importance to further

deepen the related understanding into porous media. The recommendations for the future work are detailed as follows,

(1) The efforts need to be made to determinate individual diffusion coefficient in alkane solvent(s)–CO_2–heavy oil systems in porous media with consideration of natural convection. Compared with the bulk liquid, a faster natural convection in porous media can be expected because of a reduced flow sectional area, which, consequently, imposes a greater impact on the mass transfer rate. Such work is supposed to effectively enhance the accuracy of the quantification associated with the mass transfer processes in heavy oil reservoirs.

(2) The techniques proposed in Chapters 4 and 5 need to be extended to quantify phase behaviour of foamy oil in porous media. More specifically, the parameters related to oil production rate and physical properties of porous media should be experimentally and theoretically analyzed and evaluated. Accordingly, distribution of pressure decline rate and changes of porosity and permeability caused by sand production can be utilized to accurately describe in-situ generation of foamy oil together with its physical properties.

(3) The coalescence and breakup of gas bubbles formed in the heavy oil are expected to be experimentally and theoretically explored. Such efforts will be greatly beneficial to not only quantify the movement of gas bubbles in the viscous liquid, but also determining the amount of entrained gas in foamy oil

which is the critical factor dominating the behaviour of foamy oil in heavy oil reservoirs.

REFERENCES

Abivin, P., Henaut, I., Arfillier, J.F., and Moan, M. Viscosity behavior of foamy oil: Experimental study and modeling. *Pet. Sci. Tech*., 26 (13), 2008.

Adepoju, O.O. *Coefficient of isothermal oil compressibility for reservoir fluids by cubic equation-of-state*. M.A.Sc. Thesis, Texas Tech University, Lubbock, TX, 2006.

Ahmadi, M.A, Zendehboudi, S., James, L.A., Elkamel, A., Dusseault, M., Chatzis, I., and Lohi, A. New tools to determine bubble point pressure of crude oils: Experimental and modeling study. *J. Pet. Sci. Eng.*, 123, 207-216, 2014.

Albartamani, N.S., Farouq Ali, S.M., and Lepski, B. Investigation of foamy oil phenomena in heavy oil reservoirs. Paper SPE 54084, presented at the SPE International Thermal Operations and Heavy Oil Symposium, Bakersfield, CA, March 17-19, 1999.

Al-Mahrhoun, M.A. The oil compressibility below bubble point pressure revisited–formulations and estimations. Paper SPE 120047, presented at the SPE Middle East Oil and Gas Show and Conference, Manama, Bahrain, March 15-18, 2009.

Alshmakhy, A.B. and Maini, B.B. Foamy-oil-viscosity measurement. *J. Can. Pet. Tech*., 51 (1), 60-64, 2012.

Amon, M., and Denson, C.D. A study of the dynamics of foam growth analysis of the growth of closely spaced spherical bubbles. *Polym. Eng. Sci*., 24 (13), 1026-1034, 1984.

Arefmanesh, A., Advani, S.G., and Michaelides, E.E. An accurate numerical solution for mass diffusion-induced bubble growth in viscous liquids containing limited dissolved gas. *Int. J. Heat Mass Trans*., 35 (7), 1711-1722, 1992.

Arora, P. and Kovscek, A.R. A mechanistic modeling and experimental study of solution gas drive. *Transp. Porous Med*., 51 (3), 237-265, 2003.

Avedisian, C.T. The homogeneous nucleation limits of liquids. *J. Phys. Chem. Ref. Data*, 14 (3), 695-729, 1985.

Bauget, F. and Lenormand, R. Mechanisms of bubble formation by pressure decline in porous media: A critical review. Paper SPE 77457, presented at the SPE Annual Technical Conference and Exhibition, San Antonio, TX, September 29-October 2, 2002.

Bennion, D.B., Mastmann, M., and Moustakis, M.L. A case study of foamy oil recovery in the Patos-Marinza Reservoir, Driza Sand, Albania. *J. Can. Pet. Tech*., 42 (3), 21-28, 2003.

Birkhoff, G., Margulies, R.S., and Horning, W.A. Spherical bubble growth. *Phys. Fluids*, 1 (3), 201-204, 1958.

Blander, M. Bubble nucleation in liquids. *Adv. Colloid Interface Sci*., 10, 1-32, 1979.

Bora, R. *Cold production of heavy oil-An experimental investigation of foamy oil flow in porous media*. Ph.D. Dissertation, University of Calgary, Calgary, AB, 1998.

Bora, R., Chakma, A., and Maini, B. Experimental investigation of foamy oil flow using a high pressure etched glass micromodel. Paper SPE 84033, presented at the SPE Annual Technical Conference and Exhibition, Denver, CO, October 5-8, 2003.

Bora, R., Maini, B.B., and Chakma, A. Flow visualization studies of solution gas drive process in heavy oil reservoirs using a glass micromodel. Paper SPE 37519, presented at the SPE International Thermal Operations and Heavy Oil Symposium, Bakersfield, CA, February 10-12, 1997.

Bories, S. and Prat, M., Isothermal nucleation and bubble growth in porous media at low supersaturations. In *Transport phenomena in porous media II*, Pop, I. and Ingham, D.B. Ed., Pergamon, Elsevier, 276-312. 2002.

Bulter, R.M. and Mokrys, I.J. Recovery of heavy oils using vaporized hydrocarbon solvents: Further development of the VAPEX process. PETSOC-SS-92-7, presented at the Technical Meeting/Petroleum Conference of the South Saskatchewan Section, Regina, SK, October 7-9, 1992.

Butler, R.M. *Thermal recovery of oil and bitumen*. Prentice Hall, Upper Saddle River, NJ, 1991.

Cable, M. and Frade, J.R. Diffusion-controlled growth of multi-component gas bubbles. *J. Mater. Sci*., 22 (3), 919-924, 1987.

Chatenever, A., Indra, M.K., and Kyte, J.R. Microscopic observations of solution gas-drive behavior. *J. Pet. Tech*., 11 (6), 13-15, 1959.

Chen, L., Li, Y., and Manasseh, R. The coalescence of bubbles–A numerical study. Presented at the Third International Conference on Multiphase Flow, ICMF'98, Lyon, France, June 8-12, 1998.

Chen, Z., Sun, J., Wang, R., and Wu, X. A pseudobubblepoint model and its simulation for foamy oil in porous media. *SPE J*., 20 (2), 239-247, 2015.

Chernov, A.A., Kedrinskey, V.K., and Pil'nik, A.A., Kinetics of gas bubble nucleation and growth in magmatic melt at its rapid decompression. *Phys. Fluid*, 26 (11), 116602-1-116602-19, 2014.

Chesters, A.K. The modelling of coalescence processes in fluid-liquid dispersions: A review of current understanding. *Chem. Eng. Res. Des*., 69 (4), 259-227, 1991.

Chueh, P.L. and Prausnitz, J.M. Vapor-liquid equilibria at high pressures: Calculation of partial molar volumes in non polar liquid mixtures. *AIChE J*., 13 (6), 1099-1107, 1967.

Civan, F. and Rasmussen, M.L. Determination of gas-diffusion and interface-mass-transfer coefficients for Quiescent reservoir liquids. *SPE J*., 11 (1), 71-79, 2006.

Claridge, E.L. and Prats, M. A proposed model and mechanism for anomalous foamy heavy oil behavior. Paper SPE 29243, presented at the SPE International Heavy Oil Symposium, Calgary, AB, June 19-21, 1995.

Coombe, D. and Maini, B. Modeling foamy oil flow. Presented at the Workshop on Foamy Oil Flow held at the Petroleum Recovery Institute, Calgary, AB, April 27, 1994.

de Mirabal, M., Gordillo, R., Rojas, G., Rodriguez, H., and Huerta, M. Impact of foamy oil mechanism on the Hamaca Oil Reserves, Orinoco Belt-Venezuela. Paper SPE 36140, presented at SPE Latin America/Caribbean Petroleum Engineering Conference, Port-of-Spain, Trinidad, April 23-26, 1996.

Delale, C.F., Hruby, J., and Marsik, F. Homogeneous bubble nucleation in liquids: The classical theory revisited. *J. Chem. Phys.*, 118 (2), 792-806, 2003.

Deryagin, B.V. A general theory for the formation of a new phase: Static cavitation in a nonvolatile liquid. *Prog. Surf. Sci.*, 45 (4-1), 15-20, 1994.

Dusseault, M. Cold production and enhanced oil recovery. *J. Can. Pet. Tech*., 32 (9), 16-18, 1993.

Dusseault, M.B. Comparing Venezuelan and Canadian heavy oil and tar sands. Paper PETSOC-2001-061, presented at the Canadian International Petroleum Conference, Calgary, AB, June 12-14, 2001.

Emera, M.K. and Sarma, H.K. A genetic algorithm-based model to predict CO_2-oil physical properties for dead and live oil. *J. Can. Pet. Tech*., 47 (2), 52-61, 2008.

Farajzadeh, R., Delil, H.A., Zitha, L.J., and Bruining, J. Enhanced mass transfer of CO_2 into water and oil by natural convection. Paper SPE 107380, presented at the SPE/ EUROPEC/EAGE Conference and Exhibition, London, UK, June 11-14, 2007.

Farkas, L. The velocity of nucleus formation in supersaturated vapors. *J. Phys. Chem*., 125, 236-242, 1927.

Farouq Ali, S.M. Heavy oil-evermore mobile. *J. Pet. Sci. Eng*., 37 (1-2), 5-9, 2003.

Firoozabadi, A. and Aronson, A. Visualization and measurement of gas evolution and flow of heavy and light oil in porous media. *SPE Res. Eval. Eng*., 2 (6), 550-557, 1999.

Firoozabadi, A. Mechanisms of solution gas drive in heavy oil reservoirs. *J. Can. Pet. Tech*., 40 (3), 15-20, 2001.

Firoozabadi, A. and Kashchiev, D. Pressure and volume evolution during gas phase formation in solution gas drive process. *SPE J*., 1 (3), 1-9, 1996.

Firoozabadi, A., Ottesen, B., and Mikkelsen, M. Measurements of supersaturation and critical gas saturation. *SPE Format. Eval*., 7 (4), 337-344, 1992.

Firoozabadi, A., Ottesen, B., and Mikkelsen, M. Reply to discussion of measurement of supersaturation and critical gas saturation. *SPE Format. Eval*., 9 (3), 159-160, 1994.

Frank, X., Dietrich, N., Wu, J., Barraud, R., and Li, H.Z. Bubble nucleation and growth in fluids. *Chem. Eng. Sci*., 62 (24), 7090-7097, 2007.

Frauenfeld, T.W., Jossy, C., Bleile, J., Krispin, D., and Ivory, J. Experimental and economic analysis of the thermal solvent and hybrid solvent processes. *J. Can. Pet. Tech*., 48 (11), 55-62, 2009.

Ganapathi, K. *Solubility and diffusivity study for light gases in heavy oil and its fractions*. M.A.Sc. Thesis, University of Regina, Regina, SK, 2009.

Geilikman, M.B. and Dusseault, M.B., Sand production caused by foamy oil flow. *Transp. Porous Med*., 35 (2), 259-272, 1999.

Geilikman, M.B., Dusseault, M.B., and Dullien, F.A.L. Dynamic effects of foamy fluid flow in sand production instability. Paper SPE 30251, presented at the SPE International Heavy oil Symposium, Calgary, AB, June 19-21, 1995.

Goodarzi, N.N., Bryan, J.L., Mai, A.T., and Kantzas, A. Novel techniques for measuring heavy-oil fluid properties. *SPE J*., 12 (3), 305-315, 2007.

Gor, G.Y. and Kuchma, A.E., Steady-state composition of two-component gas bubble growing in a liquid solution: Self-similar approach. *J. Chem. Phys*., 131 (23), 234705-1-234705-6, 2009.

Gor, G.Y., Kuchma, A.E., and Kuni, F.M. Gas bubble growth dynamics in a supersaturated solution: Henry's and Sievert's solubility laws. In *nucleation theory and applications*, Schmelzer, J.W.P. Ed., JINR, Dubna, 213-233, 2011.

Guerrero-Aconcha, U., Salama, D., and Kantzas, A. Diffusion coefficient of *n*-alkanes in heavy oil. Paper SPE 115346, presented at the SPE Annual Technical Conference and Exhibition, Denver, CO, September 21-24, 2008.

Gupta, S.C. and Gittins, S.D. Christina lake solvent aided process pilot. *J. Can. Pet. Tech*., 45 (9), 15-18, 2006.

Handy, L.L. A laboratory study of oil recovery by solution gas drive. *Pet. Trans*. *AIME.*, 213, 310-315, 1958.

Hayduk, W. and Cheng, S.C. Review of relation between diffusivity and solvent viscosity in diluted liquid solutions. *Chem. Eng. Sci*., 26 (5), 635-646, 1976.

Homayouni, S.S., Mehrnia, M.R., Mostoufi, N., Rajabi, M., and Yazdani, A. Bubble size distribution in oil-based bubble columns. *Chem. Eng. Tech*., 31 (11), 1668-1675, 2008.

Irani, M., and Ghannadi, S. Understanding the heat-transfer mechanism in the steam-assisted gravity-drainage (SAGD) process and comparing the conduction and convection flux in bitumen reservoirs. *SPE J*., 18 (1), 134-145, 2013.

Islam, M.R. and Chakma, A. Mechanics of bubble flow in heavy oil reservoirs. Paper SPE 20070, presented at the SPE California Regional Meeting, Ventura, CA, April 4-6, 1990.

Istchenko, C.M. and Gates, I.D. Well/wormhole model of cold heavy-oil production with sand. *SPE J*., 19 (2), 260-269, 2014.

Ivory, J., Frauenfeld, T., and Jossy, C. Thermal solvent reflux and thermal solvent hybrid experiments. *J. Can. Pet. Tech*., 49 (2), 23-31, 2010.

Jones, S.F., Evans, G.M., and Galvin, K.P. Bubble nucleation from gas cavities-A review. *Adv. Colloid Interface Sci*., 80 (1), 27-50, 1999.

Joseph, D.D., Kamp, A.M., and Bai, R. Modeling foamy oil flow in porous media. *Int. J. Multiphase Flow*, 28 (10), 1659-1686, 2002.

Kamath, J. and Boyer, R.E. Critical gas saturation and supersaturation in low-permeability rocks. *SPE Format. Eval*., 10 (4), 247-253, 1995.

Kamp, A.M., Heny, C., Andarcia, L., Lago, M., and Rodriguez, A. Experimental investigation of foamy oil solution gas driven. Paper SPE 69725, presented at the SPE International Thermal Operations and Heavy Oil Symposium, Porlamar, Venezuela, March 12-14, 2001.

Kashchiev, D. and Firoozabadi, A. Kinetics of the initial stage of isothermal gas phase formation. *J. Chem. Phys*., 98 (6), 4690-4699, 1993.

Katz, J.L. and Blander, M. Condensation and boiling: corrections to homogeneous nucleation theory for nonideal gases. *J. Colloid Interface Sci*., 42 (3), 496-502, 1973.

Kennedy, H.T. and Olson, C.R. Bubble formation in supersaturated hydrocarbon mixtures. *J. Pet. Tech.*, 4 (11), 271-278, 1952.

Kortekaas, T.F.M. and van Poelgeest, F. Liberation of solution gas during pressure depletion of virgin watered-out oil reservoirs. *SPE Res. Eng*., 6 (3), 329-335, 1991.

Kraus, W.P., McCaffrey, W.J., and Boyd, G.W. Pseudo-bubble point model for foamy oils. Paper CIM 93-45, presented at the 44th Annual Technical Conference of the Petroleum Society of CIM, Calgary, AB, May 9-12, 1993.

Kumar, A., Jaiswal, D.K., and Kumar, N. Analytical solutions of one-dimensional advection-diffusion equation with variable coefficients in a finite domain. *J. Earth Syst. Sci*., 118 (5), 539-549, 2009.

Kumar, R. and Mahadevan, J. Well-performance relationships in heavy-foamy-oil reservoirs. *SPE Prod. Oper.*, 27 (1), 2012.

Kumar, R. and Pooladi-Darvish, M. Effect of viscosity and diffusion coefficient on the kinetics of bubble growth in solution-gas drive in heavy oil. *J. Can. Pet. Tech*., 40 (3), 30-37, 2001.

Kumar, R. *Solution-gas drive in heavy oil-gas mobility and kinetics of bubble growth*. M.A.Sc. Thesis, University of Calgary, Calgary, AB, 1999.

Kumar, R., Pooladi-Darvish, M., and Okazawa, T. Effect of depletion rate on gas mobility and solution gas drive in heavy oil. *SPE J*., 7 (2): 213-220, 2002.

Laari, A. and Turunen, I. Prediction of coalescence properties of gas bubbles in a gas-liquid reactor using persistence time measurements. *Chem. Eng. Res. Des*., 83 (7), 881-886, 2005.

Leung, S.N., Park, C.B., Xu, D., Li, H., and Fenton, R.G. Computer simulation of bubble-growth phenomena in foaming. *Ind. Eng. Chem. Res.*, 45 (23), 7823-7831, 2006.

Li, D. Coalescence between small bubbles: Effects of bulk and surface diffusion. *Chem. Eng. Sci*., 51 (14), 3623-3630, 1996.

Li, H. and Yang, D. Determination of individual diffusion coefficients of solvent-CO_2 mixture in heavy oil using pressure-decay method. *SPE J*., 21 (1), 131-143, 2016.

Li, H. and Yang, D. Modified α function for the Peng-Robinson equation of state to improve the vapor pressure prediction of non-hydrocarbon and hydrocarbon compounds. *Energy Fuels*, 25 (1), 215-223, 2011.

Li, H. and Yang, D. Phase behaviour of C_3H_8/*n*-C_4H_{10}/heavy-oil systems at high pressures and elevated temperatures. *J. Can. Pet. Tech*., 52 (1), 30-40, 2013.

Li, H. *Phase behaviour and mass transfer of solvent(s)-CO_2-heavy oil systems under reservoir conditions*. Ph.D. Dissertation, University of Regina, Regina, SK, 2013.

Li, H., Sun, H., and Yang, D. Effective diffusion coefficients of gas mixture in heavy oil under constant pressure conditions. *Heat Mass Transfer*, available online DOI:10.1007/s00231-016-1919-x, 2016.

Li, H., Yang, D., and Tontiwachwuthikul, P. Experimental and theoretical determination of equilibrium interfacial tension for the solvent(s)-CO_2-Heavy oil systems. *Energy Fuels*, 26 (3), 1776-1786, 2012.

Li, H., Zheng, S., and Yang, D. Enhanced swelling effect and viscosity reduction of solvent(s)/CO_2/heavy-oil systems. *SPE J*., 18 (4), 695-707, 2013a.

Li, W., Mamora, D.D., and Li, Y. Solvent-type and -ratio impacts on solvent-aided SAGD process. *SPE Res. Eval. Eng*., 14 (3), 320-331, 2011.

Li, X. and Yortsos, Y.C. Theory of multiple bubble growth in porous media by solute diffusion. *Chem. Eng. Sci*., 50 (8), 1247-1271, 1995.

Li, X. and Yortsos, Y.C. Visualization and numerical studies of bubble growth during pressure depletion. Paper SPE 22589, presented at the 66th SPE Annual Technical Conference and Exhibition, Dallas, TX, October 6-9, 1991.

Li, X., Li, H., and Yang, D. Determination of multiphase boundaries and swelling factors of solvent(s)–CO_2–heavy oil systems at high pressures and elevated temperatures. *Energy Fuels*, 27 (3), 1293-1306, 2013b.

Li, X., Yang, D., and Fan, Z. Phase behaviour and viscosity reduction of CO_2-heavy oil systems at high pressures and elevated temperatures. Paper SPE 170057, presented at the SPE Heavy Oil Conference, Calgary, AB, June 10-12, 2014.

Li, Z. and Dong, M. Experimental study of carbon dioxide diffusion in oil-saturated porous media under reservoir conditions. *Ind. Eng. Chem. Res*., 48 (20), 9307-9317, 2009.

Li, Z. *Study of gas diffusion in liquid-saturated porous media for oil recovery and CO_2 sequestration*. Ph.D. Dissertation, University of Regina, Regina, SK, 2006.

Lillico, D.A., Babchin, A.J., Jossy, W.E., Sawatzky, R.P., and Yuan, J.-Y. Gas bubble nucleation kinetics in a live heavy oil. *Colloids Surf. A*, 192, 25-38, 2001.

Luigi, A., Saputelli, B., Carlas, M. Canache, P., and Lopez, E. Application of a nonequilibrium reaction model for describing horizontal well performance in foamy oils. Paper SPE 50414, presented at the SPE International Conference on Horizontal Well Technology, Calgary, AB, November 1-4, 1998.

Luo, H. and Kantzas, A. Investigation of diffusion coefficients of heavy oil and hydrocarbon solvent systems in porous media. Paper SPE 113995, presented at the SPE Symposium on Improved Oil Recovery, Tulsa, OK, April 20-23, 2008.

Luo, H. *Coalescence, breakup and liquid circulation in bubble column reactors*. Ph.D. Dissertation, University of Trondheim, Trondheim, Norway, 1993.

Mackay, E.J., Henderson, G.D., Tehrani, D.H., and Danesh, A. The importance of interfacial tension on fluid distribution during depressurization. *SPE Reserv. Eval. Eng.*, 1 (5), 408-415, 1998.

Maini, B.B. Foamy oil flow in heavy oil production. *J. Can. Pet. Tech*., 35 (6), 21-24, 1996.

Maini, B.B. Foamy-oil flow. *J. Pet. Tech*., 53 (10), 54-64, 2001.

Maini, B.B., Sarma, H.K., and George, A.E. Significance of foamy-oil behaviour in primary production of heavy oils. *J. Can. Pet. Tech*., 32 (9), 50-54, 1993.

Marrucci, G. A theory of coalescence. *Chem. Eng. Sci*., 24 (6), 975-958, 1969.

Marufuzzaman, M. and Henni, A. Solubility and diffusivity of propane in heavy oil and its SARA fractions. *Can. J. Chem. Eng*., 92 (8), 1421-1431, 2014.

Mastmann, M., Moustakis, M.L., and Bennion, B. Predicting foamy oil recovery. Paper SPE 68860, presented at the SPE Western Regional Meeting, Bakersfield, CA, March 26-30, 2001.

Meyer, R.F. and Attanasi, E.D. Heavy oil and natural bitumen-strategic petroleum resources. *U.S. Geological Survey Fact Sheet 70-03*, online version 1.0, 2003.

Milind, D., Nutakki, R., and Orr, F.M. Jr. Schmidt-Wenzel and Peng-Robinson equations of state for CO_2/hydrocarbon mixtures: Binary interaction parameters and volume translation factors. *SPE Adv. Tech. Ser*., 1 (2), 142-151, 1993.

Mitchell, B.J. Test data fill theory gap on using foam as a drilling fluid. *Oil Gas J*., 69 (36), 96-100, 1971.

Moghaddam, R.N., Rostami, B., Pourafshary, P., and Fallahzadeh, Y. Quantification of density-driven natural convection for dissolution mechanism in CO_2 sequestration. *Transp. Porous Med*., 92 (2), 439-456, 2011.

Moulu, J.C. Solution-gas drive: Experiments and simulation. *J. Pet. Sci. Eng.*, 2 (4), 379-386, 1989.

Or, C., Sasaki, K., Sugai, Y., Nakano, M., and Imai, M. Numerical simulation of CO_2 gas microbubble of foamy oil. *Energy Proc*., 63, 7821-7829, 2014.

Oxtoby, D.W. Nucleation of first-order phase transitions. *Acc. Chem. Res*., 31 (2), 91-97, 1998.

Pal, R., Yan, Y., and Masliyah, J. Rheology of emulsions. In *Emulsions: fundamentals and applications in the petroleum industry*, Schramm, L.L. Ed., American Chemical Society, Washington, DC, 131-170, 1992.

Patel, R.D. Bubble growth in a viscous Newtonian liquid. *Chem. Eng. Sci*., 35 (11), 2352-2356, 1980.

Payvar, P. Mass transfer-controlled bubble growth during rapid decompression of a liquid. *Int. J. Heat Mass Trans*., 30 (4), 699-706, 1987.

Pedersen, K.S., Christensen, P.L., and Shaikh, J.A. *Phase behavior of petroleum reservoir fluids* (2^{nd} Edition). CRC Press, Boca Raton, FL, 242-245, 2014.

Péneloux, A., Rauzy, E., and Freze, R. A consistent correction for Redlich-Kwong-Soave volumes. *Fluid Phase Equilib*., 8 (1), 7-23, 1982.

Peng, D. and Robinson, D.B. A new two-constant equation of state. *Ind. Eng. Chem. Fundam.*, 15 (1), 59-64, 1976.

Pooladi-Darvish, M. and Firoozabadi, A. Solution-gas drive in heavy oil reservoirs. *J. Can. Pet. Tech*., 38 (4), 54-61, 1999.

Poon, D. and Kisman, K. Non-Newtonian effects on the primary production of heavy oil reservoirs. *J. Can. Pet. Tech*., 31 (7), 55-59, 1992.

Reguera, D. and Miguel, R.J. Non-equilibrium thermodynamics for nucleation kinetics. In *Experimental thermodynamics volume X*: *Non-equilibrium thermodynamics with applications*, Bedeaux, D, Kjelstrup, S., and Sengers, J.V. Ed., RSC, Cambridge, UK, 314-337, 2015.

Renner, T.A. Measurement and correlation of diffusion coefficients for CO_2 and rich-gas applications. *SPE Reserv. Eng*., 3 (2), 517-523, 1988.

Riazi, M.R. A new method for experimental measurement of diffusion coefficients in reservoir fluids. *J. Pet. Sci. Eng*., 14 (3-4), 235-250, 1996.

Romero, D.J., Fernandez, B., and Rojas, G. Thermodynamic characterization of a PVT of foamy oil. Paper SPE 69724, presented at the SPE International Thermal Operations and Heavy Oil Symposium, Porlamar, Margarita Island, Venezuela, March 12-14, 2001.

Roscoe, S. The viscosity of suspensions of rigid spheres. *Br. J. Appl. Phys*., 3 (8), 267-269, 1952.

Rosner, D.E. and Epstein, M. Effects of interface kinetics, capillarity and solute diffusion on bubble growth rates in highly supersaturated liquids. *Chem. Eng. Sci.*, 27 (12), 69-88, 1972.

Sachs, W. The diffusional transport of methane in liquid water: Method and result of experimental investigation at elevated pressure. *J. Pet. Sci. Eng*., 21 (3-4), 153-164, 1998.

Sahni, A., Gadelle, F., Kumar, M., Tomutsa, L., and Kovscek, A.R. Experiments and analysis of heavy-oil solution-gas drive. *SPE Res. Eval. Eng*., 7 (3), 217-229, 2004.

Santos, R.G., Loh, W., Bannwart, A.C., and Trevisan, O.V. An overview of heavy oil properties and its recovery and transportation methods. *Braz. J. Chem. Eng*., 31 (3), 571-590, 2014.

Sarma, H. and Maini, B. Role of solution gas in primary production of heavy oils. Paper SPE 23631, presented at the SPE Latin America Petroleum Engineering Conference, Caracas, Venezuela, March 8-11, 1992.

Scriven, L.E. On the dynamics of phase growth. *Chem. Eng. Sci.* 10 (1-2), 1-13, 1959.

Seljom, P. Unconventional oil and gas production. *IEA-ETSAP technology brief P02*, May, 2010.

Sheikha, H. and Pooladi-Darvish, M. The effect of pressure-decline rate and pressure gradient on the behavior of solution-gas drive in heavy oil. *SPE Res. Eval. Eng*., 12 (3), 390-398, 2009.

Shen, C. and Batycky, J.P. Observation of mobility enhancement of heavy oils flowing through sand pack under solution gas drive. *J. Pet. Can. Tech*., 38 (4), 46-53, 1999.

Sheng, J.J. *Foamy oil flow in porous media*. Ph.D. Dissertation, University of Alberta, Edmonton, AB, Canada, 1997.

Sheng, J.J., Hayes, R.E., and Maini, B.B. A dynamic model to simulate foamy oil flow in porous media. Paper SPE 36750, presented at the SPE Annual Technical Conference and Exhibition, Denver, CO, October 8-9, 1996.

Sheng, J.J., Hayes, R.E., Maini, B.B., and Tortike, W.S. A proposed dynamic model for foamy oil properties. Paper SPE 30253, presented at the SPE International Heavy Oil Symposium, Calgary, AB, June 19-21, 1995.

Sheng, J.J., Hayes, R.E., Maini, B.B., and Tortike, W.S. Modelling foamy oil flow in porous media. *Transp. Porous Med*., 35 (2), 227-258, 1999a.

Sheng, J.J., Maini, B.B., Hayes, R.E., and Tortike, W.S. A non-equilibrium model to calculate foamy oil properties. *J. Can. Pet. Tech.*, 38 (4), 38-45, 1999b.

Sheng, J.J., Maini, B.B., Hayes, R.E., and Tortike, W.S. Critical review of foamy oil flow. *Transp. Porous Med*., 35 (2), 157-187, 1999c.

Shi, Y. and Yang, D. Experimental and theoretical quantification of nonequilibrium phase behaviour and physical properties of foamy oil under reservoir conditions. *J. Energy Resour. Tech.*, available online, DOI: 10.1115/1.4036960, 2017a.

Shi, Y. and Yang, D. Experimental and theoretical quantification of non-equilibrium phase behaviour and physical properties of foamy oil under reservoir conditions. Paper OMAE2017-62194, presented at the ASME Ocean Offshore and Arctic Engineering OMAE 2017 Conference, Trondheim, Norway, June 25-30, 2017b.

Shi, Y. and Yang, D. Non-equilibrium phase behaviour and mass transfer of alkane solvent(s)–CO_2–heavy oil systems under reservoir conditions. Presented at the 25th Williston Basin Petroleum Conference, Regina, SK, May 2-4, 2017c.

Shi, Y. and Yang, D. Quantification of a single gas bubble growth in solvent(s)-CO_2-heavy oil systems with consideration of multicomponent diffusion under non-equilibrium conditions. *J. Energy Resour. Tech*., 139 (2), 022909-1-022908-11, 2017d.

Shi, Y., Li, X., and Yang, D. Experimental and theoretical determination of foamy oil properties under non-equilibrium conditions. Presented at the 36th IEA-EOR Collaborative Project Workshop & Symposium, Sapporo, Japan, September 9-11, 2015.

Shi, Y., Li, X., and Yang, D. Nonequilibrium phase behaviour of alkane solvent(s)-CO_2-heavy oil systems under reservoir conditions. *Ind. Eng. Chem. Res*., 55 (10), 2860-2871, 2016.

Shi, Y., Zheng, S., and Yang, D. Determination of individual diffusion coefficients of solvents-CO_2-heavy oil systems with consideration of natural convection induced by swelling effect. *Int. J. Heat Mass Tran*., 107, 572-585, 2017.

Slettebø, E.S. *Separation of gas from liquids in viscous systems*. M.A.Sc. Thesis, Norwegian University of Science and Technology, Trondheim, Norway, 2009.

Smith, G. U.S. seen as biggest oil producer after overtaking Saudi. *Bloomberg*, https://www.bloomberg.com/news/articles/2014-07-04/u-s-seen-as-biggest-oil-producer-after-overtaking-saudi, 2014.

Smith, G.E. Fluid flow and sand production in heavy-oil reservoirs under solution-gas drive. *SPE Prod. Eng*., 3 (2), 169-180, 1988.

Song, L., Kantzas, A., and Bryan, L.J. Experimental measurement of diffusion coefficient of CO_2 in heavy oil using X-ray computed-assisted tomography under reservoir

conditions. Paper SPE 137545, presented at the SPE Canadian Unconventional Resources and International Petroleum Conference, Calgary, AB, October 19-21, 2010.

Stewart, C.R., Hunt, E.B. Jr., Schneider, F.N., Geffen, T.M., and Berry, V.J. Jr. The role of bubble formation in oil recovery by solution gas drives in limestones. *J. Pet. Tech*., 5 (12), 21-28, 1954.

Sun, H., Li, H., and Yang, D. Coupling heat and mass transfer for a gas mixture–heavy oil system at high pressures and elevated temperatures. *Int. J. Heat Mass Tran.*, 74 (7), 173-184, 2014.

Sun, X., Zhang, Y., Li, X., Cui, G., and Gu, J. A case study on foamy oil characteristics of the Orinoco Belt, Venezuela. *Adv*. *Pet. Explor. Dev.*, 5 (1), 37-41, 2013.

Szekely, J. and Fang, S.-D. Non-equilibrium effects in the growth of spherical gas bubbles due to solute diffusion–II: The combined effects of viscosity, liquid inertia, surface tension and surface kinetics. *Chem. Eng. Sci*., 28 (12), 2127-2140, 1973.

Szekely, J. and Martins, G.P. Non-equilibrium effects in the growth of spherical gas bubbles due to solution diffusion. *Chem. Eng. Sci*., 26 (1), 147-159, 1971.

Taylor, G.I. The viscosity of a fluid containing small drops of another fluid. *Proc. Roy. Soc*. *London A*, 138 (834), 41-48, 1932.

Teja, A.S. and Sandler, A.I. A corresponding states equation for saturated liquid densities. II. Applications to the calculation of swelling factors of CO_2-crude oil systems. *AIChE J*., 26 (3), 341-345, 1980.

Tharanivasan, A.K., Yang, C., and Gu, Y. Comparison of three different interface mass transfer models used in the experimental measurement of solvent diffusivity in heavy oil. *J. Pet. Sci. Eng*., 44 (3-4), 269-282, 2004.

Thomas, F.B., Young, J., Tomas, Z.R., and Hill, J.A. Towards quantifying non-equilibrium gas evaluation in heavy oil. *CETI J*., 2 (1), 9-17, 2014.

Uddin, M. Numerical studies of gas exsolution in a live heavy oil reservoir. SPE Paper 97739, presented at the SPE International Thermal Operations and Heavy Oil Symposium, Calgary, AB, November 1-3, 2005.

Upreti, S.R. and Mehrotra, A.K. Diffusivity of CO_2, CH_4, C_2H_6, and N_2 in Athabasca bitumen. *Can. J. Chem. Eng*., 80 (1), 116-125, 2002.

Upreti, S.R., Mehrotra, A.K. Experimental measurement of gas diffusivity in bitumen: Results for carbon dioxide. *Ind. Eng. Chem. Res*., 39 (4), 1080-1087, 2000.

Volmer, M. and Weber, A. Nucleus formation in supersaturated systems. *J. Phys. Chem*., 119, 277-301, 1925.

Wang, J., Yuan, Y., Zhang, L., and Wang, R. The influence of viscosity on stability of foamy oil in the process of heavy oil solution gas drive. *J. Pet. Sci. Eng.*, 66 (1-2), 69-74, 2009.

Wang, R., Qin, J., Chen, Z., and Zhao, M. Performance of drainage experiments with Orinoco Belt heavy oil in a long laboratory core in simulated reservoir conditions. *SPE J*., 13 (4), 474-479, 2008.

Ward, C.A. and Levart, E. Conditions for stability of bubble nuclei in solid surfaces contacting a liquid-gas solution. *J. Appl. Phys*., 56 (2), 491-500, 1984.

Wen, Y., Bryan, J., and Kantzas, A. Estimation of diffusion coefficients in bitumen solvent mixtures as derived from low field NMR spectra. *J. Can. Pet. Tech*., 44 (4), 29-35, 2005.

Wieland, D.R. and Kennedy, H.T. Measurements of bubble frequency in cores. *Pet. Trans. AIME*., 210, 122-125, 1957.

Wilt, P.M. Nucleation rates and bubble stability in water carbon dioxide solutions. *J. Colloid Interface Sci*., 112 (2), 530-538, 1986.

Wong, R.C.K. and Maini, B.B. Gas bubble growth in heavy oil-filled sand packs under undrained unloading. *J. Pet. Sci. Eng.*, 55 (3-4), 259-270, 2007.

Xiao, L. and Zhao, G. Integrated study of foamy oil flow and wormhole structure in CHOPS through transient pressure analysis. Paper SPE 165538, presented at the SPE Heavy Oil Conference, Calgary, AB, June 11-13, 2013.

Yang, C. and Gu, Y. A new method for measuring solvent diffusivity in heavy oil by dynamic pendant drop shape analysis (DPDSA). *SPE J*., 11 (1), 48-57, 2006a.

Yang, C. and Gu, Y. Accelerated mass transfer of CO_2 in reservoir brine due to density-driven natural convection at high pressures and elevated temperatures. *Ind. Eng. Chem. Res.*, 45 (8), 2430-2436, 2006b.

Yang, C. and Gu, Y. Diffusion coefficients and oil swelling factors of carbon dioxide, methane, ethane, propane and their mixtures in heavy oil. *Fluid Phase Equilib*., 243 (1-2), 64-73, 2006c.

Yang, D. and Gu. Y. Determination of diffusion coefficients and interface mass-transfer coefficients of the crude oil-CO_2 system by analysis of the dynamic and equilibrium interfacial tensions. *Ind. Eng. Chem. Res*., 47 (15), 5447-2455, 2008.

Yang, D., Tontiwachwuthikul, P., and Gu, Y. Dynamic interfacial tension method for measuring the gas diffusion coefficient and the interface mass transfer coefficient in a liquid. *Ind. Eng. Chem*. Res., 45 (14), 4999-5008, 2006.

Yarranton, H.W., van Dorp, J.J., Verlaan, M.L., and Lastovka, V. Wanted dead or live: Crude-cocktail viscosity-A pseudocomponent method to predict the viscosity of dead oils, live oils, and mixtures. *J. Can. Pet. Tech*., 52 (3), 176-191, 2013.

Yortsos, Y.C. and Parlar, M. Phase change in binary systems in porous media: application to solution-gas drive. Paper SPE 19697, presented at the 64th SPE Annual Technical Conference and Exhibition, San Antonio, TX, October 8-11, 1989.

Yortsos, Y.C. Discussion of pressure and volume evolution during gas phase formation in solution gas drive processes. *SPE J*., 2 (2), 223-227, 1997.

Yousifi, A.E., Zarcone, C., and Bories, S. Physical mechanisms for bubble growth during solution gas drive. Paper SPE 38921, presented at the SPE Annual Technical Conference and Exhibition, San Antonio, TX, October 5-8, 1997.

Zeldovich, J.B. On the theory of new phase formation, cavitation. *Acta Phys. URSS*, 18 (1), 1-22, 1943.

Zheng, S. and Yang, D. Determination of diffusion coefficients of C_3H_8/*n*-C_4H_{10}/CO_2/ heavy-oil systems at high pressures and elevated temperatures by dynamic volume analysis. *SPE J*., available online, DOI: 10.2118/179618-PA, 2016.

Zheng, S. and Yang, D. Experimental and theoretical determination of diffusion coefficients of CO_2-heavy oil systems by coupling heat and mass transfer. *J. Energy Resour. Tech*., 139 (2), 022901-1-022901-15, 2017.

Zheng, S., Li, H., Sun, H., and Yang, D. Determination of diffusion coefficient for

solvent-CO_2 mixtures in heavy oil with consideration of swelling effect. *Ind. Eng. Chem. Res*., 55 (6), 1533-1549, 2016a.

Zheng, S., Sun, H., and Yang, D. Coupling heat and mass transfer for determining individual diffusion coefficient of a hot C_3H_8-CO_2 mixture in heavy oil under reservoir conditions. *Int. J. Heat Mass Tran*., 102, 251-263, 2016b.